The importance of including knee joint laxity in dynamic musculoskeletal simulations of movement

by

Anne Schmitz

A dissertation submitted in partial fulfillment of

the requirements for the degree of

Doctor of Philosophy

(Biomedical Engineering)

at the

UNIVERSITY OF WISCONSIN-MADISON

2012

Date of final oral examination: 11/19/12

The dissertation is approved by the following members of the Final Oral Committee:

Darryl G. Thelen, Professor, Mechanical and Biomedical Engineering
Dan Negrut, Associate Professor, Mechanical Engineering
Heidi-Lynn Ploeg, Associate Professor, Mechanical and Biomedical Engineering
Ray Vanderby Jr., Professor, Biomedical Engineering
Geoffrey Baer, Assistant Professor, Orthopedics and Rehabilitation





ProQuest LLC.
789 East Eisenhower Parkway
P.O. Box 1346
Ann Arbor, MI 48106 - 1346

# Acknowledgements

Thank you to all who have supported me: my husband James, my daughter Lilah, my sister Kristen, my brother Nick, my mother Patty, and father Jaye. I couldn't have done it without them. A special thank you is deserved by my advisor Darryl Thelen for his patience and mentorship. Thank you to all my lab mates and everyone I have met here at the UW. I will never forget my time here. Thank you to my funding sources as well: NIH T32 AG000213 (P.I. Sanjay Asthana) and kinesiology 318 teaching assistant to Kreg Gruben.

# Abstract

Musculoskeletal simulations of human movement are often used to estimate soft tissue and joint contact loads. However, traditional modeling approaches use a serial approach that does not account for knee joint laxity when simulating movement. In the traditional approach, a multibody dynamics model is used to calculate muscle forces needed to produce skeletal movement. Then, these muscle forces are applied as boundary conditions to a detailed joint model to solve for soft tissue loading. However, the dynamic musculoskeletal models often assume a one degree of freedom kinematic knee joint that behaves independent of load. The overall goal of this work was to investigate the coupling of multibody dynamics and soft tissue mechanics. This goal was achieved by completing the following three objectives.

Objective 1: Empirically assess how *in vivo* knee kinematics vary with quadriceps loading

Rationale: Musculoskeletal models often assume that joints are simply kinematic constraints. However in reality, joint kinematics vary with loading, which can influence the line of action and moment arm of a muscle about the knee. Hypothesis: The *in vivo* tibiofemoral finite helical axis and patellar tendon moment arm will exhibit load-dependent behavior. Methods: Dynamic MRI imaging techniques were used to measure three-dimensional knee kinematics under controlled loading conditions. Eight subjects performed cyclic knee flexion/extension tasks against inertial and elastic loads, which induced quadriceps activity with knee flexion and extension, respectively. For both loading conditions, the tibiofemoral finite helical axis was calculated as well as the patellar tendon's moment arm with respect to this axis. Results: Quadriceps loading in a flexed knee induced a significant inferior shift of the finite helical axis, which diminished the patellar tendon moment arm. Since the quadriceps load induced during flexion in the experiment was similar to that seen during the load-acceptance phase of gait, this load-dependence may be important to consider in gait simulations. Relevance: Since the quadriceps

load induced during flexion in the experiment was similar to that seen during the load-acceptance phase of gait, this load-dependence may be important to consider in gait simulations.

Objective 2: Investigate whether a muscle-actuated computational knee model that includes ligament compliance and tibiofemoral contact could emulate *in vivo* kinematic patterns. Rationale: Since the knee exhibits load-dependent behavior *in vivo*, a framework should be developed to couple multibody dynamics and soft tissue loads. Hypothesis: Similar to what was seen *in vivo*, the finite helical axis will shift inferiorly when the quadriceps are loaded in flexion, thus diminishing the moment arm of the patellar tendon. Methods: We started with a generic lower extremity model with 44 muscles, 6 joints, and 18 degrees of freedom. The kinematic knee joint was replaced by a six degree of freedom tibiofemoral joint. This knee model included 19 ligaments represented by non-linear springs as well as an elastic foundation model to calculate tibiofemoral cartilage contact loads. The one degree of freedom patellofemoral joint was constrained to move within a path relative to the femoral groove with patellar tendon and quadriceps forces acting on either end of the patella. A co-simulation framework was implemented in which neuromusculokeletal dynamics and knee mechanics were simultaneously solved using a computed muscle control algorithm. Results: The co-simulation framework predicted similar load-dependent variations in knee kinematics as seen *in vivo,* specifically that quadriceps loading at flexed angles induces anterior tibial translation and superior patellar translation. The model predicted internal rotation with quadriceps loading, which was not seen experimentally. However, the model agrees with other *ex vivo* studies on quadriceps function. Relevance: These results demonstrate the relevance and potential for co-simulating musculoskeletal dynamics and soft tissue loads.

Objective 3: Use the co-simulation framework to investigate the influence of knee laxity on tibiofemoral kinematics and kinetics during walking. Rationale: The load-dependent behavior of the knee is evident in intact healthy knees and may even more important to consider in pathological cases where injury can alter joint laxity and surgery can alter the properties of both reconstructed and donor

tissues. These effects are particularly relevant when using models to characterize cartilage and muscle loads. Hypothesis: When the quadriceps are maximally loaded during stance, the models with laxity will exhibit an anteriorly translated and internally rotated tibia in comparison to a kinematic joint assumption. These will in turn affect the moment arm of the patellar tendon and thus predictions of quadriceps loading. Methods: Using the developed co-simulation technique from objective 2, muscle activation patterns were computed that drove a lower extremity musculoskeletal model to track normal hip, knee, and ankle flexion patterns during gait. Results: During the load acceptance phase of gait, the models with laxity predicted increased anterior tibia translation and internal tibia rotation due to quadriceps loading. These variations in tibiofemoral kinematics resulted in a more inferior finite helical axis, a diminished patellar tendon moment arm, and increased quadriceps loading, relative to what would be computed using a traditional kinematic knee model. Simulating gait with an ACL-deficient knee shifted tibia plateau cartilage contact posteriorly and laterally. Relevance: Shifts in cartilage loading after surgery are thought to contribute to early onset knee osteoarthritis.

We have shown that load-dependent variations in secondary joint kinematics affect muscle actions by using a modified computed muscle control algorithm to co-simulate soft tissue loads and musculoskeletal dynamics during gait. This is the first study to predict changes in cartilage contact loading between a healthy and ACL-deficient knee. This framework could be further used to explore surgical and rehabilitative strategies to restore normal knee mechanics after injury and disease.

# Table of Contents

# Chapter 1: Introduction

The knee is an important load-bearing joint, unique from other joints in that there are three compartments (two tibiofemoral and one patellofemoral) with menisci to distribute loads (McDermott and Amis, 2006) and soft tissues as the major stabilizing factors, as opposed to articular geometry (Elsevier, 2008). Causing over 55 million doctor visits a year, the knee is the most frequently injured joint (Dunkin, 2009). Osteoarthritis, the most common form of arthritis, occurs more in the knee than any other joint (Oliveria, et al., 2005). Therefore, knee models are built to study normal joint function, prevention of problems, and treatments.

These models range in complexity from a hinge joint (Asano, et al., 2005; Reinbolt, et al., 2005) to a complex continuum representation using finite element analysis (Dhaher, et al., 2010) and have been used to estimate immeasurable forces (i.e. muscle forces and soft tissue loads) and to perform 'what-if' studies. For example, (van der Krogt, et al., 2012) used simplified joint models to study how muscle weakness affected normal walking. (Shelburne, et al., 2005a) used a discrete element model of the knee, a model that includes cartilage loads and spring representations for ligaments, to predict hamstring and quadriceps forces that could be used to restore normal joint function in a knee without an anterior cruciate ligament. (Dhaher and Kahn, 2002) used a finite element model to determine how quadriceps forces affect patellofemoral cartilage loads, often the cause of patellofemoral pain.

However, a serial approach is typically used to estimate these internal knee loads (Fernandez and Pandy, 2006). First, muscle forces are calculated using a simplified model of knee (e.g. hinge joint), where the joint is assumed to behave independently of load (a.k.a. a kinematic joint) (Anderson and Pandy, 1999; Anderson and Pandy, 2001; Reinbolt, et al., 2005). These muscle forces are then used as boundary conditions to a more detailed joint model to calculate soft tissue loading. However, knee

behavior is load-dependent (Dyrby and Andriacchi, 2004; Tsaopoulos, et al., 2007; Westphal and Thelen, 2009), and it is unclear how important it is to account for this when muscle forces are calculated.

Rather than using a serial approach, others have simultaneously predicted muscle forces and soft tissue loads, coupling musculoskeletal dynamics and soft tissue mechanics. (Halloran, et al., 2009) coupled a musculoskeletal model of the lower extremity with a finite element model of the foot to determine neuromuscular coordination patterns to optimize jumping. However, this was constrained to the sagittal plane. (Lin, et al., 2010) simultaneously predicted muscle forces and contact forces at the knee during gait but did not consider ligament forces. Both of these techniques used surrogate models for the soft tissue mechanics. Surrogate models are computationally in-expensive when generated but need to be re-generated if model parameters are changed (e.g. articular geometry), thus limiting its flexibility. Therefore, a co-simulation framework needs to be developed that is 3D, does not use a surrogate model, and incorporates ligaments. Once developed, this co-simulation framework can be used to investigate how ligament injury leads to long-term complications.

In an ACL deficient (ACLd) knee, osteoarthritis typically develops 5 to 15 years later (Lohmander, et al., 2007) due to changes in cartilage contact locations that arise from abnormal kinematics (Chaudhari, et al., 2008). The tibia was shown to be more internally rotated in ACLd knees during walking (Andriacchi and Dyrby, 2005; Georgoulis, et al., 2003; Stergiou, et al., 2007). (Andriacchi, et al., 2006) has shown that an internal rotational offset of 5 degrees could increase cartilage volume loss by 44% compared to a non-rotated knee. Changes in cartilage loads are also thought to progress osteoarthritis (Andriacchi, et al., 2004). A co-simulation framework that predicts these changes in cartilage loading may be used to investigate the effectiveness of treatment strategies like neuromuscular training to restore normal function.

There were four goals of this dissertation:

1. To create a 3D knee model including cartilage contact, ligaments, and muscles acting across the tibiofemoral and patellofemoral joints (for use in a co-simulation framework)
2. To develop a co-simulation framework validated against *in vivo* measures of knee kinematics and knee extensor function measured with dynamic MRI
3. To quantify differences in predicted kinematics, knee extensor mechanics, and muscle forces predicting during gait using co-simulation and a kinematic knee assumption
4. To predict changes in cartilage loading patterns between an intact and an ACL-deficient knee

# Chapter 2: Background

## Knee Anatomy and Soft Tissue Function

The development of computational models requires an understanding of how the soft tissue structures of the knee restrain motion. There are four main ligaments (Figure 1): anterior cruciate ligament (ACL), posterior cruciate ligament (PCL), medial collateral ligament (MCL), and lateral collateral ligament (LCL).

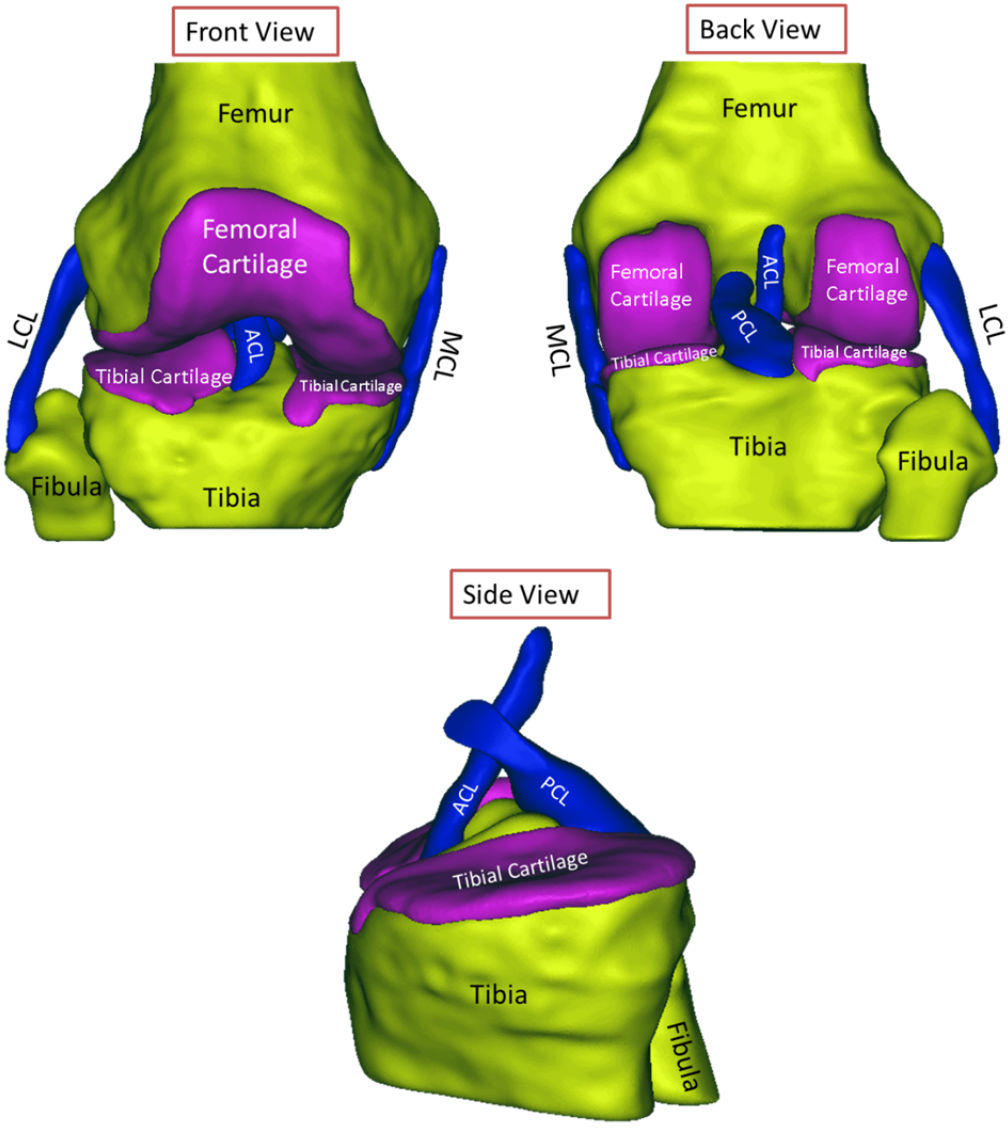


Figure 1: Anatomy of the knee without the patella and menisci.

The anterior cruciate ligament (ACL) and posterior cruciate ligament (PCL) primarily restrict anterior and posterior tibial translation, respectively; to a lesser extent, the cruciate ligaments also help control lateral and rotary motion (Bonnin, et al., 1996; Brantigan and Voshell, 1941; Butler, et al., 1980; Fu, et al., 1993; Fukubayashi, et al., 1982; Girgis, et al., 1975; Gollehon, et al., 1987; Grood, et al., 1981; Grood, et al., 1988; Haimes, et al., 1994; Hsieh and Walker, 1976; Kanamori, et al., 2000; Kersh, 2010; Levy, et al., 1982; Markolf, et al., 1976; Sakane, et al., 1999; Shoemaker and Markolf, 1985; Sullivan, et al., 1984).

The cruciates are composed of bundles that allow them to restrain anterior-posterior motion at all flexion angles (Figure 2). At extended knee angles, both ACL bundles resist anterior motion while the posteromedial (PM) bundle of the PCL resists posterior motion; at more flexed knee angles, the anteromedial (AM) bundle of the ACL resists anterior motion while the anterolateral (AL) bundle of the PCL resists posterior motion (Bowman Jr and Sekiya, 2010; Girgis, et al., 1975).

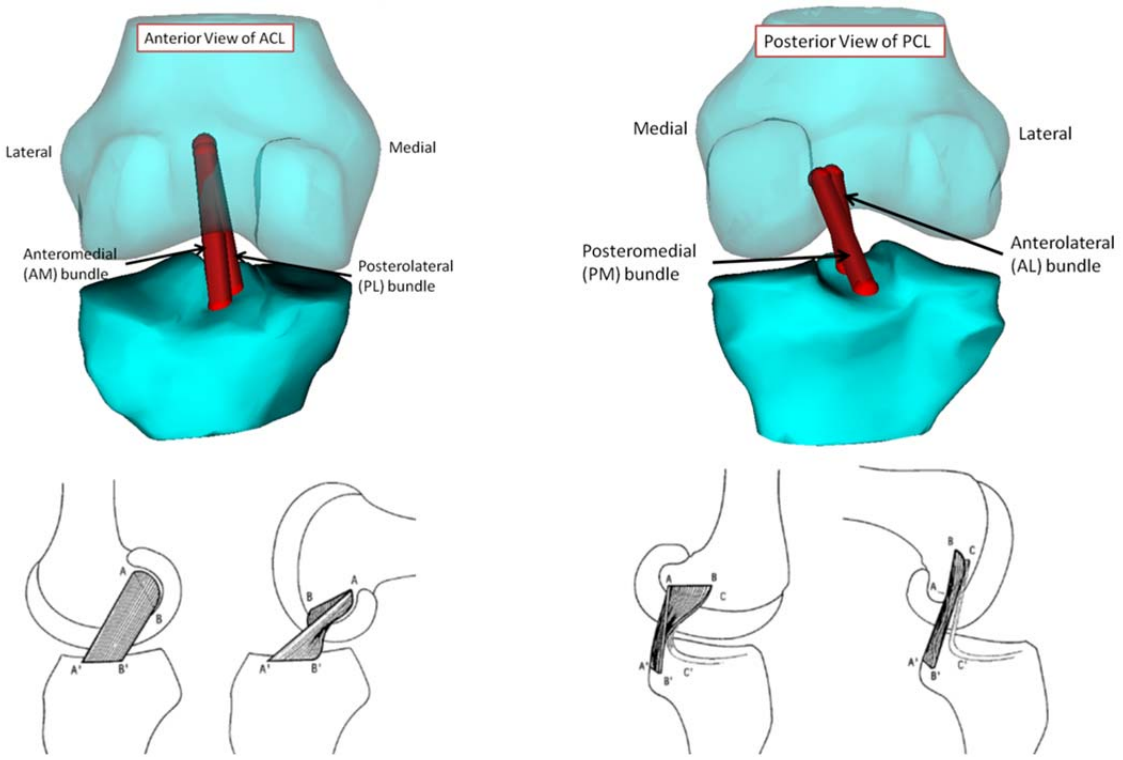


**Figure 2: (Top left) Anterior view of a right knee showing the two bundles of the ACL. (Bottom left) Both bundles are in tension at extension, but only the AM bundle is tight at more flexed angles. Picture from (Bowman Jr and Sekiya, 2010; Girgis, et al., 1975; Pandy and Sasaki, 1998). (Top right) Posterior view of a right knee showing the two bundles of the PCL. (Bottom right) The AL bundle is tighter than the PM bundle at more flexed angles. Picture from (Girgis, et al., 1975).**

The lateral collateral ligament (LCL) and medial collateral ligament (MCL) provide rotational and lateral stability. The LCL primarily restricts varus angulation (Fu, et al., 1993; Gollehon, et al., 1987; Grood, et al., 1988; Kersh, 2010; Seering, et al., 1980) along with lateral motion in extension and rotary motion in extension and slight flexion (Brantigan and Voshell, 1941; Grood, et al., 1981; Wang and Walker, 1974), more specifically external rotation (Gollehon, et al., 1987; Markolf, et al., 1976; Seering, et al., 1980) and possibly internal rotation as well (Kersh, 2010). The main function of the MCL is to restrain internal-external rotation and valgus angulation (Haimes, et al., 1994; Markolf, et al., 1976; Seering, et al., 1980; Shoemaker and Markolf, 1985), and secondarily to control lateral motion (Brantigan and Voshell, 1941; Grood, et al., 1981; Hsieh and Walker, 1976; Markolf, et al., 1976; Wang

and Walker, 1974). The collateral ligaments may also provide some slight anterior-posterior stabilization (Butler, et al., 1980; Haimes, et al., 1994; Markolf, et al., 1976; Shoemaker and Markolf, 1985).

The posterior capsule (Figure 3) helps control lateral and rotary motion (Brantigan and Voshell, 1941), more specifically external rotation (Haimes, et al., 1994; Markolf, et al., 1976) and possibly anterior-posterior translation (Bonnin, et al., 1996; Markolf, et al., 1976).

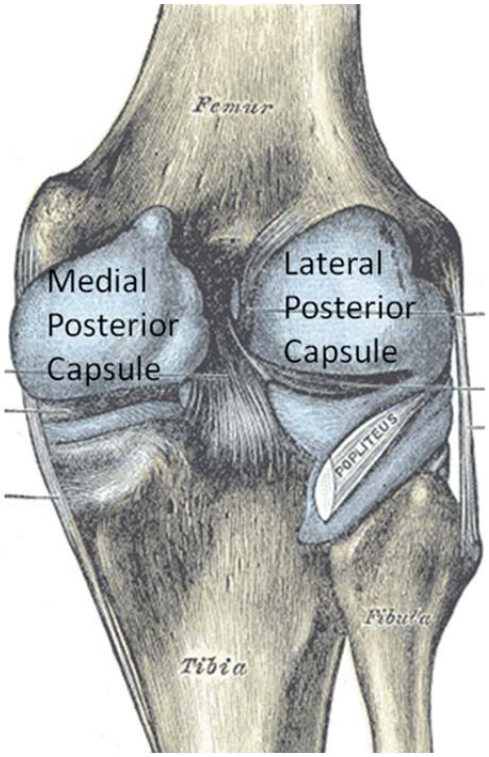


**Figure 3: Posterior view of the knee with posterior capsules shown in blue. Picture from (Gray, 1918).**

The principal functions of the menisci (Figure 4) are load transmission and shock absorption (Aagaard and Verdonk, 1999; Messner and Gao, 1998). Another important function is to fill any 'dead-space' between the femur and tibia to increase joint congruity (Allen and Caldwell, 1995; Simon, et al., 1973). This helps the menisci in their secondary function, to enhance stability of the knee in anterior-posterior translation, varus-valgus rotation, and internal-external rotation in the ACL deficient (ACL-d) (Thompson and Fu, 1993; Wang and Walker, 1974) and possibly the ACL intact knee (Kersh, 2010; Markolf, et al., 1981; Seale, et al., 1981). The medial meniscus limits anterior tibial translation in the

ACL-d knee (Allen, et al., 2000; Bargar, et al., 1980; Bonnin, et al., 1996; Levy, et al., 1982; Markolf, et al., 1984; Shoemaker and Markolf, 1986) whereas the lateral meniscus does not (Levy, et al., 1989). The lateral meniscus may act as a primary stabilizer in medial-lateral translation (Kersh, 2010). The menisci also help to cushion and prevent hyperextension and hyperflexion (Brantigan and Voshell, 1941).

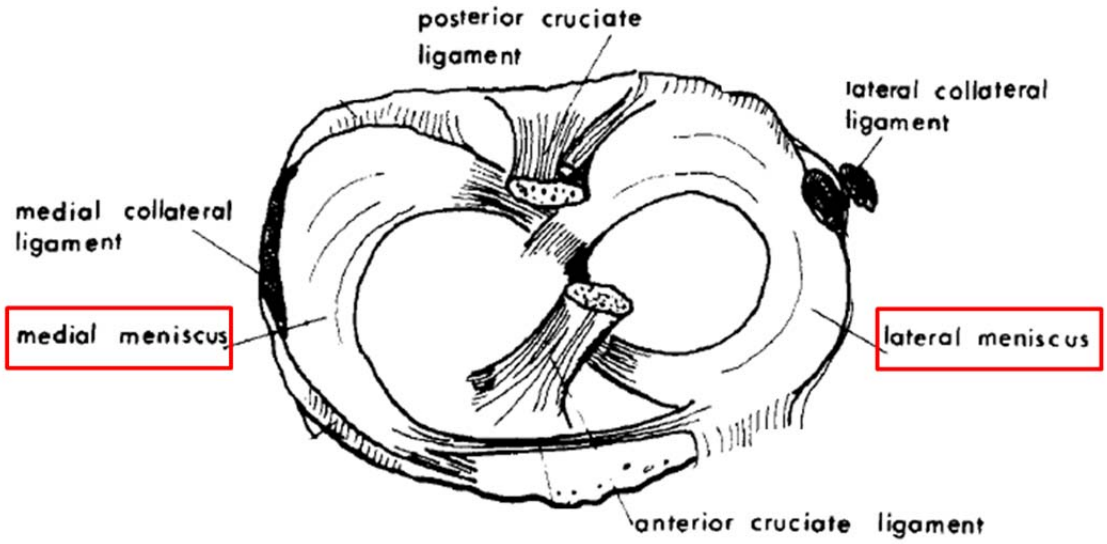


**Figure 4: Anatomy of the knee with the menisci highlighted. Picture from (Seedhom, 1979).**

Table 1 summarizes the primary restraints to knee motion.

**Table 1:** Summary of primary ligament restraining function

| Degree of Freedom | Primary Restraint |
|---|---|
| **Anterior Translation** | ACL (both bundles in extension and anteromedial bundle at more flexed knee angles) |
| **Posterior Translation** | PCL (posteromedial bundle at extension and anterolateral bundle at more flexed angles) |
| **Medial Translation** | - |
| **Lateral Translation** | LCL in extension<br>Posterior capsule |
| **Internal Rotation** | MCL |
| **External Rotation** | MCL<br>LCL in extension and slight flexion<br>Posterior capsule |
| **Varus Angulation** | LCL |
| **Valgus Angulation** | MCL |

# Movement simulations

Movement simulations can be used to predict immeasurable muscle forces, ligament loading, and cartilage contact during movement. Pandy provides a nice review of how computational modeling can be used with gait measures to study muscle and joint function in human locomotion (Pandy and Andriacchi, 2010). These simulations typically involve a forward dynamics simulation and a computational model. Only the forward dynamics simulation will be explained in more detail.

## Forward Dynamics Simulation

A forward dynamics simulation is typically used to answer 'what if' situations. For example, if the ACL is damaged and removed, how will the knee move? A forward dynamics simulation involves integrating a set of ordinary differential equations for muscle dynamics (activation dynamics and musculotendon dynamics) and equations of motion to compute simulated kinematics from muscle excitations (Figure 5). These muscle excitations can either be from electromyography measurements or calculated via a computed muscle control algorithm (Thelen and Anderson, 2006b).

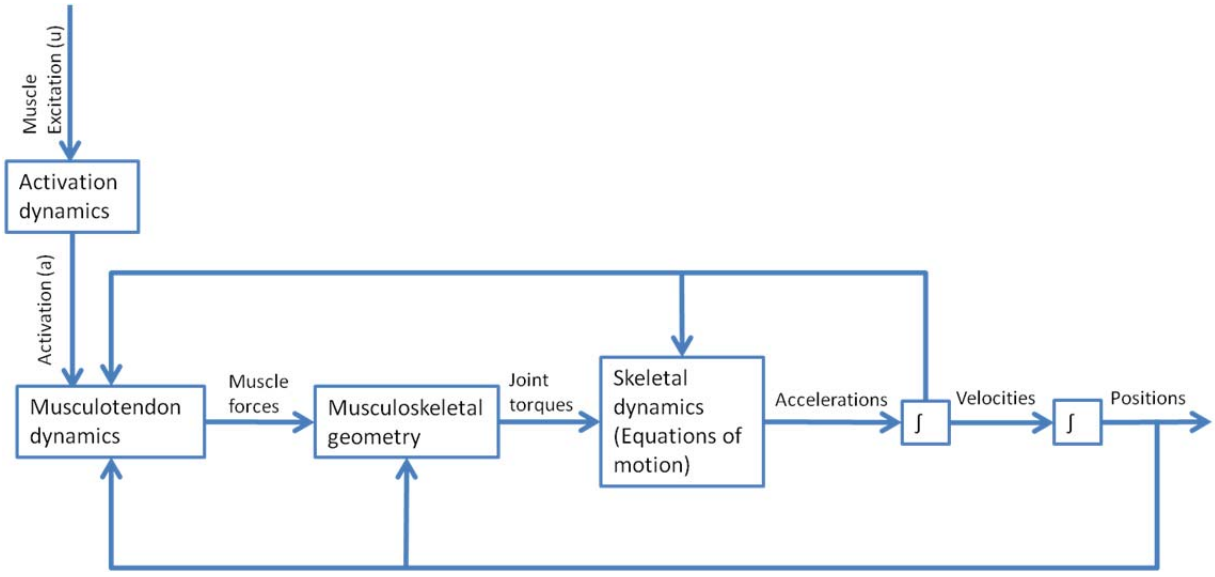


**Figure 5: A forward dynamic simulation integrates ordinary differential equations for muscle dynamics and the equations of motion to calculate kinematics from muscle excitations. Figure adapted from (Pandy, 2001).**

## Moment Arms

In the equations of motion for a system of bodies, muscle moment arms determine how much torque muscle forces produce about a joint. Therefore, moment arms are an important aspect of movement simulations. Only two techniques to calculate moment arms will be presented here: the tendon excursion method and the finite helical axis method. A comprehensive review of other techniques in the literature used to calculate muscle moment arms can be found in (Tsaopoulos, et al., 2006).

A common technique to calculate a muscle's moment arm is by the tendon excursion method. The work done in changing the length of a muscle is converted to potential energy in the ligament and kinetic energy of bone motion. The ligament is assumed inextensible in this method so the potential energy is ignored, leaving just the kinetic energy of the bones. Work is force (F) times a change in distance (dl) or torque (M) times a change in angle (dΘ). Therefore, this method can be expressed as the total work done to change the length of the muscle is converted to a six degree of freedom motion (3 translations and 3 rotations of the bone, denoted by subscripts 1,2, and 3) (Eq 1).

$$F(dl)=M_1 d\theta_1 + M_2 d\theta_2 + M_3 d\theta_3 + F_1 dx_1 + F_2 dx_2 + F_3 dx_3 \quad \text{Eq 1}$$

Torque divided by force is the moment arm. Therefore, the moment arm for each degree of freedom is given by Eq 2.

$$\text{moment arm}_n = \frac{dl}{d\theta_n} \quad \text{Eq 2}$$

To account for ligament stretch, other authors have used the finite helical axis (FHA) method where the moment arm is the shortest distance between the line of action of the muscle and the finite helical axis (Eq 3) (Krevolin, et al., 2004; Pandy, 1999; Sheehan, 2007a).

$$\text{moment arm} = \left| \vec{\mathbf{r}}^{OQ} \cdot \left( \hat{\mathbf{u}}^{M} \times \hat{\mathbf{u}}^{FHA} \right) \right| \quad \text{Eq 3}$$

In this equation, $\mathbf{r}^{OQ}$ is a position vector from any point O on the FHA to any point Q on the muscle's tendon line of action, $\mathbf{u}^{M}$ a unit vector along the muscle's line of action, and $\mathbf{u}^{FHA}$ a unit vector along the FHA.

# Chapter 3: Knee Model

## Introduction

Traditionally, cartilage loads are estimated using a serial approach (Kim, et al., 2009; Shelburne, et al., 2005b; Taylor, et al., 2004). A musculoskeletal model is first used to estimate muscle forces via optimization (Thelen, et al., 2003). Then, these muscle forces are applied to a computational joint model to estimate cartilage loading. However, the musculoskeletal model used to compute muscle forces typically represents the knee joint as a kinematic joint that behaves invariant of load, which others have suggested is not true (Dyrby and Andriacchi, 2004; Tsaopoulos, et al., 2007; Westphal, 2009).

Simultaneous prediction of musculoskeletal dynamics and soft tissue deformation has been used to couple a musculoskeletal model and finite element model of the foot (Halloran, et al., 2009) and knee implant (Lin, et al., 2010), thus circumventing the kinematic joint assumption. The large computational cost of solving a finite element model at every time step was avoided by development of a surrogate model. However, the initial generation of a surrogate model is costly and must be re-generated if a part of the detailed model is changed (e.g. articular geometry). Therefore the goal of this work was to construct a discrete element model of the tibiofemoral and patellofemoral joint that could be solved quickly within the context of whole body movement.

## Methods

### Articular Geometry

The articulating geometry of a right femur (bone and cartilage) was obtained from the MRI of a male subject 29 years old, 185 cm in height, and 113 kg (Bradford, 2011). This geometry was compared to data in the literature to ensure it was an average size femur (Figure 6).

(1)
**ACL1: 69**
Dargel: 69.3 ± 2.50 (male)
63.1 ± 3.82 (female)
Mensch: 67.9 +- 3.3 (male cadavers)
69.9 +- 2.6 (female cadavers)
70.3 +- 4.3 (male in vivo)
62.6 +- 2.3 (female in vivo)
Yoshioka: 72 +- 4.0 (males)
65 +- 3.7 (females)
Seedhom: 69.0 +- 3.2 (male cadavers)
65.0 +- 3.0 (female cadavers)
74.6 +- 4.5 (in vivo males)
67.8 +- 3.5 (in vivo females)

(2)
**ACL1: 32**
Dargel: 30.6 ± 1.25 (male)
26.0 ± 0.85 (female)
Mensch: 31.4 +- 2.6 (male cadavers)
26.6 +- 1.5 (female cadavers)
31.4 +- 2.3 (male in vivo)
26.5 +- 6.0 (female in vivo)
Rostlund: 26 – 37
Seedhom: 29.5 +- 1.7 (male cadavers)
28.2 +- 1.3 (female cadavers)
32.4 +- 2.2 (in vivo males)
27.1 +- 1.5 (in vivo females)

(3)
**ACL1: 29**
Dargel: 32.3 ± 4.22 (male)
28.4 ± 2.40 (female)
Mensch: 29.9 +- 2.6 (male cadavers)
24.5 +- 1.5 (female cadavers)
29.2 +- 2.2(male in vivo)
24.5 +- 1.2(female in vivo)
Rostlund: 23 – 34
Seedhom: 28.4 +- 1.8 (male cadavers)
13.2 +- 1.6 (female cadavers)
31.3 +- 1.7 (in vivo males)
27.1 +- 1.5 (in vivo females)

(5)
**ACL1: 18**
Dargel: 19.3 ± 1.99 (male)
19.0 ± 2.74 (female)
Mensch: 20.8 +- 3.6 (male cadavers)
18.7 +- 2.5 (female cadavers)
22.6 +- 6.0 (male in vivo)
18.9 +- 1.5 (female in vivo)
Yoshioka: 13 +- 3.1 (males)
11 +- 4.0 (females)
Seedhom: 21.8 +- 2.3 (male cadavers)
17.7 +- 2.4 (female cadavers)
21.7 +- 3.0 (in vivo males)
20.8 +- 2.5 (in vivo females)

(6)
**ACL1: 35**
Dargel: 32.5 ± 2.63 (male)
30.3 ± 2.46 (female)

(7)
**ACL1: 80**
Dargel: 80.9 ± 3.53 (male)
71.5 ± 3.95 (female)
Mensch: 81.1 +- 3.4 (male cadavers)
69.7 +- 2.7 (female cadavers)
82.1 +- 4.7 (male in vivo)
69.9 +- 2.6 (female in vivo)
Yoshioka: 83 +- 3.9 (males)
72 +- 4.7 (females)
Seedhom: 80.0 +- 4.8 (cadaver males)
74.0 +- 4.0 (cadaver females)
86.0 +- 5.3 (in vivo males)
75.0 +- 3.8 (in vivo females)

(9)
**ACL1: 38**
Dargel: 39.2 ± 3.85 (male)
37.0 ± 4.16 (female)
Yoshioka: 38 +- 2.4 (males)
32 +- 2.5 (females)

(12)
**ACL1: 86**
Griffin: 84.1 +- 4.4 (males)
74.1 +- 4.6 (females)

(12) Along transepicondylar axis rather than projected onto an axial plane
**ACL1: 89**
Yoshioka: 90 +- 6.1 (males)
80 +- 6.1 (females)

(13)
**ACL1: 87**
Rostlund: 75 – 95

(14)
**ACL1: 70**
Yoshioka: 70 +- 4.3 (male)
63 +- 4.5 (female)

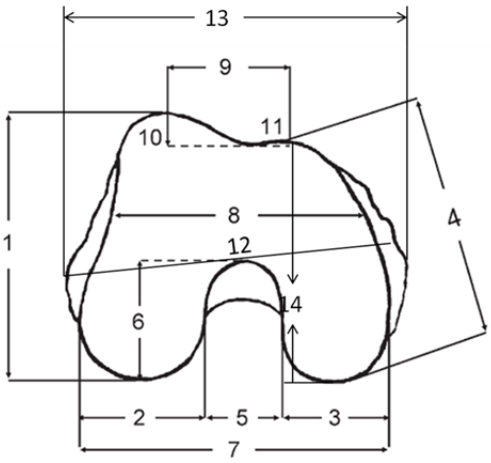


**Figure 6: Comparison of subject (denoted as ACL1) with femur geometry measurements from the literature (Dargel, et al., 2010; Griffin, et al., 2000; Mensch and Amstutz, 1975; Röstlund, et al., 1989; Seedhom, et al., 1972; Yoshioka, et al., 1987). All measurements are in mm.**

The tibial plateaus were modeled as two planes with the slopes based on geometric descriptions of 23 cadaver knees (Garg and Walker, 1990). The lateral plateau sloped 7 degrees posteriorly and 2 degrees laterally while the medial plateau sloped 2 degrees posteriorly and medially (Kim, 1996; Pandy, et al., 1997). These planes were positioned so at full extension, the tibia was abducted 0.0 deg and tibial origin was 0.404 m inferior to the femoral origin (Arnold, et al., 2010).

## Tibiofemoral Joint

### Generalized Coordinates

The body fixed coordinate systems for the femur and tibia are displayed in Figure 7. The origin of the femur coordinate system was placed at the center of the femoral head with the x-axis pointing anteriorly, the y-axis superiorly, and the z-axis to the right (laterally for the right knee) (Arnold, et al., 2000; Delp, 1990). The y-axis was placed along a line connecting the femoral head and the center of the femoral condyles. The tibial coordinate system was located at the midpoint of the femoral condyles with the knee in full extension. Consistent with the femur coordinate system, the axes were oriented with the x-axis pointing anteriorly, the y-axis superiorly, and the z-axis to the right (laterally for the right knee) (Arnold, et al., 2000; Delp, 1990).


Figure 7: The body fixed coordinate systems of the femur and tibia for the right knee.

The tibiofemoral joint consisted of six generalized coordinates: three translations followed by three rotations about the x, y, and z-axes. These translations were defined as the location of the tibia origin with respect to the femur origin, expressed in the femur coordinate system. Rotation angles between the bones were calculated using a body fixed 3-1-2 rotation of the tibia with respect to the femur. Rotation about the +z-axis was termed extension, +x as adduction, and +y as internal rotation. With the knee in full extension, both coordinate systems were aligned (all rotation angles 0.0) with the tibia displaced -0.404 m in the y direction and -0.001 m in the z direction (Arnold, et al., 2010).

## Contact

Contact forces between the bones were calculated and applied using two steps: collision detection and force calculation. For collision detection, the femur including the articular cartilage was discretized into 6096 triangles (Figure 8).

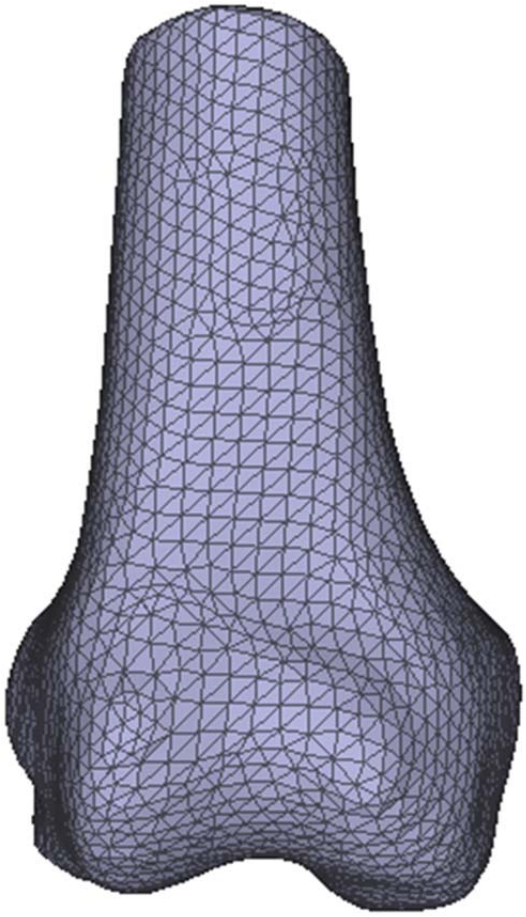

Figure 8: Discretized geometry of the femur, including the articular cartilage.

At each point in time, the position of each triangle centroid with respect to the corresponding tibial plane origin (medial or lateral) was calculated. Using this position vector, along with the normal vector to the tibial plane, the penetration depth of each triangle was computed. If the center penetration depth was greater than or equal to zero, contact was present and a contact force calculated for this triangle-plane interface using a linear elastic foundation model (Eq 4) as used by (Anderson, et al., 2010c; Blankevoort and Huiskes, 1991; Blankevoort, et al., 1991b; Caruntu and Hefzy, 2004; Kim, 1996; Pandy, et al., 1997; Shelburne, et al., 2004). Cartilage was modeled as an elastic layer resting on a rigid foundation of bone. Other assumptions included deformation of this elastic layer to be normal to the foundation (medial/lateral expansion of the cartilage is neglected); area of contact to be large

compared to the cartilage layer thickness; and the normal displacements of the cartilage to be small during loading. Cartilage parameters used were modulus of 5 MPa, Poisson's ratio of 0.45, no damping, and a uniform thickness of 3 mm for each bone (Blankevoort and Huiskes, 1991; Blankevoort, et al., 1991b; Caruntu and Hefzy, 2004; Kim, 1996; Li, et al., 2005; Pandy, et al., 1997; Shelburne, et al., 2004).

$$F = A\frac{E\,(1-\nu)}{(1+\nu)(1-2\nu)}\frac{d}{h} \qquad \text{Eq 4}$$

In this equation, F = force between contacting objects, A = area of contact (used the area of the contacting triangle), E = elastic modulus of cartilage, $\nu$ = Poisson's ratio of cartilage, d = penetration depth, and h = combined thickness of femur and tibia cartilage.

## Patellofemoral Joint

### Generalized Coordinates

The body fixed coordinate system for the patella was placed at the proximal pole of the patella with the x-axis pointing anteriorly, the y-axis superiorly, and the z-axis to the right (laterally for the right knee) (Figure 9) (Arnold, et al., 2000; Delp, 1990).


Figure 9: The body fixed coordinate systems of the femur and patella for the right knee.

The patellofemoral joint consisted of one degree of freedom, translation of the patella along the y-axis of the femur, with translation along the x-axis and rotation about the z-axis prescribed as functions of this degree of freedom (Figure 10). These translations were defined as the location of the patella origin with respect to the femur origin, expressed in the femur coordinate system. With the knee in full extension, both coordinate systems were aligned with the patella displaced -0.366 m along the y-axis (Arnold, et al., 2010). There was no contact model between the patella and femur.

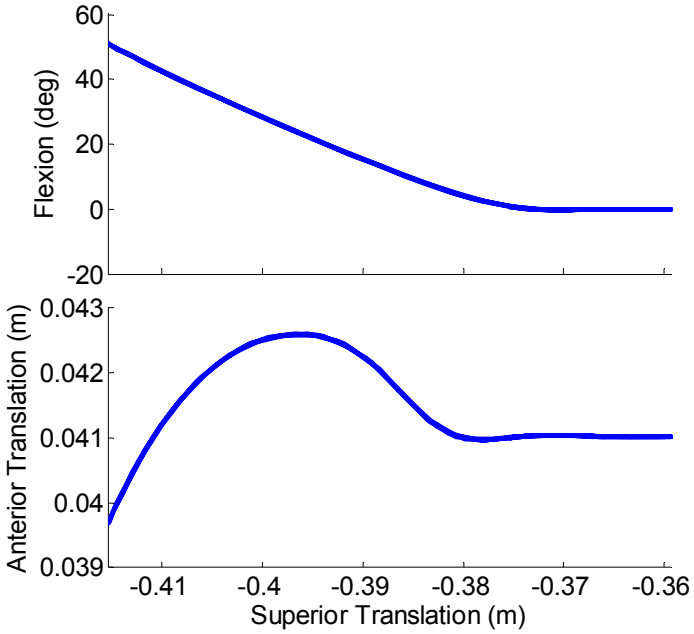


**Figure 10: The anterior-posterior translation and flexion-extension angle of the patella were prescribed functions of superior-inferior translation.**

## Ligaments

The model consisted of 19 ligament bundles (Figure 11). To approximate the path from origin to insertion, ligament geometries were represented as line segments. The origin and insertions of the ACL and PCL bundles were placed using anatomical landmarks (Edwards, et al., 2007; Girgis, et al., 1975; Gray, 1918; Kopf, et al., 2009; Petersen and Zantop, 2007) as well as the PFL and LCL (Davies, et al., 2004; Meister, et al., 2000). The MCL bundles were positioned using data by (Shelburne, et al., 2006).

The posterior capsule bundles were located according to (Abdel-Rahman and Hefzy, 1998). The patellar tendon was positioned according to (Arnold, et al., 2010).

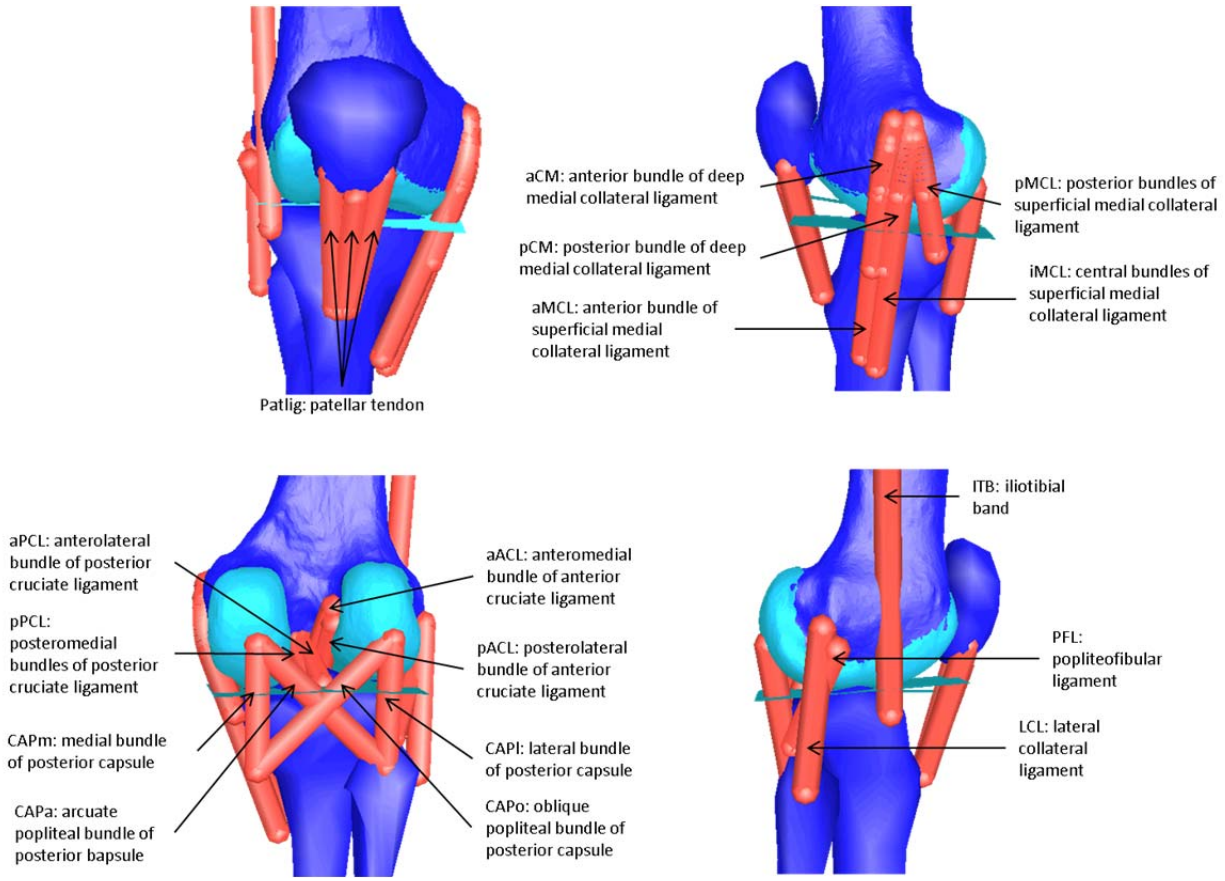


**Figure 11: Nineteen ligament bundles were included in the model.**

Table 2 displays the attachment points of the ligaments.

Table 2: Coordinates of ligament attachments in local segment frames.

| Ligament | Tibial Attachment (m) | Femoral/Patellar Attachment (m) |
|---|---|---|
| aACL | (0.0029, -0.0215, 0.0003) | (-0.018, -0.399, 0.0062) |
| pACL | (0.0023, -0.0216, 0.0034) | (-0.0179, -0.4051, 0.0063) |
| aPCL | (-0.0215, -0.0241, 0.0018) | (-0.0017, -0.4113, -0.0046) |
| pPCL | (-0.0214, -0.0303, 0.0015) | (-0.0035, -0.4116, -0.008) |
| aMCL | (0.01042, -0.08125, -0.01078) | (0.00129, -0.38946, -0.04106) |
| iMCL | (0.00466, -0.0858, -0.01287) | (-0.00546, -0.38937, -0.04157) |
| pMCL | (-0.01721, -0.03464, -0.03148) | (-0.00546, -0.38937, -0.04157) |
| aCM | (0.00756, -0.0419, -0.02847) | (0.00129, -0.38946, -0.04157) |
| pCM | (0.00261, -0.0419, -0.02847) | (-0.00546, -0.38937, -0.04157) |
| LCL | (-0.01999, -0.0601, 0.04066) | (-0.01568, -0.405, 0.04274) |
| PFL | (-0.02509, -0.045, 0.02916) | (-0.0106, -0.4123, 0.0439) |
| CAPa | (-0.025, -0.05627, 0.02627) | (-0.0322, -0.4134, -0.0248) |
| CAPl | (-0.025, -0.05627, 0.02627) | (-0.0355, -0.4118, 0.0253) |
| CAPo | (-0.025, -0.05627, -0.02373) | (-0.0355, -0.4118, 0.0253) |
| CAPm | (-0.025, -0.05627, -0.02373) | (-0.0322, -0.4134, -0.0248) |
| patlig | (0.0282, -0.0579, 0.0057) | (0.0021, 0.0015, 0.0001) |
| Med_patlig | (0.0287, -0.0587, -0.0019) | (0.0022, 0.0053, -0.0084) |
| Lat_patlig | (0.0282, -0.0579, 0.0084) | (0.0022, 0.0053, 0.0103) |

To avoid penetration of the femur with the PFL and MCL, wrapping surfaces were included (Figure 12 and Table 3).

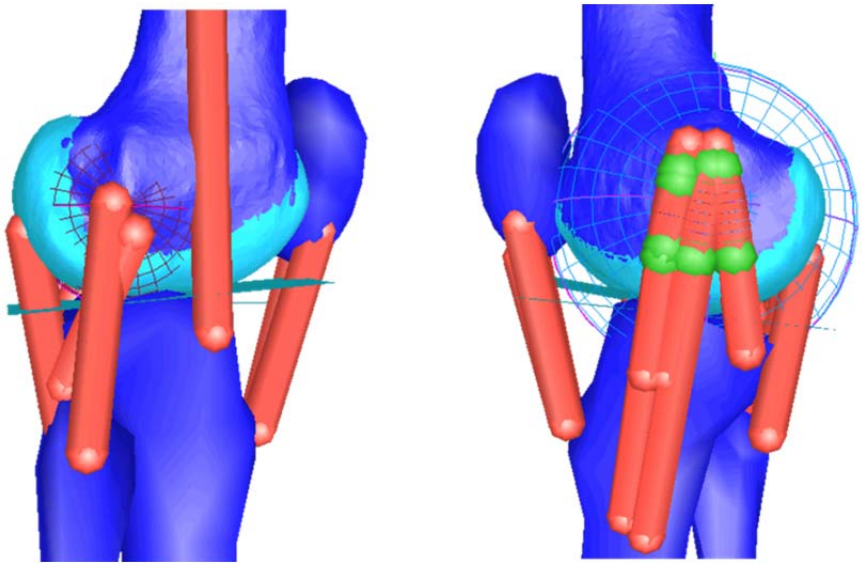

Figure 12: The PFL and MCL wrapped about the femur.

Table 3: Wrapping object parameters

| Wrapping Object | Geometry | Location in Femur |
|---|---|---|
| PFL and femur | Sphere with radius 0.024 m | (-0.0123, -0.4056, 0.020) |
| MCL and femur | Sphere with radius 0.044 m | (-0.0066, -0.4025, 0.0003) |

Ligaments were modeled as nonlinear elastic springs (Figure 13 and Eq 5 through Eq 7) with linear damping (Blankevoort and Huiskes, 1991; Blankevoort, et al., 1991b; Shelburne, et al., 2011; Shelburne, et al., 2006; Wismans, et al., 1980).

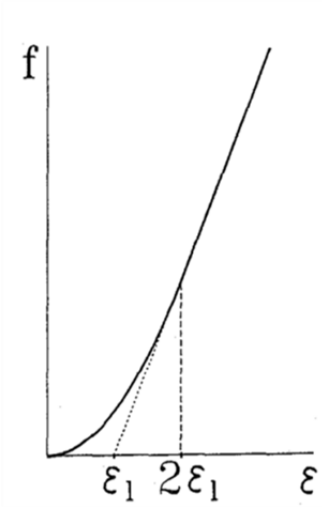


Figure 13: Figure from (Blankevoort and Huiskes, 1991). Ligaments were modeled with a nonlinear force (f) – strain (ε) curve. $\varepsilon_l$ is the transition strain, ε the current ligament strain calculated from zero-load length and current length, and f the force.

$$f = \frac{1}{4}\frac{k\varepsilon^2}{\varepsilon_l} + c\dot{l} \qquad 0 \le \varepsilon \le 2\varepsilon_l \qquad \text{Eq 5}$$

$$f = k(\varepsilon - \varepsilon_l) + c\dot{l} \qquad \varepsilon > 2\varepsilon_l \qquad \text{Eq 6}$$

$$f = 0 \qquad \varepsilon < 0 \qquad \text{Eq 7}$$

In these equations, $\varepsilon_l$ is the transition strain, ε the current ligament strain calculated from zero-load length and current length, k the ligament stiffness, c the damping coefficient, $\dot{l}$ the rate of change of the ligament length, and f the force in the ligament. The damping coefficient was set at 10.0 Ns/m for all ligaments. The transition strain at which the force-strain behavior transitioned from nonlinear to linear behavior was set at 0.03 (Blankevoort and Huiskes, 1991; Butler, et al., 1986). Properties of ligaments

such as reference strain (strain in the ligament at full extension) and stiffness were adapted from (LaPrade, et al., 2005; Shelburne, et al., 2004; Shin, et al., 2007). The model values for the ligament properties and how they compare to the literature are shown in Table 4. A literature review of *ex vivo* and *in silico* ligament properties can be found in Appendix A. Since the ligament model required the current ligament strain to calculate force, the reference strain for each ligament was used to set the zero-load length (slack length) of the ligament (Blankevoort and Huiskes, 1991). At the beginning of each simulation, the model was put into a reference configuration and the length of each ligament retrieved (reference length). Then the user specified reference strains were used in conjunction with the reference length to calculate the required slack lengths.

**Table 4: Comparison of Model Ligament Parameters with Literature**

| Ligament | Model Stiffness (N/strain) | Literature Range (from tensile testing of tissue) | Literature Range (from other musculoskeletal models) | Model Reference Strain (-) | Literature Range (from other musculoskeletal models) | Model Slack Length (mm) | Literature Range (mm) from *ex vivo* or *in vivo* data | Model Reference Length (mm) | Literature Range (mm) from *ex vivo* or *in vivo* data |
|---|---|---|---|---|---|---|---|---|---|
| **aACL** | 4000 | Total stiffness 1100 to 9300 | 1000 to 5000 | 0.02 | 0 to 0.093 | 34 | 22.15 to 36.5 | 35 | 32.5 +- 2.8 |
| **pACL** | 4000 | | 1500 to 5000 | 0.02 | 0.01 to 0.10 | 29 | | 29 | 27.6 +- 5.2 |
| **aPCL** | 4000 | Total stiffness 1000 to 12200 | 2600 to 9000 | -0.12 | -0.39 to 0.004 | 30 | 29.5 to 32 | 27 | 25 to 31 |
| **pPCL** | 1600 | | 1580 to 9000 | -0.05 | -0.12 to 0.05 | 32 | | 30 | 32 to 46 |
| **aMCL** | 2000 | Total stiffness 6200 to 7100 | Total stiffness 5160 to 14500 | 0.02 | -0.274 to 0.10 | 100 | - | 102 | 21 to 112 |
| **iMCL** | 2000 | | | 0.02 | | 104 | | 106 | |
| **pMCL** | 4000 | | | 0.05 | | 50 | | 53 | |
| **aCM** | 2000 | | | 0.02 | | 58 | | 59 | |
| **pCM** | 2000 | | | 0.05 | | 57 | | 60 | |
| **LCL** | 3000 | 1300 to 3400 | 2000 to 8000 | 0.05 | -0.25 to 0.1 | 57 | 48.7 to 50.9 | 60 | 51.5 to 74 |
| **PFL** | 2000 | 1900 | - | -0.05 | - | 45 | - | 43 | 42.6 +- 7.3 |
| **CAPa** | 1500 | - | Total stiffness 2000 to 8100 | 0.05 | -0.18 to 0.1 | 66 | - | 69 | - |
| **CAPl** | 2000 | | | 0.05 | | 48 | | 50 | |
| **CAPo** | 1500 | | | 0.05 | | 68 | | 71 | |
| **CAPm** | 2000 | | | 0.05 | | 46 | | 48 | |
| **ITB** | 5000 | 4800 to 8700 | - | 0.00 | - | 571 | 490 to 540 | 571 | - |
| **PT** | 6000 | Total stiffness 13000 to 28000 | inextensible | 0.00 | inextensible | 48 | 41.5 to 57.8 | 48 | 45 to 52 |
| **Medial PT** | 6000 | | | 0.00 | | 52 | | 52 | |
| **Lateral PT** | 6000 | | | 0.00 | | 51 | | 51 | |

## Muscles

The vastii muscles were included when using the model to simulate passive flexion-extension and stiffness behavior. Inclusion of these is consistent with experimental cadaveric studies which kept the extensor mechanism intact when assessing stiffness and passive behavior (Figure 14). The geometry and wrapping were the same as those used by (Arnold, et al., 2010) with properties shown in Table 5 using a Hill-type model to characterize the passive force characteristics of the vastii (Zajac, 1989).

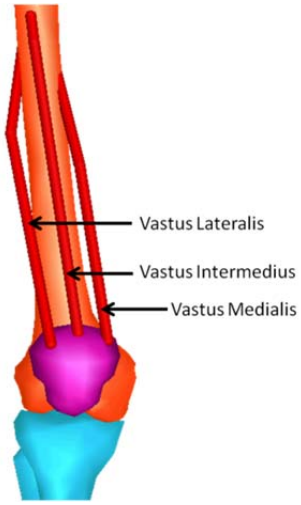


Figure 14: The vastii muscles were included to keep the knee extensor mechanism intact.

Table 5: Properties of vastii muscles

| Muscle | Optimal Fiber Length (cm) | Pennation Angle (deg) | Maximum Strength (N) | Tendon Slack Length (cm) |
|---|---|---|---|---|
| **Vastus intermedius** | 9.92 | 4.54 | 1024.2 | 10.6 |
| **Vastus Lateralis** | 9.94 | 18.38 | 2255.4 | 13.0 |
| **Vastus Medialis** | 9.68 | 29.61 | 1443.7 | 11.2 |

## Dynamics

The knee model was created using the SIMM Dynamics Pipeline (MusculoGraphics, Evanston, IL, USA), which uses SD/Fast (Symbolic Dynamics, Mountainview CA, USA) to generate all equations of motion. The mass properties and overall bone dimensions were consistent with those of a 75 kg male (de Leva, 1996b; Delp, 1990).

## Model Verification

The following loading conditions and constraints were applied to assess the capacity of the knee model to emulate behavior measured in cadaveric knees:

- passive flexion/extension of the tibia (0 to 70 deg flexion)
- axial rotation torque (5 Nm)
- anterior/posterior force (100 N)
- varus/valgus torque (10 Nm)

To simulate the experimental setups, gravity was neglected and the ITB ligament removed for all of the following verification tests.

### Passive Flexion/Extension Test

The model was used to simulate passive flexion/extension as measured experimentally by (Markolf, et al., 1976; Wilson, et al., 2000). In this simulation, the knee was fixed at full extension with all other tibiofemoral degrees of freedom unconstrained and allowed to come to an equilibrium position; then tibiofemoral flexion/extension was prescribed (Figure 15) with the other tibiofemoral degrees of freedom still unconstrained. The knee was only flexed up to 70 degrees since this is the maximum flexion angle the knee reaches in gait (Lafortune, et al., 1992). The movement of the most posterior tibial attachment point of the ACL from the equilibrium position was analyzed and compared with (Wilson, et al., 2000).

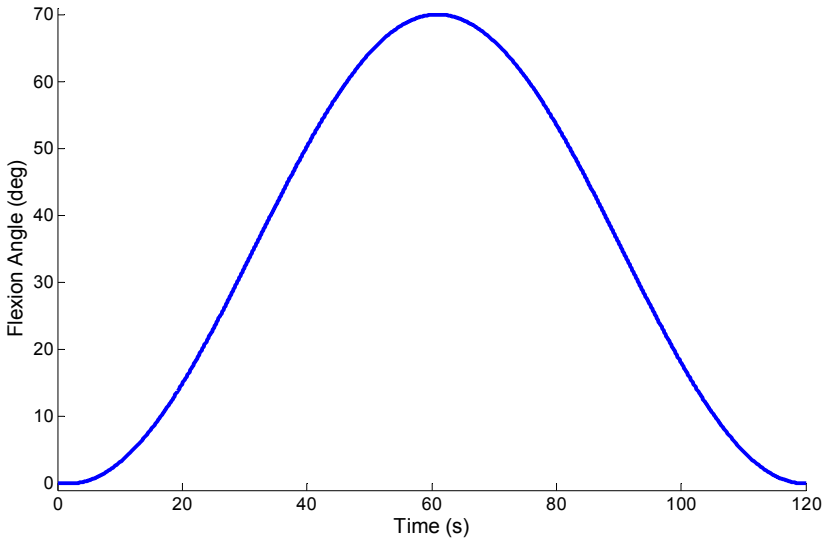


Figure 15: Flexion angle prescribed in the passive flexion/extension test.

## Axial Rotation Stiffness Test

A 5 Nm internal and external rotational torque were applied to the tibia (Figure 16) and the resulting axial rotation measured and compared with the literature (Anderson, et al., 2010b; Coobs, et al., 2007; Coobs, et al., 2010; Griffith, et al., 2009; Markolf, et al., 1981; Markolf, et al., 1976; Shoemaker and Markolf, 1985; Tsai, et al., 2010). For the entire test, the tibiofemoral flexion angle was fixed and all other degrees of freedom unconstrained. Flexion angles of 0, 15, 20, 30, 40, 45, and 60 were considered. First, the model settled at an equilibrium position. Then, a 5 Nm axial torque was applied to the tibia. However, to be consistent with the experimental setups in the literature, the direction of the torque was defined with respect to the fixed femur frame (Figure 17) so the applied torque would not change direction as the tibia moved. Finally, the axial rotation of the tibia with respect to the neutral configuration was measured and compared to the literature. The neutral configuration was defined as the inflection point of the applied torque versus rotation curve, where zero axial torque was applied.

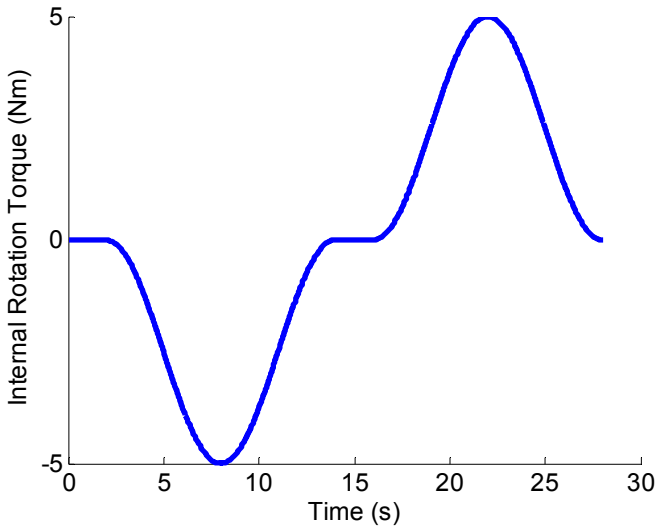


Figure 16: Magnitude of axial rotation torque applied to the tibia in full extension.

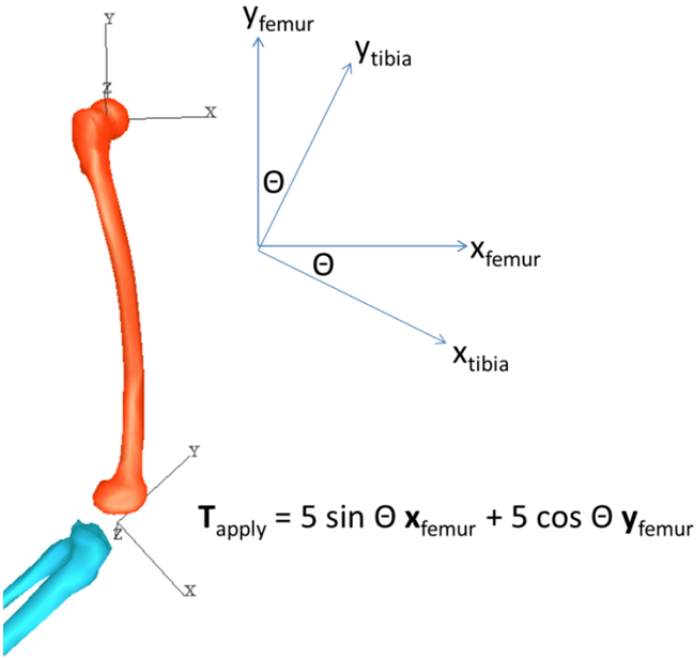


Figure 17: An axial torque of 5 Nm was applied to the tibia. This torque, $T_{apply}$, was defined in the femur frame by the equation shown where Θ is the tibiofemoral flexion angle. A -5 was used in the equation to apply an external rotation torque.

## Anterior/ Posterior Stiffness Test

The tibia was subjected to a 100 N anterior and posterior force (Figure 18) with the resulting translation and coupled axial rotation measured and compared with the literature (Gollehon, et al.,

1987; Levy, et al., 1989; Markolf, et al., 1981; Markolf, et al., 1976; Shoemaker and Markolf, 1985; Sullivan, et al., 1984). Throughout the simulation, the tibia was fixed at a prescribed tibiofemoral flexion angle. Flexion angles of 0, 15, 30, 45, 60, and 75 were considered. After the model settled at an equilibrium position, an anterior and posterior force was applied to the tibia. Similar to the axial rotation test, the direction of the force was defined with respect to the fixed femur frame (Figure 19) so the applied force would not change direction as the tibia moved. The medial/lateral position of the point force application (Figure 19) was applied to match the coupled internal rotation seen in the literature when an anterior force is applied. The coupled axial rotation and anterior/posterior translation of the tibia with respect to the neutral configuration were measured and compared to the literature. This translation was the movement of the point of force application (Figure 20). The neutral configuration was defined as the inflection point of the applied force versus translation curve, where zero force was applied.

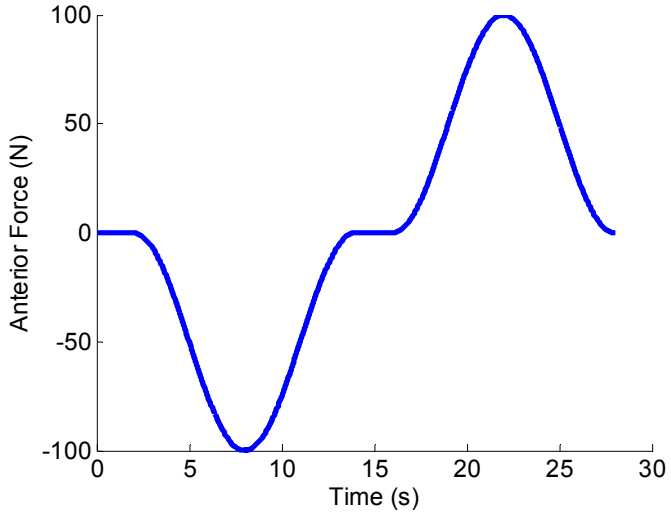


**Figure 18: Magnitude of anterior/posterior force applied to the tibia in full extension.**

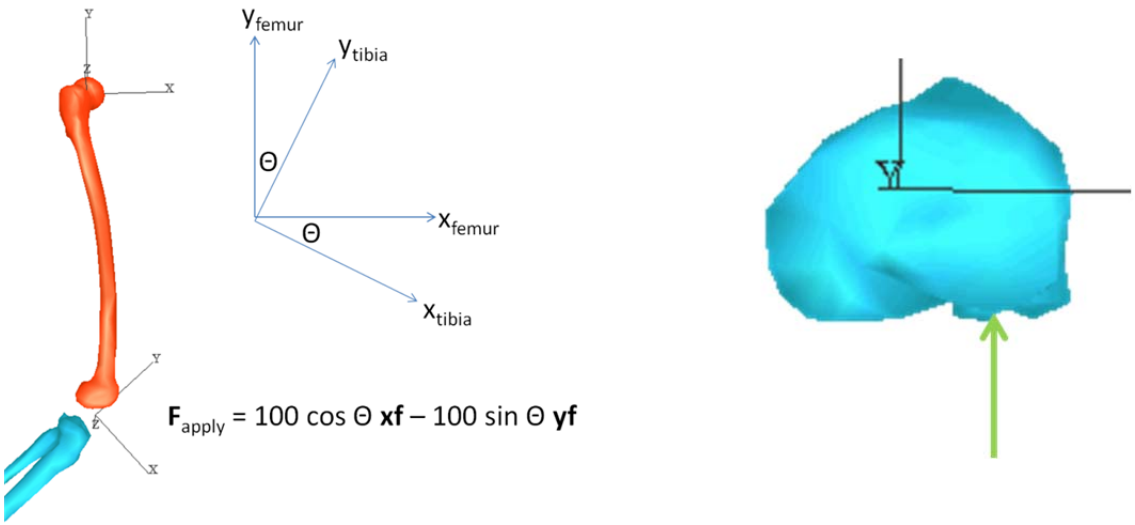


**Figure 19: An anterior/posterior force of 100 Nm was applied to the tibia. (left) This force, $F_{apply}$, was defined in the femur frame by the equation shown where Θ is the tibiofemoral flexion angle. A -100 was used in the equation to apply a posterior force. (right) The point of force application was positioned to match the coupled internal rotation seen in the literature that accompanies anterior translation.**

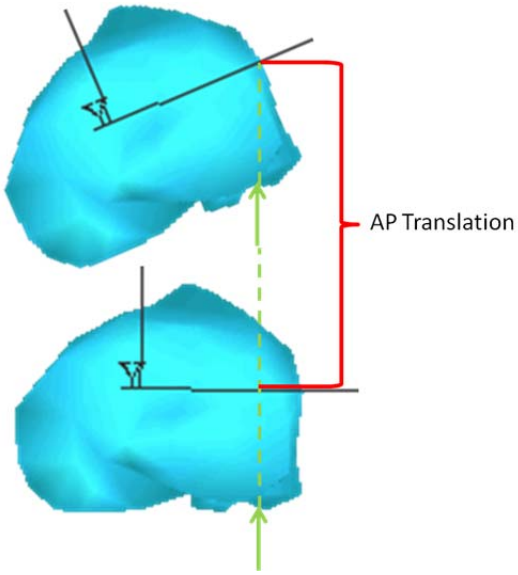


**Figure 20: The anterior/posterior translation of the tibia was measured at the point of force application.**

## Varus/Valgus Stiffness Test

A 10 Nm varus and valgus torque were applied to the tibia (Figure 21) and the resulting rotation measured and compared with the literature (Anderson, et al., 2010a; Coobs, et al., 2007; Gollehon, et

al., 1987; Griffith, et al., 2009; Markolf, et al., 1981; Markolf, et al., 1976; Tsai, et al., 2010). For the entire test, the tibiofemoral flexion angle was fixed and all other degrees of freedom unconstrained. Flexion angles of 0, 15, 20, 30, 40, 45, 60, and 75 were considered. First, the model settled at an equilibrium position. Then, a varus/valgus torque was applied to the tibia. However, to be consistent with the experimental setups in the literature, the direction of the torque was defined with respect to the fixed femur frame (Figure 22) so the applied torque would not change direction as the tibia moved. Finally, the rotation of the tibia with respect to the neutral configuration was measured and compared to the literature. The neutral configuration was defined as the inflection point of the applied torque versus rotation curve, where zero varus/valgus torque was applied.

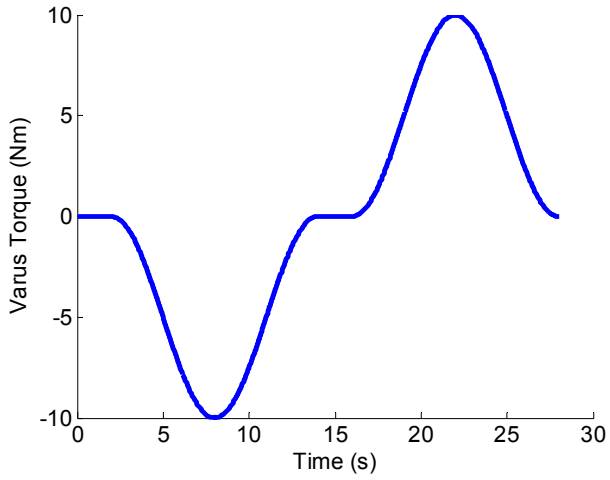


**Figure 21: Magnitude of varus/valgus torque applied to tibia in full extension.**

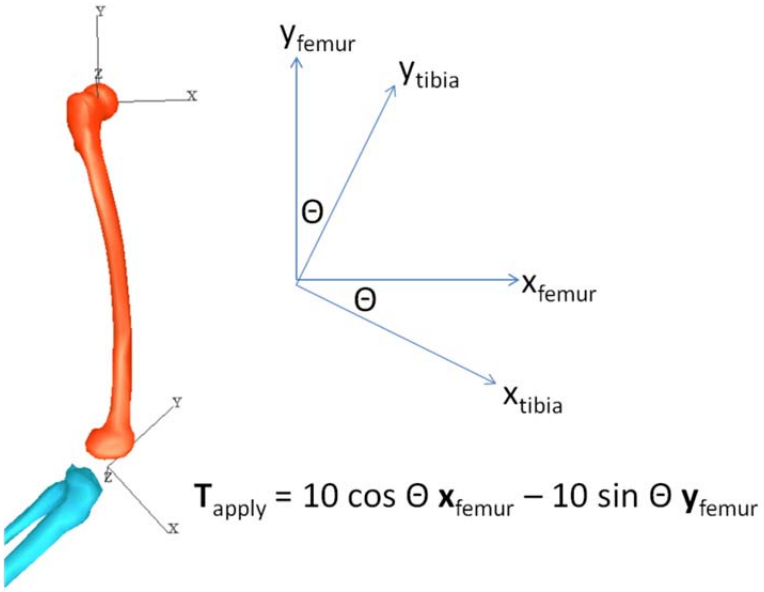


Figure 22: A varus/valgus torque of 10 Nm was applied to the tibia. This torque, $T_{apply}$, was defined in the femur frame by the equation shown where Θ is the tibiofemoral flexion angle.

## Ligament Function

The force and torque each ligament exerted on the tibia was calculated during the stiffness tests to assess ligament function (Figure 23). For example, when an anterior-posterior force was applied, the anterior-posterior component of each ligament force on the tibia was calculated.

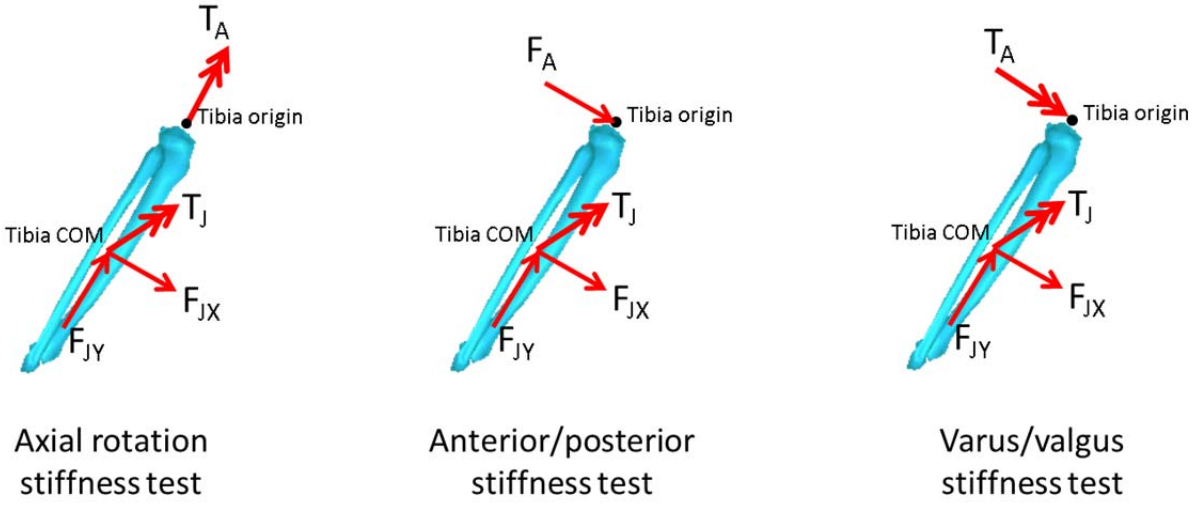


Figure 23: Free body diagrams of the tibia for each of the stiffness tests. $T_A$ and $F_A$ are the applied torque and force, respectively. $T_J$ and $F_J$ are the torque and force of the ligaments and femur acting on the tibia.

# Results

## Passive Flexion/Extension Test

The passive motion of the model is consistent with that seen *ex vivo* (Figure 24). However, the model does show greater hysteresis in axial rotation than seen experimentally. The maximum ligament strain reached by any ligament was 12% in the posterior bundle of the PCL. This is slightly greater than the 10% strain limit other models have used (Amiri, et al., 2007; Blankevoort, et al., 1991a).

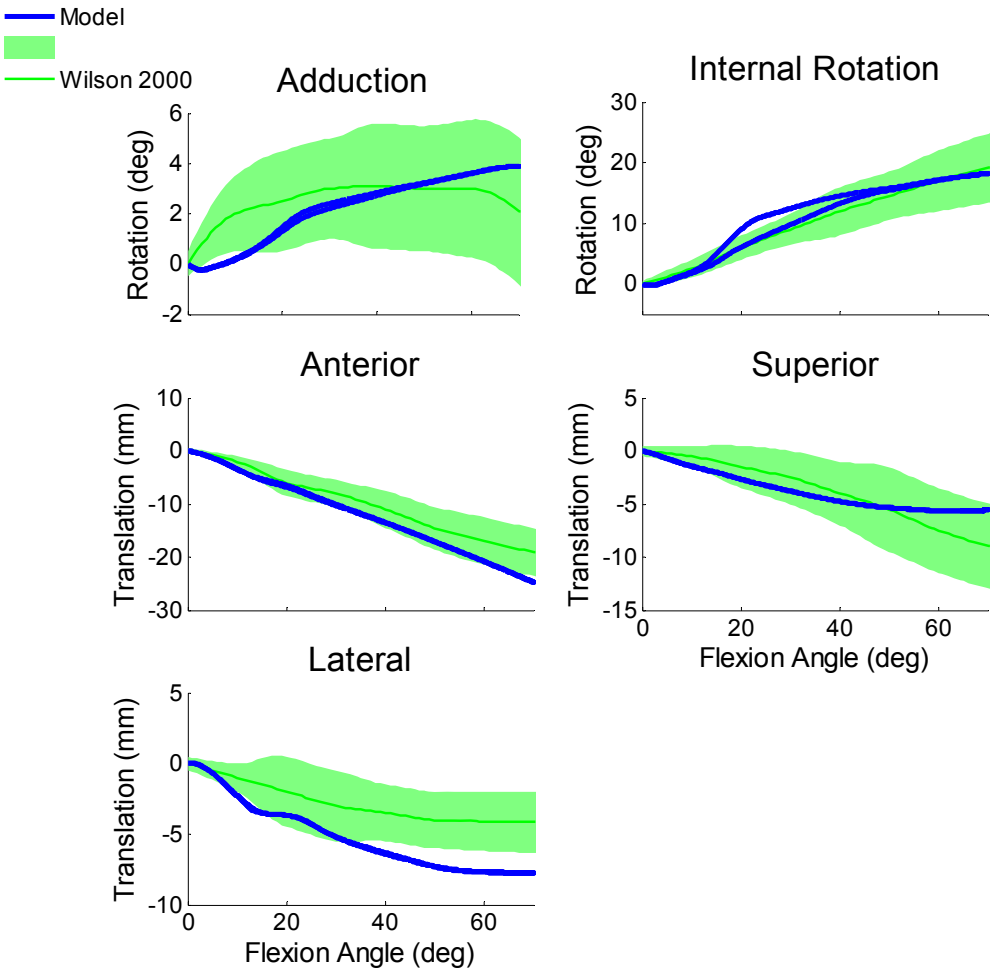


Figure 24: Passive motion of the model compared with ex vivo data (Wilson, et al., 2000).

## Stiffness Tests

Shown in Figure 25 through Figure 30 are the rotations and translations resulting from an applied axial torque, anterior/posterior force, and varus/valgus torque, along with the force and torques of each ligament on the tibia.

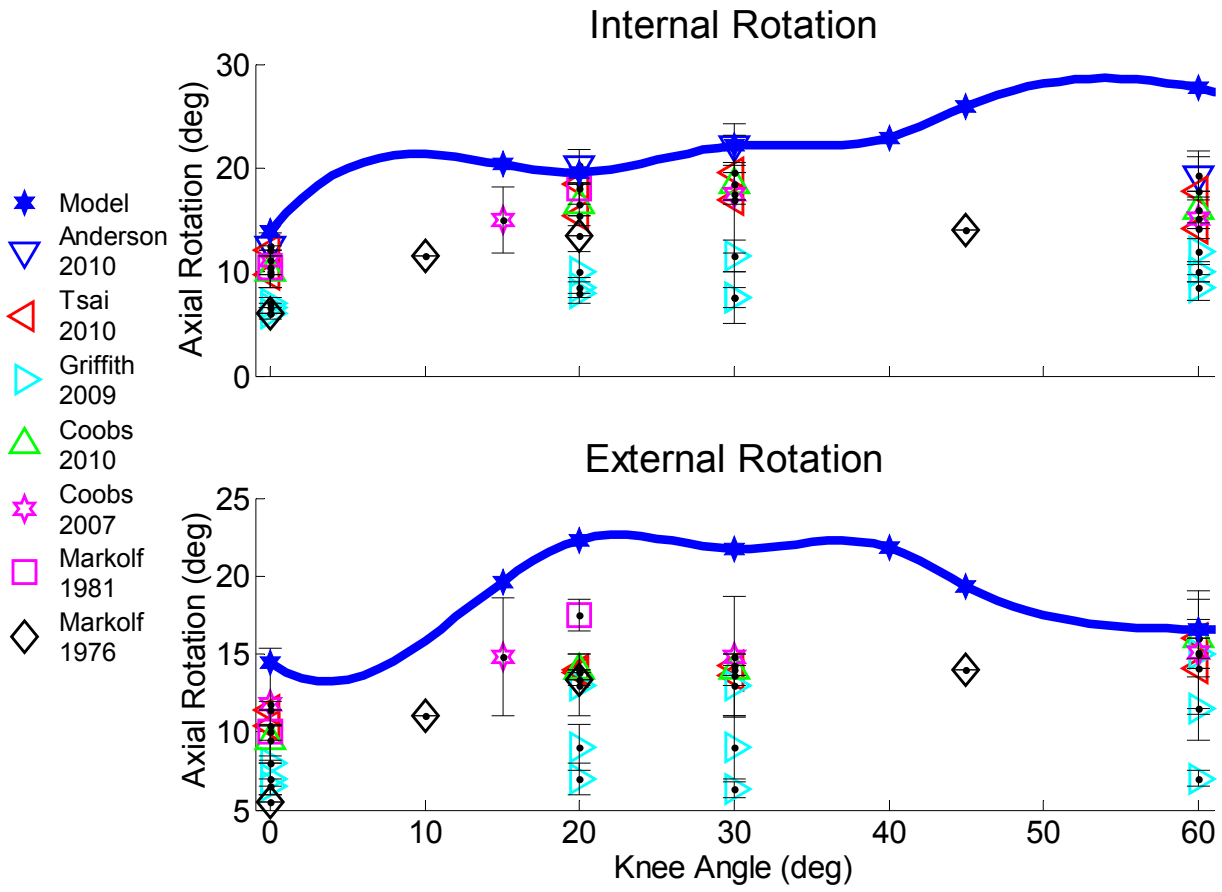


Figure 25: Rotation resulting from 5 Nm torque applied about the long axis of the tibia for the model and literature (Anderson, et al., 2010a; Coobs, et al., 2007; Coobs, et al., 2010; Griffith, et al., 2009; Markolf, et al., 1981; Markolf, et al., 1976; Tsai, et al., 2010).

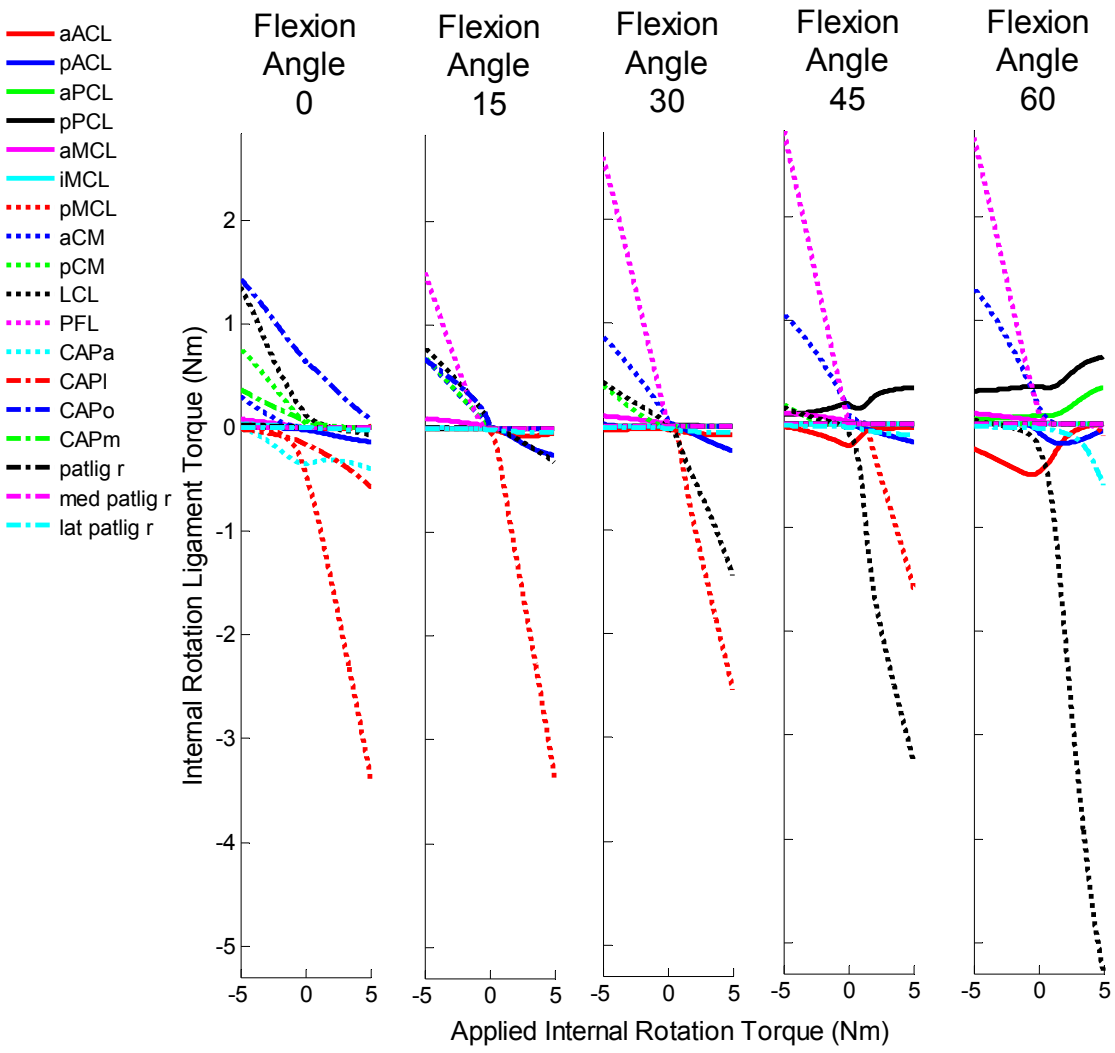


Figure 26: The axial torque each ligament in the model applies to the tibia when an axial torque is applied.

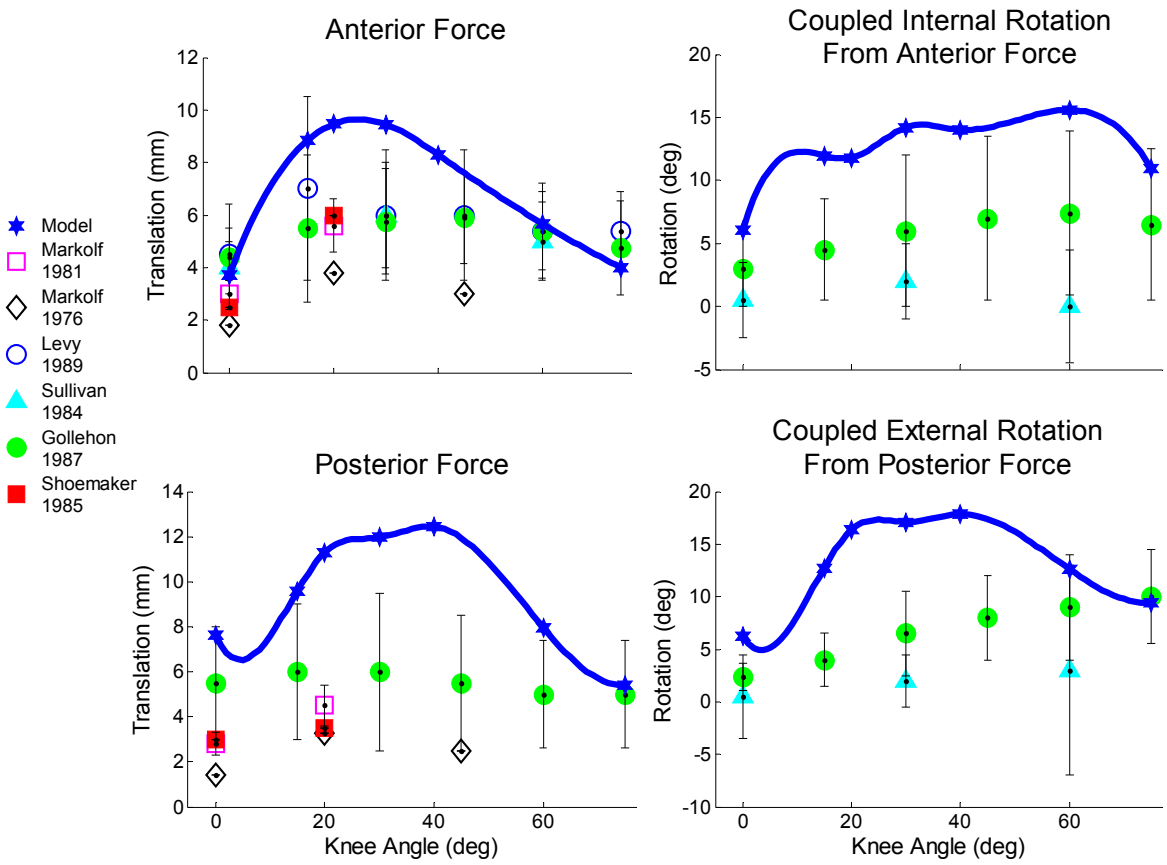


**Figure 27: Translation and rotation resulting from 100 N applied to the tibia for the model and literature (Gollehon, et al., 1987; Levy, et al., 1989; Markolf, et al., 1981; Markolf, et al., 1976; Shoemaker and Markolf, 1985; Sullivan, et al., 1984).**

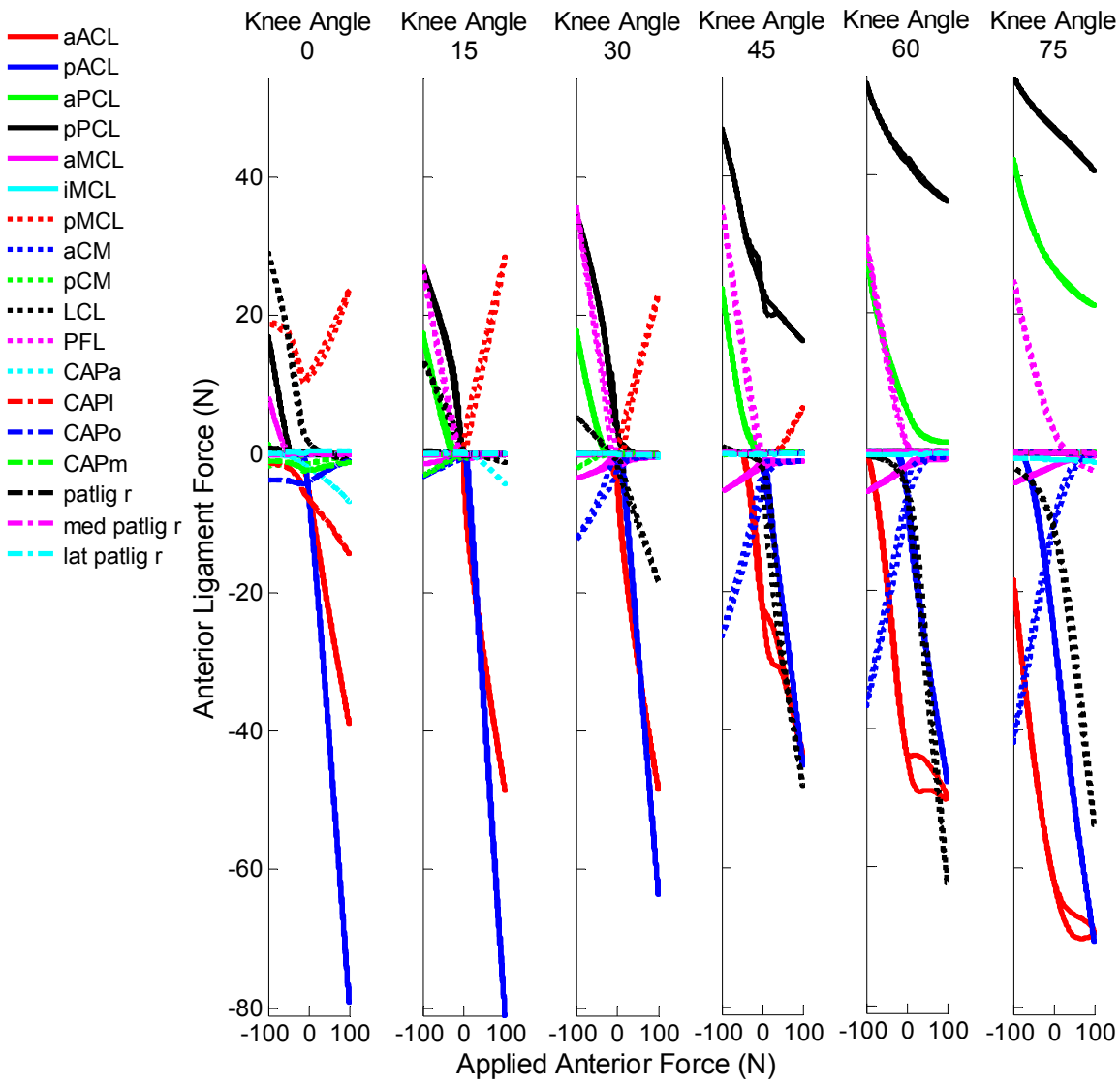


**Figure 28: The anterior-posterior force each ligament in the model applies to the tibia when an anterior-posterior force is applied.**

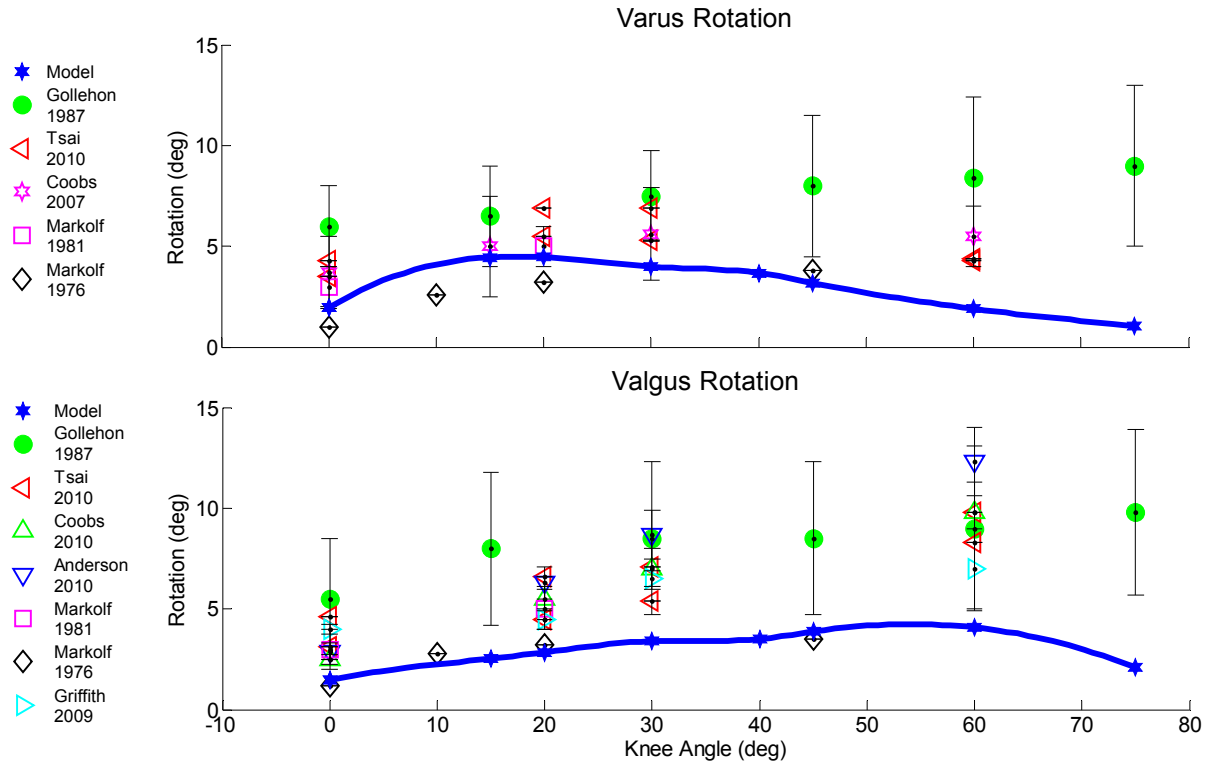


**Figure 29: Rotation resulting from 10 Nm varus/valgus torque applied to the tibia for the model and literature (Anderson, et al., 2010a; Coobs, et al., 2007; Gollehon, et al., 1987; Griffith, et al., 2009; Markolf, et al., 1981; Markolf, et al., 1976; Tsai, et al., 2010).**

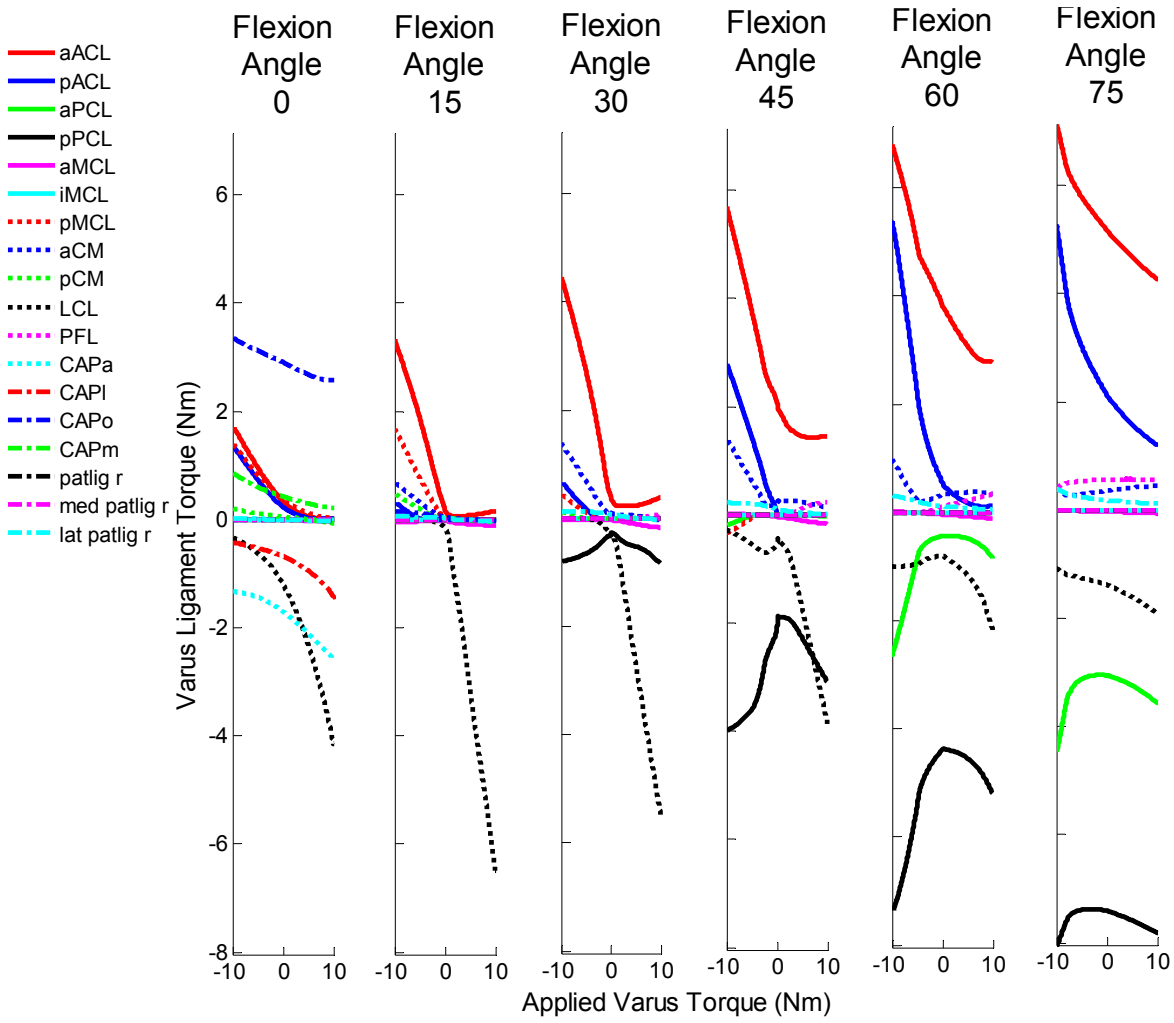


Figure 30: The varus/valgus torque each ligament in the model applies to the tibia when a varus/valgus torque is applied.

# Discussion

The passive motion of the model agrees fairly well with the literature. However, according to the stiffness tests, the model seems slightly lax in axial rotation and posterior translation as well as tight in varus/valgus rotation. The model was not tuned to the stiffness tests since this might produce unrealistic ligament properties. For example, to increase axial rotation stiffness the stiffness and/or reference strain of the LCL would need to be increased beyond literature values (Table 4). This also holds for the PCL to increase posterior translational stiffness. Varus/valgus rotation may be stiff due to the cartilage properties used. Ligament functions in the model are consistent with the literature (Table 6).

**Table 6: Comparison of ligament function between the model and literature**

| Degree of Freedom | Primary Restraint in Literature | Primary Restraint in Model |
|---|---|---|
| **Anterior Translation** | ACL (both bundles in extension and anteromedial bundle at more flexed knee angles) | ACL (aACL at more flexed angles) |
| **Posterior Translation** | PCL (posteromedial bundle at extension and anterolateral bundle at more flexed angles) | PCL (aPCL recruited at more flexed angles)<br>LCL (at more extended angles)<br>PFL (at more extended angles) |
| **Internal Rotation** | MCL | pMCL<br>LCL (at more flexed angles) |
| **External Rotation** | MCL<br>LCL in extension and slight flexion<br>Posterior capsule | Posterior capsule<br>LCL<br>aCM<br>PFL |
| **Varus Angulation** | LCL | LCL<br>PCL (at flexed angles) |
| **Valgus Angulation** | MCL | Posterior capsule<br>ACL (at flexed angles) |

There are a number of limitations to consider in this knee model. The ligaments were represented as spring elements, rather than deformable 3D representations that account for spatial variations in strain. The articular geometry of the tibial plateaus was represented by planes when computing contact forces between the tibia and femur. In addition, the a one degree of freedom

patellofemoral joint allowed for patella glide to occur as a result of patellar tendon stretch but did not allow for non-sagittal rotations or translations. These choices were made for computational reasons so the model could be quickly solved within the context of whole body movement. Menisci were not included in the model. (Markolf, et al., 1981) has shown that removal of the menisci increased anterior-posterior laxity by 1 to 3.6 mm and axial rotation laxity by 2.4 to 4.6 degrees, which may account for some of the excessive posterior translation and axial rotation seen in model.

In conclusion, a musculoskeletal model of the knee was developed that included cartilage contact and ligaments with the intention of being incorporated into simulations of whole body movement. The model was minimally tuned and provides reasonable estimates of the passive properties of the knee as seen *ex vivo*.

# Chapter 4: The Effect of External Loading on the 3D Patellar Tendon Moment Arm Measured with Dynamic MRI

## Introduction

Musculoskeletal models are often used to predict internal knee loads during movement. For example, models have been used to investigate knee ligament injury risk during cutting maneuvers (McLean, et al., 2003), to identify causes of anterior knee pain (Besier, et al., 2009), and to compare the effect of various rehabilitation strategies on internal knee loading (Neptune and Kautz, 2000). Such applications require consideration of the coupled influence of muscle, ligament, and cartilage contact forces within the knee. Hence, knee models have steadily become more sophisticated over time to include detailed articular surface geometries, soft tissue properties, and muscular actions across both the tibiofemoral and patellofemoral joints (Abdel-Rahman and Hefzy, 1998; Blankevoort and Huiskes, 1991; Caruntu and Hefzy, 2004; Dhaher, et al., 2010; Lin, et al., 2010; Shelburne, et al., 2006; Shin, et al., 2007). However, it remains challenging to assess the capacity of knee models to accurately represent *in vivo* behavior.

Traditionally, model predictions of knee kinematics are compared to *ex vivo* experimental measures of load-displacement behavior at the joint level (Anderson, et al., 2010a; Coobs, et al., 2010; Gollehon, et al., 1987; Griffith, et al., 2009; Tsai, et al., 2010; Walker, et al., 1988). However, under *in vivo* conditions, muscle forces can substantially alter both skeletal kinematics and cartilage loading. Traditional motion capture technology can be used to track knee kinematics during movement but has limited accuracy to measure tibiofemoral translations (Manal, et al., 2003) and secondary rotations in the transverse and frontal planes (Akbarshahi, et al., 2010).

Emerging techniques in dynamic imaging have allowed investigators to begin to track three-dimensional *in vivo* knee kinematics (Barrance, et al., 2007; Draper, et al., 2008; Seisler and Sheehan, 2007; Sheehan, 2007b; Sheehan, et al., 2009). For example, dynamic magnetic resonance imaging (MRI) techniques have been used to assess the time-varying tibiofemoral kinematics, finite helical axis, and patellar tendon moment arm during unloaded knee extension (Seisler and Sheehan, 2007; Sheehan, 2007a). We recently used dynamic MRI to show that small variations in external loading can significantly alter *in vivo* kinematic behavior at both the tibiofemoral and patellofemoral joints (Westphal, 2009). These load-dependent changes may be important to consider in clinical applications since kinematic changes could alter the finite helical axis and musculotendon moment arms. Indeed, a recent *in vivo* study showed that the patellar tendon moment arm with quadriceps contraction varies by 6% between a relaxed and fully contracted state (Tsaopoulos, et al., 2007). However that study only considered two-dimensional knee motion and did not have a model to investigate the potential underlying mechanisms.

The first objective of this study was to assess how the *in vivo* tibiofemoral finite helical axis and patellar tendon moment arm vary with loading. The second objective was to investigate the capacity of a muscle-actuated knee model to emulate load-dependent behavior observed *in vivo* (Westphal, et al., 2012). To do this, we first modified a lower extremity model to include a 6 degree of freedom tibiofemoral joint that included cartilage contact, ligaments, and muscles acting across the joint. We then used the model to predict knee kinematics, tibiofemoral rotation axis, and patellar tendon moment arm during a knee flexion-extension task performed against an external elastic and inertial load. These model predictions were directly compared to *in vivo* measures obtained by dynamically imaging subjects performing knee flexion-extension under similar loading conditions. Finally to better understand the model, we assessed the sensitivity of model predictions to variations in ligament properties.

# Methods

## Lower Extremity Model

We started with a lower limb musculoskeletal model that included 44 musculotendons acting about the hip, knee, and ankle joints (see Appendix B) (Arnold, et al., 2010). The one degree of freedom (dof) knee in the model was replaced by a six dof tibiofemoral joint (Shelburne, et al., 2006; Shin, et al., 2007) and a one dof patellofemoral joint. Nineteen ligament bundles were represented (Figure 31): the MCL (5 bundles), LCL (1 bundle), popliteofibular ligament (1 bundle), ACL (2 bundles), PCL (2 bundles), posterior capsule (4 bundles), iliotibial band (ITB), and patellar tendon (3 bundles). Each ligament was represented as a nonlinear spring (Blankevoort and Huiskes, 1991; Blankevoort, et al., 1991b; Shelburne, et al., 2011; Shelburne, et al., 2006; Wismans, et al., 1980) with origins and insertions based on anatomical landmarks (Abdel-Rahman and Hefzy, 1998; Arnold, et al., 2010; Davies, et al., 2004; Edwards, et al., 2007; Girgis, et al., 1975; Gray, 1918; Kopf, et al., 2009; Petersen and Zantop, 2007; Shelburne, et al., 2006) and wrapping about the femoral condyles accounted for.

The geometry of the distal femur and cartilage was segmented from high resolution MRI images (Bradford, 2011) of a young male knee with average femoral geometry (29 years old, 185 cm in height, 113 kg, and 87 mm epicondylar width). The medial and lateral tibial plateaus were modeled as planes with the medial plateau sloping two degrees posteriorly and medially and the lateral plateau sloping seven degrees posteriorly and two degrees laterally (Shelburne, et al., 2006). Tibiofemoral contact forces were computed via an elastic foundation model with cartilage properties of 5 MPa for elastic modulus, 0.45 for Poisson's ratio, and 3 mm uniform thickness for each bone (Li, et al., 2005; Shelburne, et al., 2006). Penetration depth was calculated as the distance between the centroid of each triangle of the femoral mesh and the plane representing the corresponding tibial plateau. The one dof patellofemoral joint allowed for the patellar translation within a constrained path relative to the femur,

with the path corresponding to that defined in the lower extremity model of (Arnold, et al., 2010). Quadriceps and patellar tendon forces were applied to the proximal and distal ends of the patella.

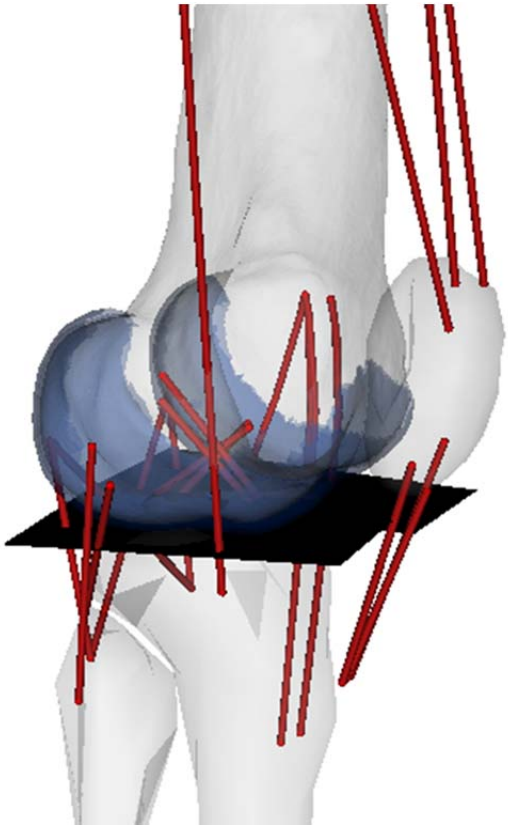

**Figure 31: The model was comprised of nineteen ligament bundles.**

**The reference strains (strains in the ligaments with the knee in full extension) and stiffnesses of the ligaments (**

Table 7) were primarily adapted from (Shelburne, et al., 2006; Shin, et al., 2007). Small adjustments of the reference strains were introduced so that the relaxed tibiofemoral rotation was approximately zero in full extension, as defined in (Arnold, et al., 2010). The knee model was used to simulate passive flexion, anterior-posterior tibia loading, and axial tibia rotation tests that have been performed in cadaveric studies (e.g. (Markolf, et al., 1981)). Model predictions of tibiofemoral translations, adduction, and internal rotation were within the range of experimental values reported in the literature (see Chapter 3).

Table 7: Ligament parameters

| Ligament | Stiffness (N/strain) | Reference Strain (-) |
|---|---|---|
| aACL | 4000 | 0.02 |
| pACL | 4000 | 0.02 |
| aPCL | 4000 | -0.12 |
| pPCL | 1600 | -0.05 |
| aMCL | 2000 | 0.02 |
| iMCL | 2000 | 0.02 |
| pMCL | 4000 | 0.05 |
| aCM | 2000 | 0.02 |
| pCM | 2000 | 0.05 |
| LCL | 3000 | 0.05 |
| PFL | 2000 | -0.05 |
| CAPa | 1500 | 0.05 |
| CAPl | 2000 | 0.05 |
| CAPo | 1500 | 0.05 |
| CAPm | 2000 | 0.05 |
| patlig | 6000 | 0.0 |
| Medial patlig | 6000 | 0.0 |
| Lateral patlig | 6000 | 0.0 |
| ITB | 5000 | 0.0 |

## *In Vivo* Knee Kinematics

High resolution static MR images were used in conjunction with dynamic MRI to track tibiofemoral and patellofemoral kinematics (Westphal, 2009). Eight healthy subjects (four male, four female, ages 22-28 years) participated. Each subject performed cyclic knee flexion-extension (30 cycles per minute) through ~35 degrees of motion within the bore of a MR scanner (Figure 32). A MRI compatible loading device was used to apply two distinct loading conditions: an elastic loading condition where subjects extended the knee against a torsional spring and an inertial condition where subjects used the quadriceps to decelerate rotating disks during knee flexion (Westphal, 2009). These elastic and inertial loading conditions induced quadriceps activity with knee extension and flexion, respectively (Figure 32). We note that quadriceps loading with knee flexion is more comparable to what is observed during the load acceptance phase of walking. Subjects performed three trials for each loading condition.

Skeletal motion was tracked using a cine phase contrast (cine-pc) sequence (Pelc, et al., 1995) to measure 3D tissue velocities during the cyclic knee flexion-extension tasks. A sagittal-oblique imaging plane (pixel size of 0.94 x 0.94 mm) was defined that bisected the femur, tibia, and patella (Figure 32). A cine sequence was used to acquire 40 frames over the motion cycle. At each frame, linear least squares was used to calculate the 3D translational and angular velocity of the femur, tibia, and patella that best agreed with measured pixel velocities (Westphal, et al., 2012). Numerical integration of the rigid body velocity data was then performed to compute the 3D translations and orientations of the bone segments throughout the motion cycle (Pelc, et al., 1995; Sheehan, et al., 1999). Six degree of freedom motion at the tibiofemoral and patellofemoral joints were then computed. 3D joint angles were determined using a Cardan rotation sequence (body fixed 3-1-2) consisting of flexion, adduction, and then internal rotation (Grood and Suntay, 1983).

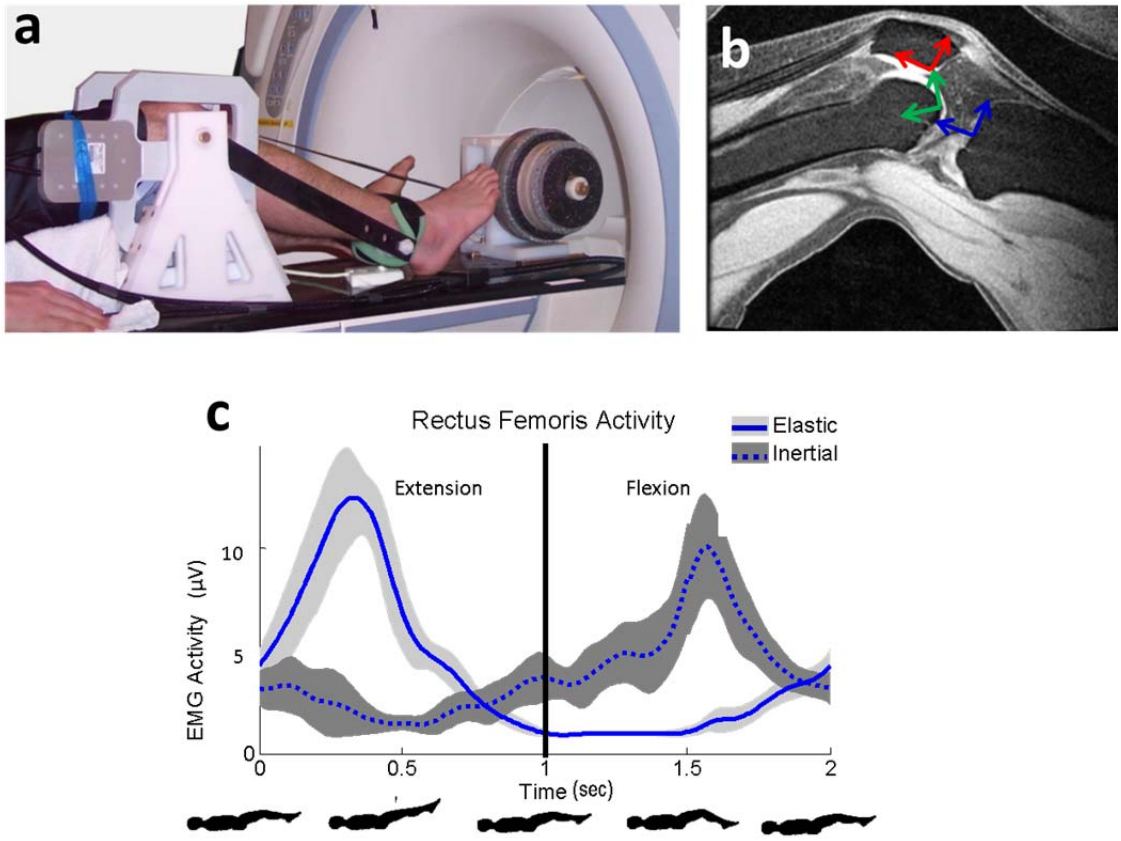


**Figure 32: (a) MR compatible loading device, (b) Sagittal-oblique imaging plane, (c) Quadriceps activity (shown for one representative subject) was induced during either knee extension (elastic loading) or flexion (inertial). Joint kinematics were reported in the bone embedded reference frames as adapted from (Sheehan, 2007b) and used in (Westphal, et al., 2012). The bone origins were placed on a sagittal oblique plane oriented along the shaft of the femur and midway through the patella. The femur origin was placed in the intercondylar notch and most inferior point. The tibia origin placed on the middle of the tibial plateau. The patellar origin positioned on the most posterior, inferior point of the bone. The y axes of the femur and tibia were oriented along the long-axis of the bones and the patellar y axis along the posterior edge of the bone. The medial-lateral axis of the femur connected the most posterior points of the femoral condyles in an axial image, with the tibia given the same axis. The medial-lateral axis of the patella was also defined using the most medial and lateral points of the bone in an axial image.**

Static MR images of the knee were collected using an IDEAL sequence (pixel size of 0.39 x 0.39 mm) (Reeder, et al., 2007), which produced four image data sets: fat, water, in-phase, and out-of-phase images. These static images were segmented (3D Slicer, Isomics, Inc., Cambridge, MA) to create subject-specific representations of the distal femur, proximal tibia, and patella (Gering, et al., 1999; Pieper, et al., 2005; Pieper, et al., 2006). The origin and insertions of the patella tendon were manually identified in these images in order to locate the local position of these points in the patella and tibia, respectively.

We computed the time-varying position and orientation of the finite helical axis (FHA) of the tibia relative to the femur assuming rigid body transformations (Berme, et al., 1990; Spoor and Veldpaus, 1980). The FHA was computed for every 5 deg increment in knee flexion. To quantify how the FHA changes under load, the intersection point of the FHA with the femoral xy plane was calculated (Sheehan, 2007b).

Using Eq 3, the patellar tendon moment arm was determined as the shortest distance between the patellar tendon line of action and the FHA (Sheehan, 2007a).

$$\text{moment arm} = |\vec{\boldsymbol{r}}^{OQ} \cdot (\hat{\boldsymbol{u}}^{PT} \times \hat{\boldsymbol{u}}^{FHA})| \qquad \text{Eq 8}$$

In this equation, $\mathbf{r}^{OQ}$ is a position vector from any point O on the FHA to any point Q on the patellar tendon line of action, $\mathbf{u}^{PT}$ a unit vector along the patellar tendon line of action, and $\mathbf{u}^{FHA}$ a unit vector along the FHA.

A two-tailed paired *t*-test was used to compare the moment arms, and the anterior and superior position of the FHA on the femoral xy plane between elastic and inertial loading conditions.

## Dynamic Simulation

The muscle-actuated lower extremity model was used to simulate knee flexion-extension tasks that were imaged. In these simulations, a time-varying external force was directly applied to the distal tibia to emulate the external loads acting on the lower limb in the elastic and inertial loading conditions. In the elastic case, a posterior tibia force linearly increased with knee extension (Figure 33). In the inertial case, the anterior tibia force linearly decreased with knee flexion (Figure 33). The elastic and inertial loads induced quadriceps activity in extension and flexion, respectively, which was consistent with what was seen experimentally.

A computed muscle control algorithm (CMC) was used to determine muscle excitations that drove the model to track a sinusoidal (0.5 Hz) knee flexion trajectory that oscillated between 5 and 45 deg of knee flexion (Thelen and Anderson, 2006b). Pelvis position, pelvic tilt (90 deg posterior), and hip flexion (20 deg) were prescribed in the simulations, reflecting the external support provided in the experimental setup (Figure 32). Ankle dorsiflexion was actively controlled by the muscles to track a desired fixed value (30 deg). At each time step in a simulation, the CMC controller computes the difference between desired and simulated generalized coordinates and speeds associated with knee flexion and ankle dorsiflexion. Based on current tracking errors, a desired set of generalized accelerations are then computed. CMC then determines a set of muscle forces that would produce the desired joint accelerations while minimizing a cost function to resolve muscle redundancy. The cost function used was the sum of muscle volume-weighted squared activations (Happee, 1994). Muscle-tendon acutators were represented by Hill-type models which accounted for activation dynamics and tendon elasticity (Zajac, 1989). Muscle excitations were computed from the desired muscle forces by inverting the activation and contraction dynamics properties of each muscle (Thelen and Anderson, 2006b). Note that CMC was only used to track knee flexion and ankle dorsiflexion, such that the other five dof at the tibiofemoral joint and the patella translation were predicted (Figure 33). The resulting

tibiofemoral and patellofemoral kinematics were filtered using a zero-lag low-pass second-order Butterworth filter with a cutoff frequency of 6 Hz (Lloyd and Besier, 2003) and subsequently used to calculate the FHA and patellar tendon moment arm.

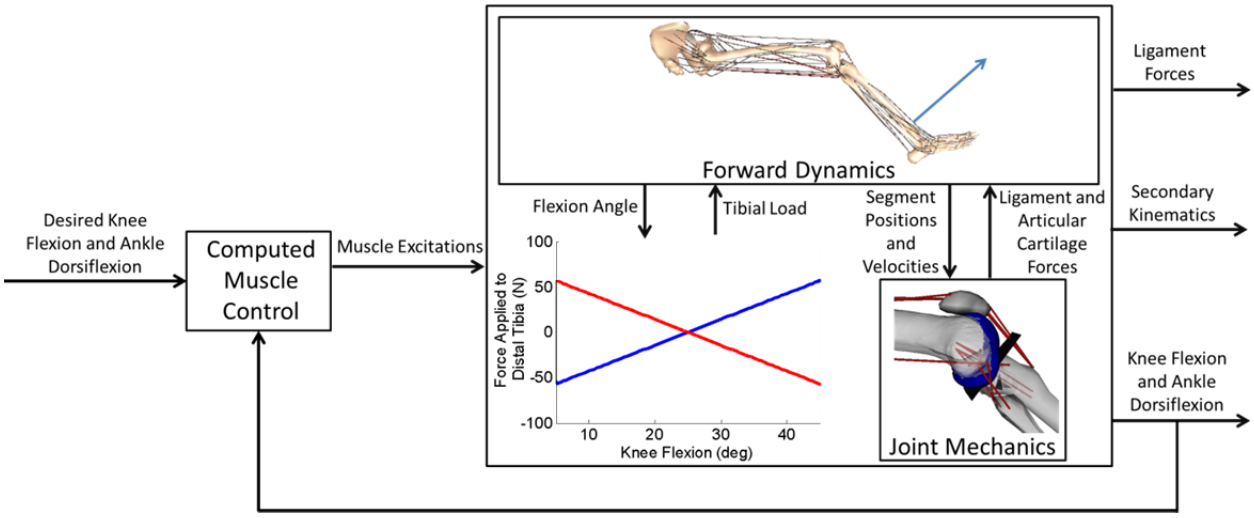


**Figure 33: Forward dynamics and joint mechanics models were integrated simultaneously when simulating the motion.**

## Sensitivity Analysis

The influence of quadriceps loading and ligament properties on the kinematics was assessed by running simulations of both the elastic and inertial loading conditions while sequentially varying the reference strain and stiffness properties of each bundle of ligaments. Ligament reference strains were increased by 0.01 and ligament stiffnesses was doubled in the sensitivity analyses (Wismans, et al., 1980). The kinematics obtained from the nominal simulation was subtracted from those obtained in each perturbed simulation.

# Results

## Tracking

The simulations were able to track the desired knee flexion angle with absolute errors averaging less than 2 deg over the motion cycle. Simulated quadriceps activities were consistent with experimental measures. Elastic loading induced maximum quadriceps activity slightly before peak knee extension. The inertial loading induced maximum quadriceps activity slightly after peak knee flexion (Figure 34).

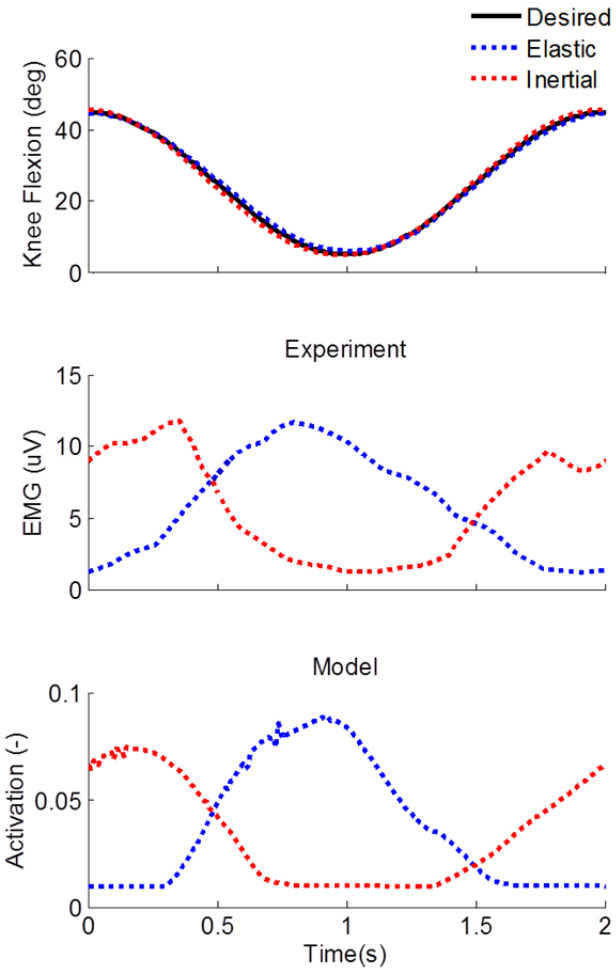


**Figure 34: (top) The simulations were able to track the prescribed flexion angle. (middle, bottom) The vastus lateralis activation patterns induced in the simulations were comparable to measured EMG.**

## Kinematics

Experimentally, we observed distinct differences in secondary tibiofemoral and patellofemoral kinematics between elastic and inertial loading conditions. Notably, the inertial loading induced greater superior patella translation (2.5 mm) and anterior tibia translation (3.5 mm) in a flexed posture, which acted to reduce the overall excursion over a motion cycle by 5.7 and 5.0 mm, respectively (Figure 35). Similar load-dependent differences in joint translations were evident in the model. The model predicted greater superior patella translation by 0.9 mm and anterior translation by 2.2 mm in a flexed posture, thus decreasing the overall excursion by 1.7 and 1.9 mm, respectively. Experimentally, we did not observe load-dependent differences in axial tibiofemoral rotation (Westphal, et al., 2012). There were slight differences in axial tibia rotation predicted by the model, with quadriceps loading inducing a shift towards internal rotation at both flexed and extended positions.

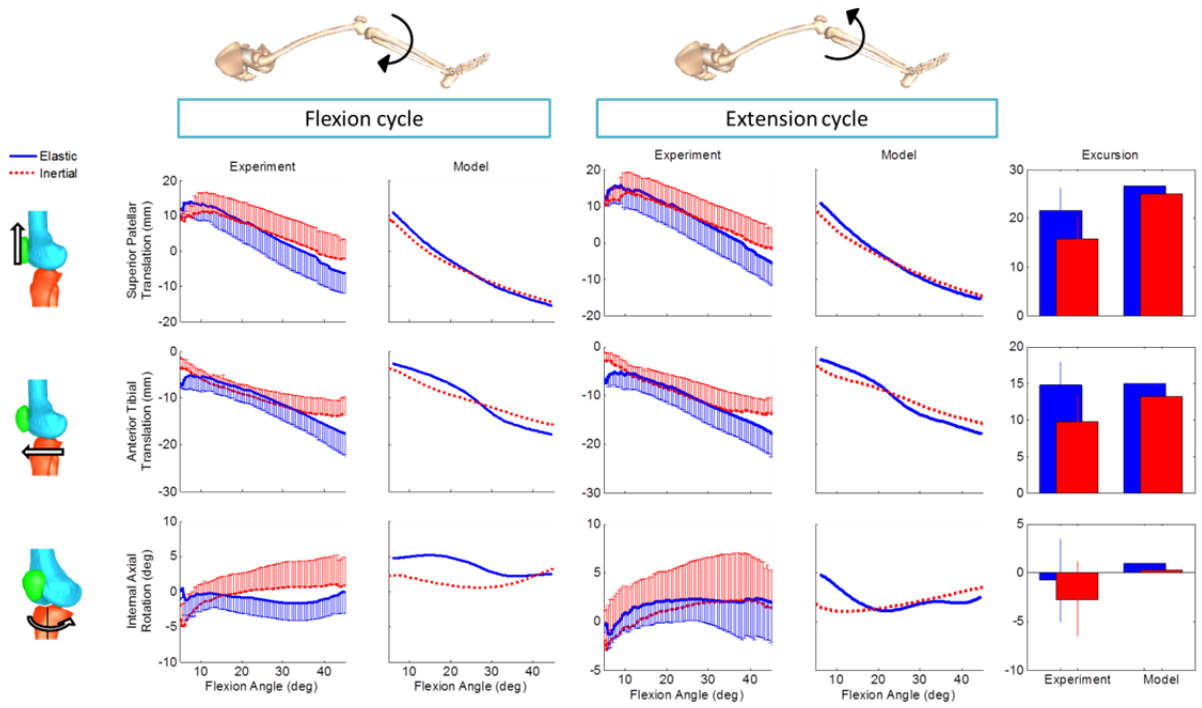


**Figure 35: Both in vivo data and model predictions show quadriceps loading to induce a superior patella and an anterior tibia. The bar plots show how the excursion (extended measure minus flexed measure) changes between the loading conditions.**

## Finite Helical Axis

The orientation of the tibiofemoral finite helical axis was mainly in the medial-lateral direction of the femur (Figure 36). At extended angles during the flexion cycle, *in vivo* quadriceps loading caused greater external rotation component in the FHA orientation. This is reflected in the slopes of the kinematic curves (Figure 35). As the tibia flexes from 15 to 20 deg, the tibia axially rotates from -0.5 to -0.8 deg in the elastic case and rotates from -0.6 to -0.1 deg in the inertial case. In the model, quadriceps loading caused an internal rotation component in the FHA orientation with both flexion and extension.

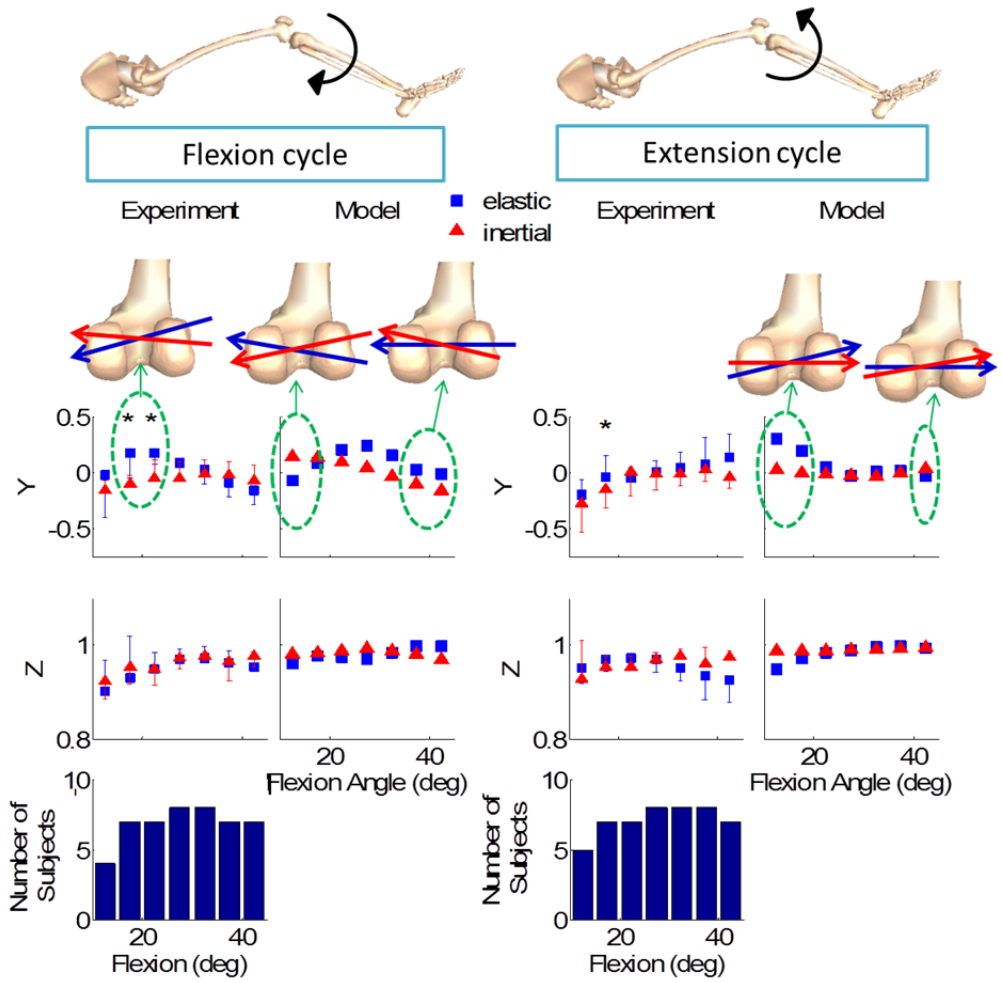


**Figure 36: Components of a unit vector along the tibiofemoral finite helical axis, expressed in the femur reference frame. Statistical significance of $p < 0.05$ is denoted as *.**

Experimentally, we observed a significant effect of loading condition on the location of the finite helical axis. Both the model and experiment predict a maximum superior shift by 20 and 21 mm, respectively, in the elastic loading condition (Figure 37). However, the model predicts the elastic condition to be anteriorly shifted by 10 mm and the experiment posteriorly by 13 mm.

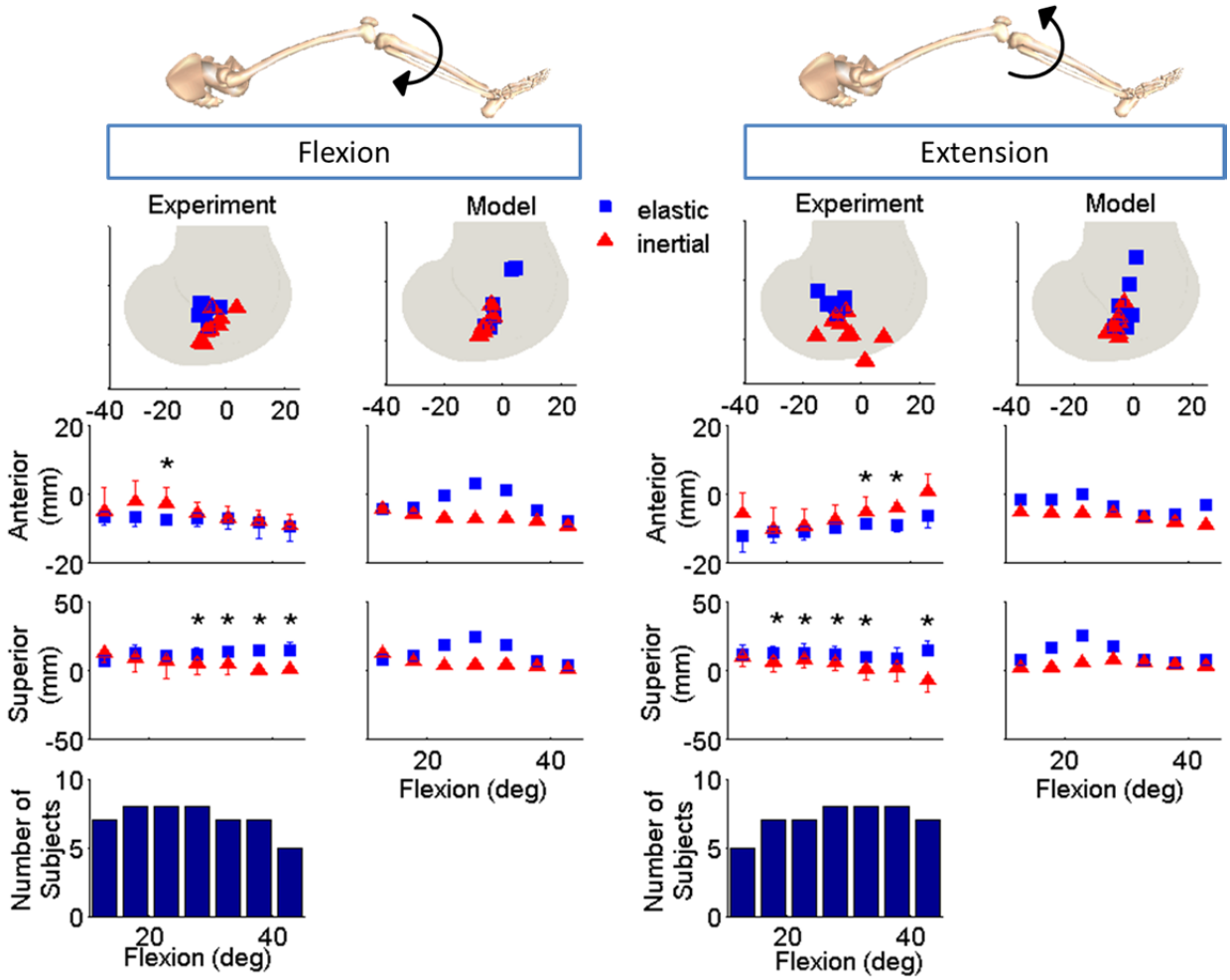


Figure 37: Location of the FHA with the sagittal plane. Statistical significance of $p < 0.05$ is denoted as *.

## Patellar Tendon Moment Arms

The image based measures of patellar tendon moment arms averaged from 25 to 46 mm. In flexed postures, the patellar tendon moment arms were significantly reduced by 11 to 18 mm with quadriceps loading (Figure 38). The model also predicted a reduction in the patellar tendon moment arms in the inertial loading case, but the magnitude of differences (up to 7 mm) were not as great as that seen experimentally (Figure 38).

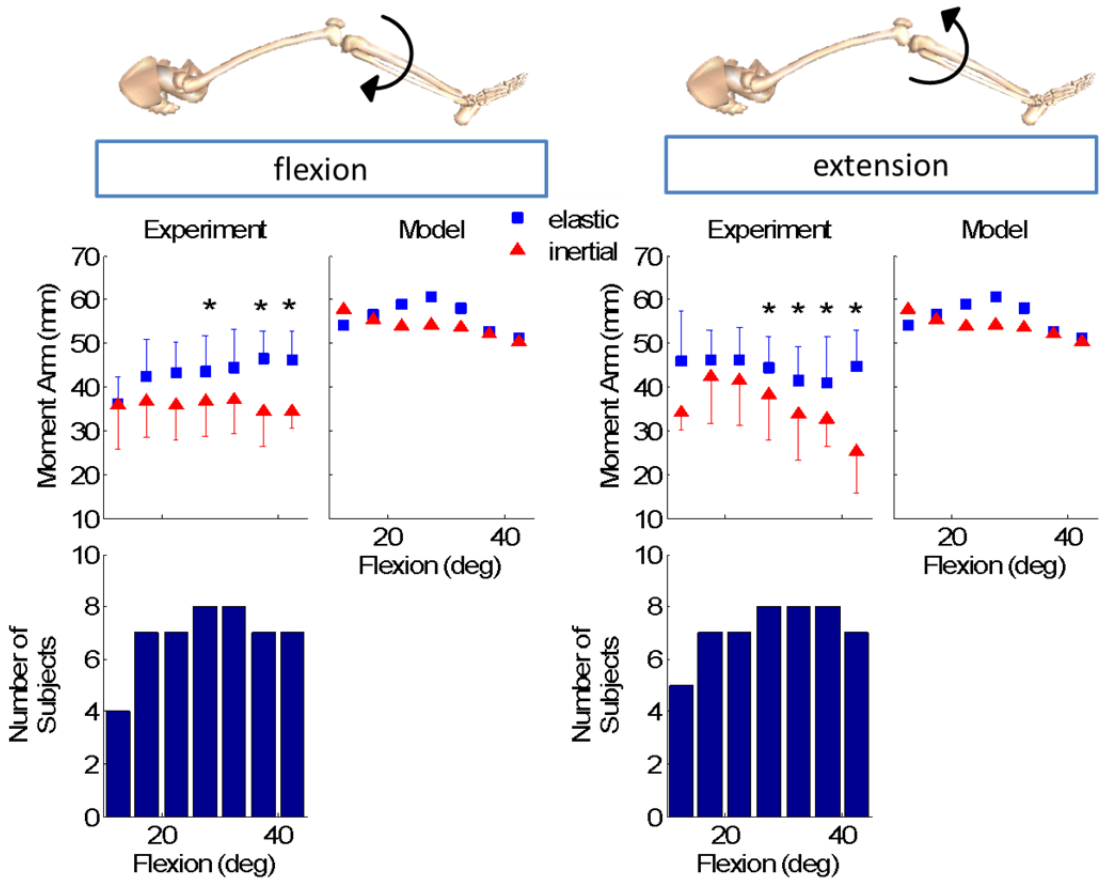


**Figure 38: The patellar tendon moment was larger in the elastic loading condition, seen both in vivo and predicted by the model. Statistical significance of $p < 0.05$ is denoted as *.**

## Sensitivity

The influence of ligament properties on secondary knee kinematics was load-dependent. As expected, superior patella translation was most dependent on the patellar tendon but was also affected by the ACL in extension. Anterior tibia translation was most dependent on the ACL in extended postures. In flexed postures, anterior tibia translation was most dependent on the deep MCL in the inertial case but more dependent on the PCL in the elastic case. Internal tibia rotation was dependent on the deep MCL and LCL/PFL at more flexed angles. At extended angles, axial rotation was influenced by the LCL/PFL, deep MCL, and superior MCL (Figure 39).

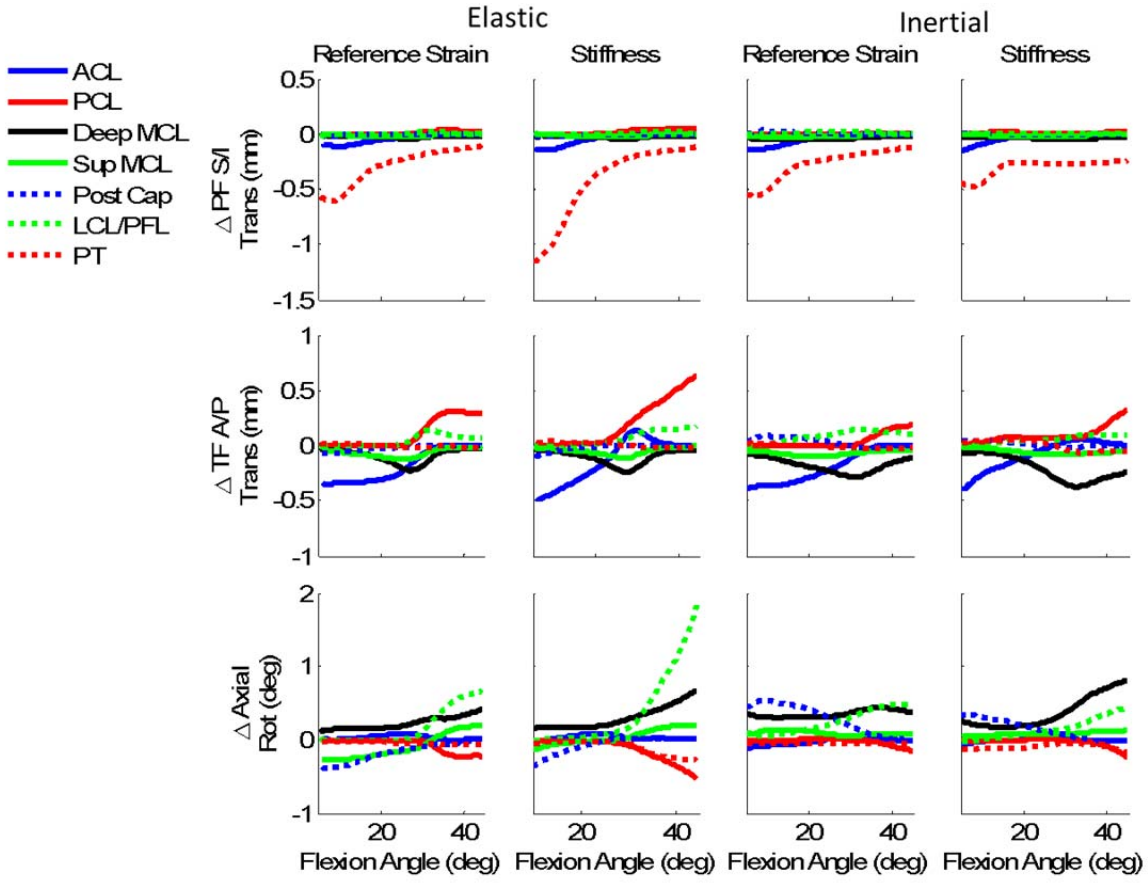


**Figure 39: The difference in kinematics (nominal subtracted from perturbed model) seen when ligament properties in the model were changed (reference strain increased by 0.01 and stiffness doubled).**

# Discussion

This study compared model predictions of knee kinematics to *in vivo* measures obtained with dynamic imaging. The results clearly show the strong influence that the timing of quadriceps loading can have on secondary tibiofemoral kinematics, patellofemoral motion, and the patellar tendon moment arm. Such load-dependent effects can alter the lines of action and moment generating capacities of muscles about the knee, and thus might be important to incorporate in muscle-actuated simulations of movement.

Consistent with *in vivo* data, the model was able to predict a reduction in anterior-posterior tibia translation and superior-inferior patella translation when quadriceps loading occurred in a flexed knee posture. Not seen experimentally, the model predicted quadriceps loading to induce internal rotation. However, the model is consistent with previous studies using *ex vivo* cadaveric setups to investigate quadriceps function (Hirokawa, et al., 1992; Li, et al., 1999).

Both the model and *in vivo* results show a diminished patellar tendon moment arm with the inertial load. However, the model under predicts the amount the moment arm is reduced. This may be due to the disagreement of the model and *in vivo* results of the anterior-posterior location of the FHA. Both show a superior shift in the elastic FHA, which would increase the moment arm of the patellar tendon. A posterior shift would increase the moment arm further, as seen *in vivo*, but the anterior shift seen in the model would act to decrease the moment arm.

The passive screw-home mechanism of the knee is internal rotation with flexion (Wilson, et al., 2000). At extended angles during the flexion cycle, *in vivo* quadriceps loading caused greater external rotation, which differs from the passive screw-home mechanism. In the model, quadriceps loading caused internal rotation with flexion (consistent with passive screw home mechanism) and extension (not consistent with passive screw home mechanism). This suggests the screw home mechanism is load-dependent.

The ligament sensitivity results seen in the model are generally consistent with prior serial dissection studies. According to a review by Masouros, anterior-posterior translation is mainly restrained by the cruciate ligaments with secondary restraints attributable to the MCL (Masouros, et al., 2010). Axial rotation is mostly modulated by the MCL, LCL, and posterior capsule, with the role of the LCL diminishing at more flexed postures (Masouros, et al., 2010). Similarly in our model, anterior-posterior translation was affected by cruciate properties as well as the MCL. Axial rotation was affected by the properties of the posterior capsule, LCL/PFL, and MCL, with the LCL/PFL not diminishing with flexion. A unique observation of the current study is that these postural-dependencies also vary with loading conditions. For example, we predicted much less influence of the posterior cruciate ligament (PCL) on posterior tibial translation when the quadriceps were loaded in flexion. The PCL became taut at about 30 deg of knee flexion, such that quadriceps loading in these postures would act to unload the PCL and hence lessen its influence on secondary motion. The model also suggests the MCL had greater influence on internal rotation when the quadriceps were loaded in flexion, while the LCL/PFL had greater influence when the quadriceps were unloaded in flexion. When the quadriceps were loaded in flexion, the anterior position of the tibia decreased the stretch of the PFL, thus decreasing its ability to restrain axial motion.

Many models assume the patellar tendon to be inextensible (Arnold, et al., 2010; Shelburne, et al., 2006) and thus would not predict a load-dependence in patellofemoral kinematics as seen in Figure 35. Our model suggests a 1.7 mm change in patellar excursion between our two loading conditions. Thus patellar tendon stretch may be important to consider when investigating the causes of patellofemoral pathologies since the degree of superior patella translation can influence where the patella resides along the trochlear groove.

The model predicted a smaller change in patellar excursion compared to the *in vivo* results. This may be due to the femoral geometry. The average epicondylar width was 84 mm for the *in vivo* subjects

and 87 mm in the model. This would cause the patella to be more posterior *in vivo*, thus changing the patellar tendon line of action to be more superior-inferiorly aligned. Therefore, even though the force in the patellar tendon may be the same in the model and *in vivo*, the *in vivo* patellar tendon has a greater superior-inferior component and hence a greater influence on the superior-inferior motion of the patellofemoral joint.

The load-dependent variations in kinematics we measured are likely functionally relevant. Peak knee extension moments in these experiments averaged from 23-33 Nm (Westphal, et al., 2012), which is comparable to that seen at the knee during the load acceptance phase of walking. The timing of quadriceps loading in the inertial condition better reflects patterns seen in locomotion activities. During both walking and running, the quadriceps undergo lengthening contractions during the load-acceptance phase with peak quadriceps loading coinciding relatively closely with peak stance phase knee flexion angle. The fact that the patellar tendon moment arm is somewhat diminished under these loading conditions could necessitate greater patellar tendon forces than would be estimated using a knee model that does not account for load-dependent changes.

There are some limitations to consider in our knee model. We represented the ligaments as spring elements, rather than deformable 3D representations that account for spatial variations in strain. In addition, the medial and lateral tibia plateaus were represented by posteriorly sloped planes when computing cartilage contact forces at the tibiofemoral joint. A one dof patellofemoral joint allowed for patella glide to occur as a result of patellar tendon stretch but did not allow for medio-lateral translation and tilt. Both of these choices were made for computational reasons since the simplified ligament and cartilage loading models could be more efficiently solved within the context of whole body movement. Since the main functions of the menisci are not to restrain motion, menisci were not included in the model (Aagaard and Verdonk, 1999; Messner and Gao, 1998).

Despite the limitations, we believe this study demonstrates the relevance and potential for simulating six degree of freedom tibiofemoral kinematics during human gait. Most current gait models utilize a simplified kinematic knee model, in which it is assumed that patellofemoral kinematics and secondary tibiofemoral kinematics can be expressed as constrained functions of knee flexion (Arnold, et al., 2010). While simulated muscle forces can be subsequently applied to a deformable knee model (e.g. (Shelburne, et al., 2006)), such a serial formulation inherently disconnects the affect that variations in secondary knee kinematics could have on muscle actions. This study clearly demonstrates that load-dependent behavior is evident in intact healthy knees and is likely even more important to consider in pathological cases where injury can alter joint laxity and surgery can alter the properties of both reconstructed and donor tissues. These effects are particularly relevant when using models to characterize the location and magnitude of articular cartilage loading. The formulation we used in this study co-simulates movement dynamics at the whole body level and tissue loading and deformation at the joint level. Such a co-simulation framework provides simultaneous estimates of movement kinematics as well as cartilage, ligament, and muscle loading which is highly relevant to understand knee mechanics function in both healthy and pathological states.

# Chapter 5: The Effect of Joint Laxity on Knee Mechanics during Gait

## Introduction

A serial modeling approach is typically used to estimate soft tissue loading and secondary joint kinematics during gait. In this approach a dynamic multibody model of the musculoskeletal system is first used to calculate muscle forces (Anderson and Pandy, 2003; Buchanan, et al., 2005), which are then applied as boundary conditions to a detailed joint model to solve for soft tissue strains, stresses, and secondary joint kinematics (Besier, et al., 2005; Fernandez and Pandy, 2006). This method could be used to investigate how secondary kinematics affect cartilage contact locations in the ACLd knee as well as how cartilage loading changes, but there are inherent assumptions that limit its predictive capabilities. The multibody dynamic models typically represent the knee as a kinematic constraint that does not vary with loading (Arnold, et al., 2010; Delp, et al., 1990). The tibiofemoral joint has been shown to exhibit load-dependent behavior during gait with internal tibia rotation varying substantially between early stance, late stance, and terminal swing (Andriacchi and Dyrby, 2005; Lafortune, et al., 1992). This load-dependent behavior of the knee may be more exaggerated in some pathological conditions, like the ACL-d knee. Laxity could alter both the line of action and the moment arms of the muscles, thereby affecting its capacity to generate joint moments and accelerations. A serial simulation assumes such effects are negligible, and hence that muscle forces are not dependent on joint laxity. Clinically, there has long been an interest in the use of muscle recruitment to compensate for excessive laxity, with a number of studies investigating the use of quadriceps avoidance and hamstring facilitation to compensate for ACLd. Variations in muscle recruitment would alter muscle forces, which are a large determinant of cartilage contact loads (Costigan, et al., 2002; Kuster, et al., 1997; Pandy and Andriacchi,

2010). It is thus important to consider how including joint laxity in musculoskeletal simulations of gait can alter soft tissue and joint loading.

Some recent biomechanical studies have introduced new approaches to address the computational challenge of considering contact and soft tissue loads within the context of whole body movement. For example, (Halloran, et al., 2009) calculated neuromuscular control needed to optimize jump height while minimizing stress patterns within a finite element model of the foot. The large computational cost of solving a finite element model at every time step within a dynamic simulation was circumvented by development of a surrogate model. However, numerical dynamic optimization was used which necessitated large computation time even when simulating with a 2D model. (Lin, et al., 2010) showed that the consideration of knee articular cartilage contact forces can substantially alter muscle force predictions during gait. However, only an inverse analysis approach was used such that one could not simulate unique movement patterns. Our approach is to simulate tibiofemoral mechanics within the context of an actively controlled muscle-actuated simulation of gait. Specifically, we used a feedforward-feedback control scheme, termed computed muscle control (CMC), to modulate muscle excitations to drive the model to track desired flexion at the knee (Thelen and Anderson, 2006a), with the model then predicting secondary tibiofemoral motions based on evolving cartilage contact, ligament, and muscle forces.

The first objective of this study was to investigate how simulations of secondary kinematics, knee extensor mechanics, and quadriceps loading differ when simulating gait with a knee that exhibits laxity versus a kinematic assumption for joint mechanics. We hypothesize that in comparison with traditional kinematic knee formulations, the models with joint laxity will exhibit an anteriorly translated and internally rotated tibia when the quadriceps are loaded during weight acceptance. We further hypothesize that this change in kinematics will affect the moment arm of the patellar tendon about the knee and thus alter quadriceps load estimates. The second objective of this study was to use the

modeling framework to investigate how an injury-induced increase in joint laxity (due to ACL deficiency) could alter secondary tibiofemoral kinematics and cartilage contact patterns. We hypothesize that ACL-deficiency alters tibiofemoral kinematics in a way that shifts tibia cartilage contact locations in the ACLd knee posteriorly.

# Methods

## Musculoskeletal Model

A musculoskeletal model of the lower limb was developed that incorporated ligaments and tibiofermoal cartilage contact (Chapter 3). We started with a generic model that included 44 musculotendons acting about the hip, knee, and ankle joints (see Appendix B) (Arnold, et al., 2010). The one degree of freedom (dof) knee in the model was replaced by a six dof tibiofemoral joint (Shelburne, et al., 2006; Shin, et al., 2007) and a one dof patellofemoral joint (Figure 40) with bone embedded reference frames consistent with (Arnold, et al., 2010). Nineteen ligament bundles were represented including the MCL (5 bundles), LCL (1 bundle), popliteofibular ligament (1 bundle), ACL (2 bundles), PCL (2 bundles), posterior capsule (4 bundles), iliotibial band (ITB), and patellar tendon (3 bundles). Each ligament was represented as a nonlinear spring with origins and insertions based on (Shelburne, et al., 2006) and wrapping about the femoral condyles accounted for. The geometry of the distal femur and cartilage was segmented from high resolution MRI images of a young male knee with average femoral geometry. The medial and lateral tibia plateaus were modeled as planes with posterior slopes of 2 and 7 deg, respectively (Shelburne, et al., 2006). Tibiofemoral contact forces were computed via an elastic foundation model (Shelburne, et al., 2006). The one dof patellofemoral joint allowed for the patella to translate within a constrained path relative to the femur, subject to quadriceps and patellar tendon forces acting on either end. The reference strains and stiffness values of the ligaments were adapted from the literature (Shelburne, et al., 2006; Shin, et al., 2007), with a minimal amount of tuning to

ensure the model replicated literature measures of passive motion, anterior-posterior stiffness, and axial rotational tibiofemoral stiffness.

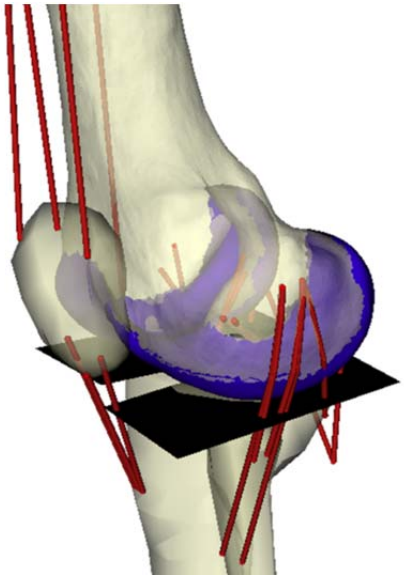

Figure 40: Knee model with cartilage contact and ligamentous restraints.

## Gait Simulation

The model was used to simulate knee motion and loading during gait. To do this, a computed muscle control (CMC, see Appendix C) (Thelen and Anderson, 2006a) algorithm was used to determine muscle excitations that drive the model to track normal hip, knee, and ankle flexion throughout a normative gait cycle (average velocity 1.47 m/s). During the simulation, measured ground reaction forces were directly applied to the feet while pelvis and non-sagittal hip kinematics were prescribed to follow measured trajectories. We generated gait simulations using three different knee representations: a 1 degree of freedom knee, an intact knee with a 6 dof tibiofemoral joint and 1 dof patellofemoral joint, and an ACLd knee where both ACL bundles were removed from the intact knee model. For the kinematic knee, the tibiofemoral translations, non-sagittal rotations, and patellofemoral motion were set to constrained functions of the knee flexion angle (Arnold, et al., 2010). The kinematic constraint functions were determined by passively flexing and extending the intact knee model and then using piecewise

cubic spline functions to describe the tibiofemoral translations, non-sagittal tibiofemoral rotations, and patella translation as a function of knee flexion (Figure 41).

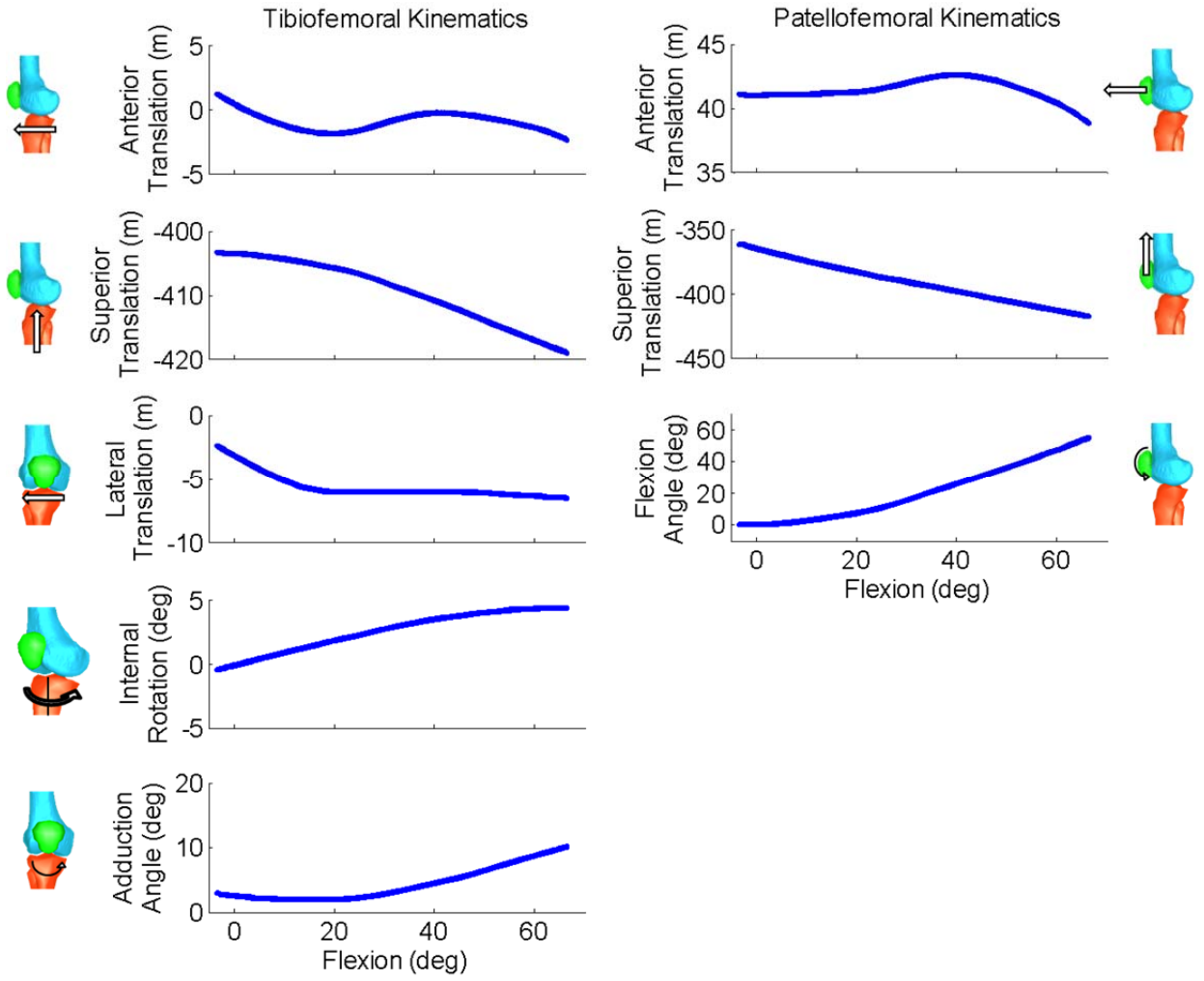


**Figure 41: Constraint functions used for the kinematic knee model.**

Note that for the intact and ACLd knee, CMC was only used to track flexion such that the other five dof at the tibiofemoral joint and the patella translation evolved as a result of muscle, ligament, and cartilage contact forces (Figure 42).

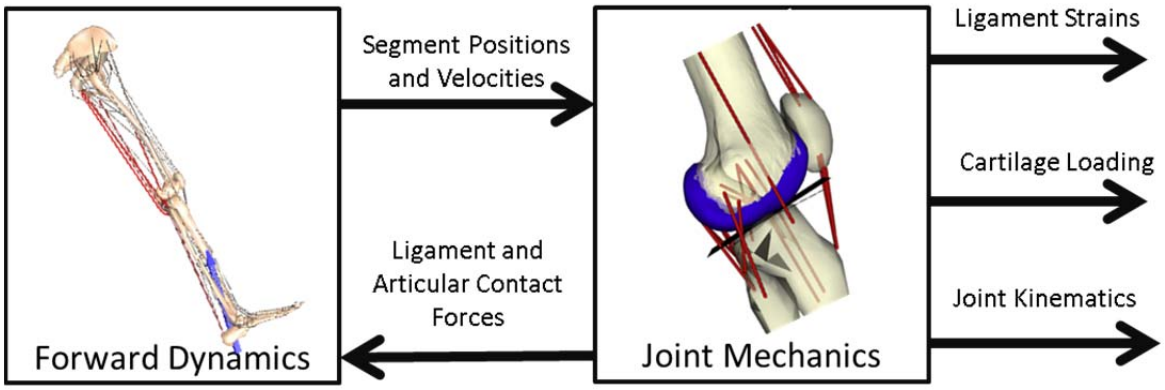


**Figure 42. Forward dynamics and joint mechanics models were integrated simultaneously when simulating gait, providing predictions of muscle forces, ligament loads, cartilage contact, and secondary knee kinematics.**

For each simulation, the resulting kinematics were lowpass filtered at 6 Hz with a second-order Butterworth filter (Lloyd and Besier, 2003). The tibiofemoral kinematics were used to compute the tibiofemoral finite helical axis (Berme, et al., 1990; Spoor and Veldpaus, 1980) and patellar tendon moment arm (Sheehan, 2007a) during distinct phases of the gait cycle. During load acceptance, the position of the tibia at 0% (heel contact) and 16% (peak stance knee flexion angle) of the gait cycle were used to determine the FHA and patellar tendon moment arm at 8%. To compute the FHA and patellar tendon during midstance, 16% and 40% (maximum knee extension angle) were used. Terminal stance was defined as 40% to 55% (opposite heel strike). 55% to 60% (toe-off) was pre-swing. Initial swing was comprised of 60% to 75% (maximum knee flexion angle). Mid-swing was set at 75% to 90% (when the tibia was vertical). Terminal swing was defined as 90% to 100% (heel strike).

# Results

## Muscle Excitation Patterns

Simulated excitation patterns were generally consistent with the timing of normative EMG patterns reported by (Winter, 1987) for each of the gait simulations considered. Notably, the models predicted semitendinosus activity during load acceptance, peak quadriceps activity during load acceptance and midstance, tibialis anterior activity just after heel strike, and soleus activity during terminal stance and pre-swing (Figure 43).

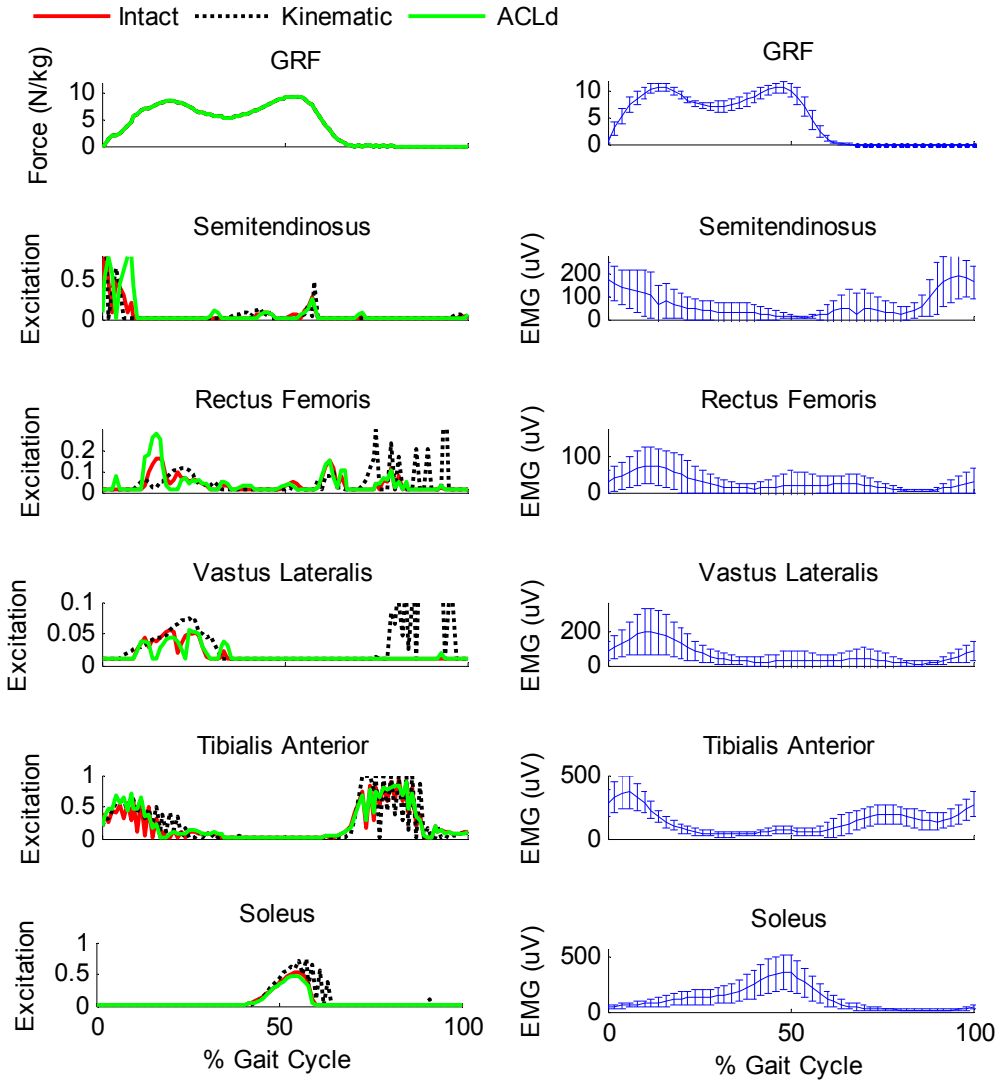


Figure 43: Comparison of muscle excitations from the model (left) to EMG (right) of (Winter, 1987).

## Effects of Joint Laxity on Knee Kinematics

All models were able to closely track normative knee flexion-extension patterns during gait (Figure 44). However, there were distinct differences in secondary tibiofemoral kinematics during stance, with the greatest variations arising in tibia translation and internal tibia rotation. During the beginning of stance, the intact knee model exhibited greater peak internal tibia rotation (4 deg), anterior tibia translation (5mm), and lateral translation (2 mm) than was assumed in the kinematic knee model. The axial rotation patterns of the intact knee was generally consistent with that directly measured using bone pins (Lafortune, et al., 1992), with peak internal rotation occurring during pre-swing, as opposed to swing phase in the kinematic knee. Compared to the intact model, anterior tibia translation and internal tibia rotation were exaggerated by 11 mm and 1deg, respectively, in the ACLd model.

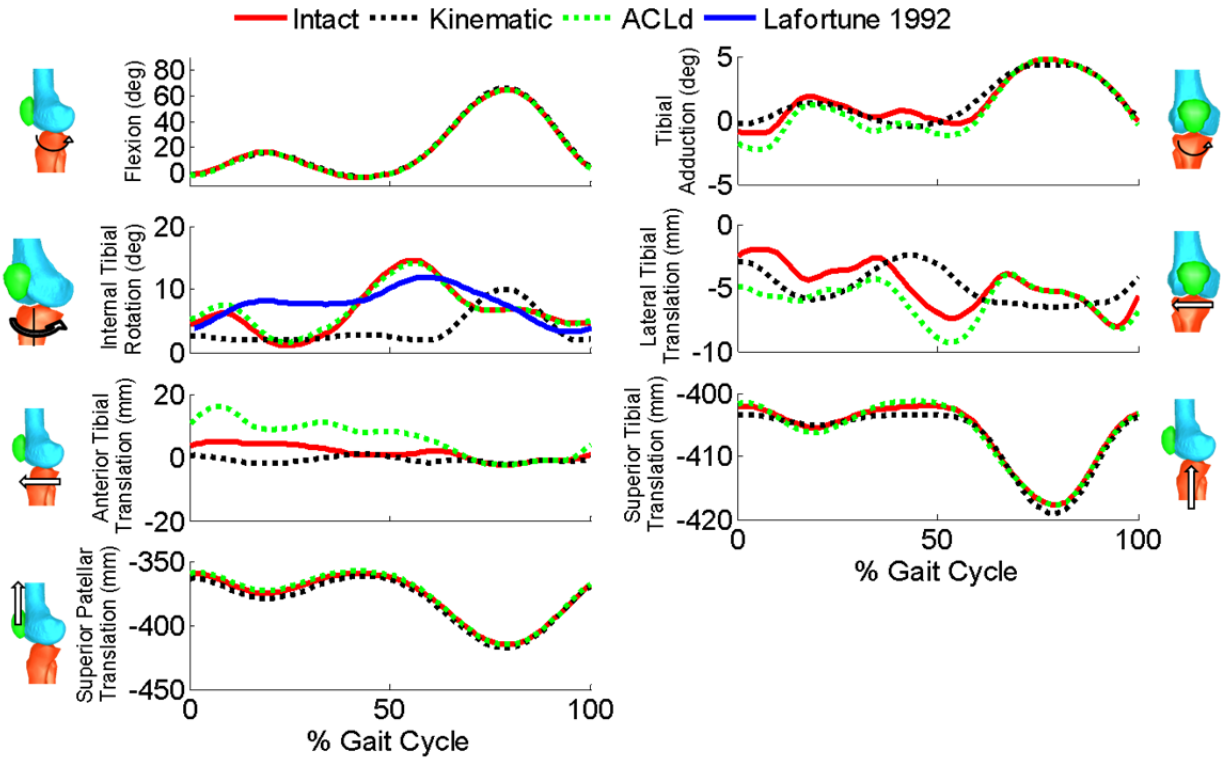


**Figure 44: When the quadriceps were maximally loaded around 20%, the model with joint laxity showed a shift towards an anteriorly and laterally translated tibia with increased internal rotation when compared with the kinematic model. Some of these effects were more exaggerated in the ACLd model.**

During beginning stance, the orientation of the FHA was mostly in the medial-lateral direction (Figure 45). Slight differences were seen between the models in the ab/adduction component when the quadriceps were loaded.

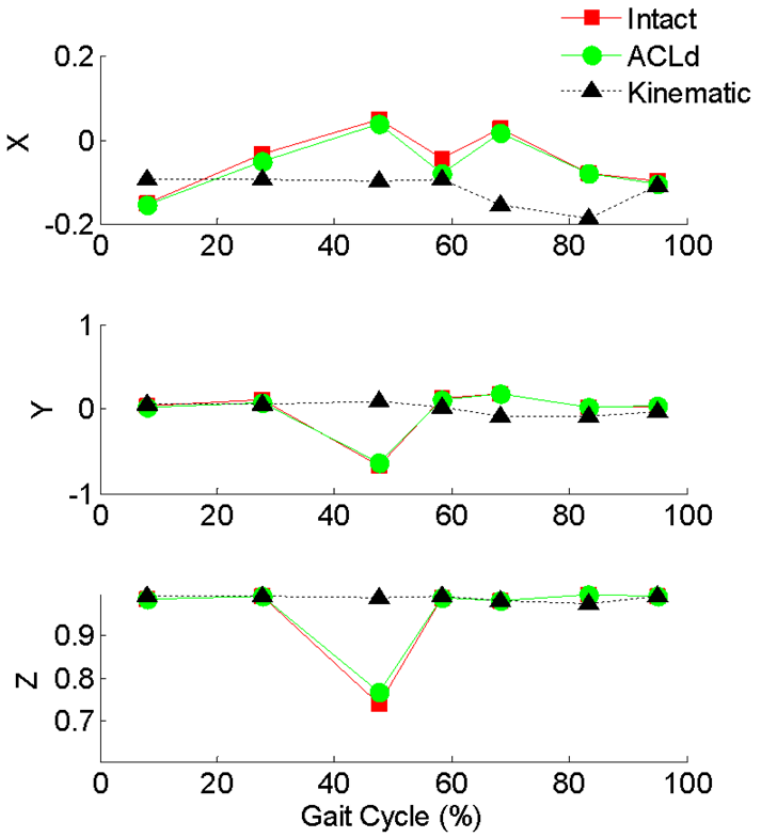


Figure 45: FHA orientation.

During initial stance, joint laxity shifted the finite helical axis inferiorly. This inferior shift was accompanied by a diminished patellar tendon moment arm by up to 6 mm in the joints with laxity, compared to the kinematic joint assumption (Figure 46).

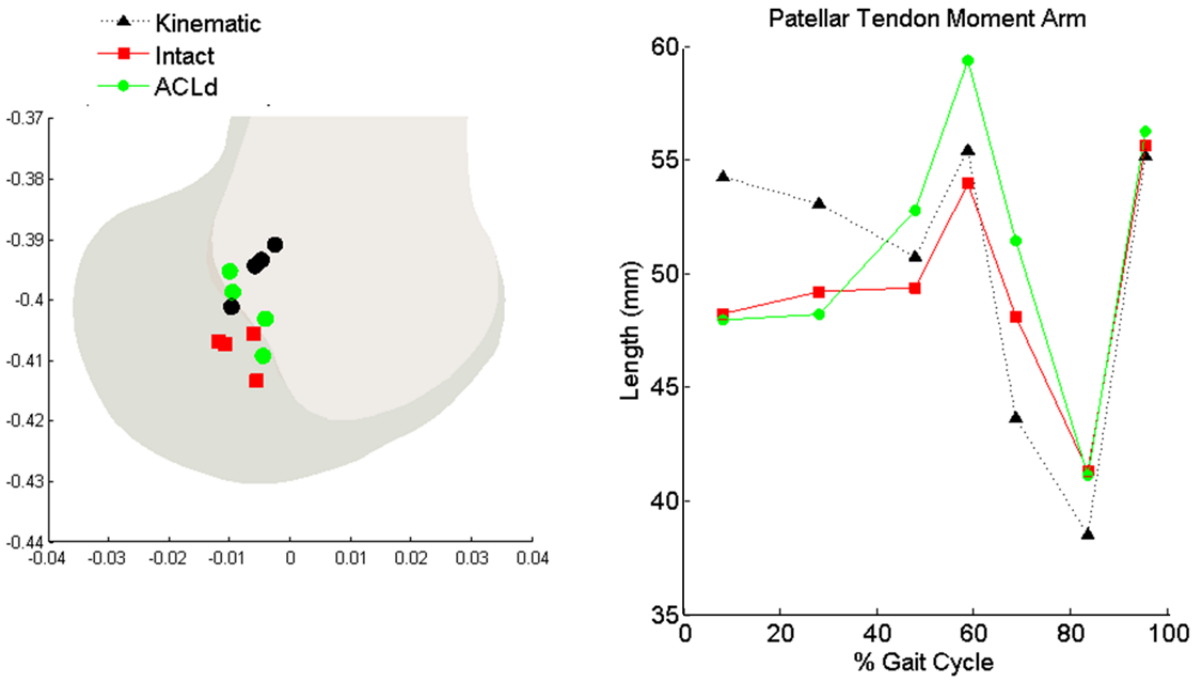


**Figure 46: (left) Intersection of the finite helical axis with the sagittal plane of the femur. During most of stance, the models with laxity showed an inferior shift in the tibiofemoral finite helical axis, (right) along with a decreased patellar tendon moment arm, compared to the kinematic model assumption.**

The forces in the ligaments were similar between the intact and ACLd model except during peak quadriceps activity where the ACLd knee showed a slight increase in the patellar tendon force (Figure 47). Notice that the kinematic model is not included since it did not contain ligaments.

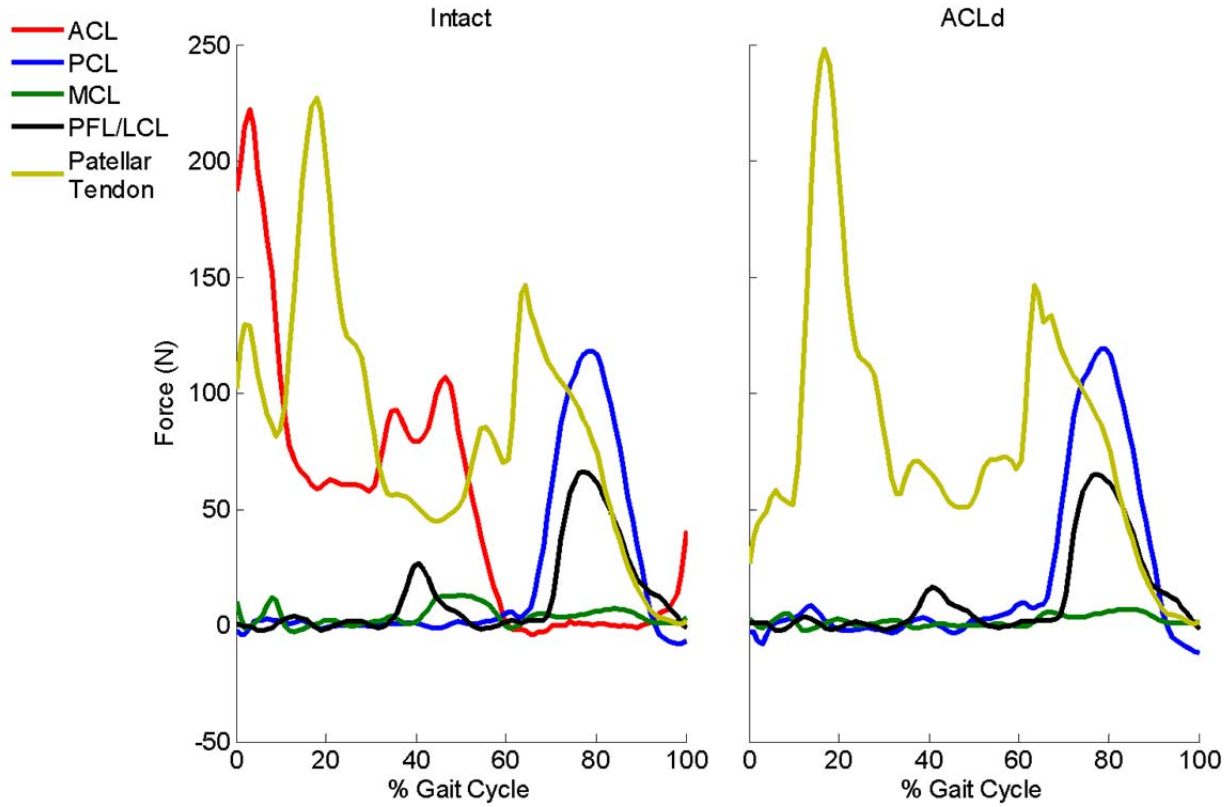


Figure 47: Ligament forces in the intact and ACLd models.

Compared to the kinematic assumption, the models with laxity predicted larger peak quadriceps loading in the vastus lateralis by 74 N (intact) and 14 N (ACLd) as well as in the rectus femoris by 163 N (intact) and 314 N (ACLd). At peak quadriceps loading, the model without the ACL showed a lower vastus lateralis force (60 N) as well as higher forces in the rectus femoris force (163 N), semimembranosus (20 N), semitendinosus (23 N), and biceps femoris long head (16 N), compared to the intact model.

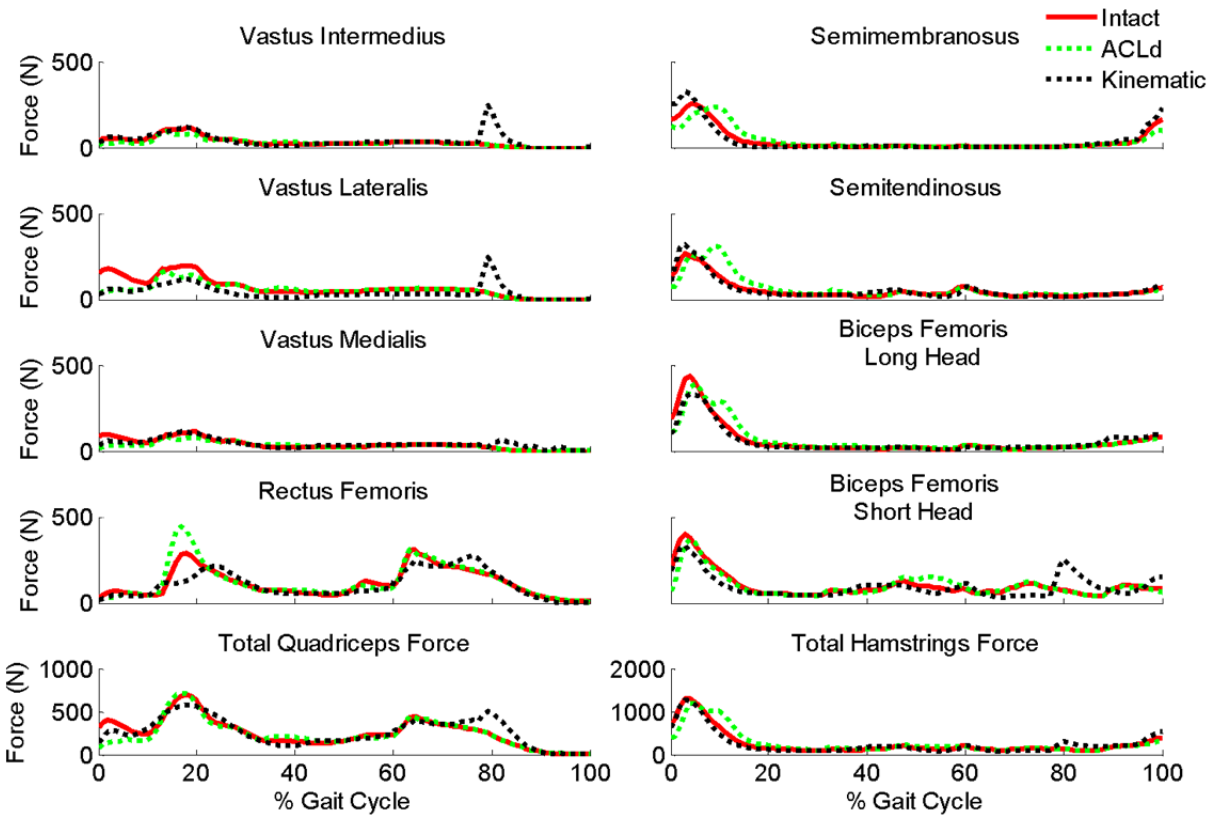


**Figure 48: The models with joint laxity predicted a larger peak quadriceps force during initial stance.**

## Cartilage Contact

The intact model predicted greater excursion of cartilage contact on the lateral tibia plateau (32 mm) than the medial plateau (14 mm). Similar cartilage contact excursion magnitudes are observed in the ACLd knee, but the cartilage contact is shifted posteriorly by an average of 5 and 4.5 mm on the medial and lateral tibial plateau, respectively. There was also a lateral shift in the cartilage contact in the ACLd model of 2.5 mm that arose from a medial shift in the tibia that persisted throughout stance (Figure 49).

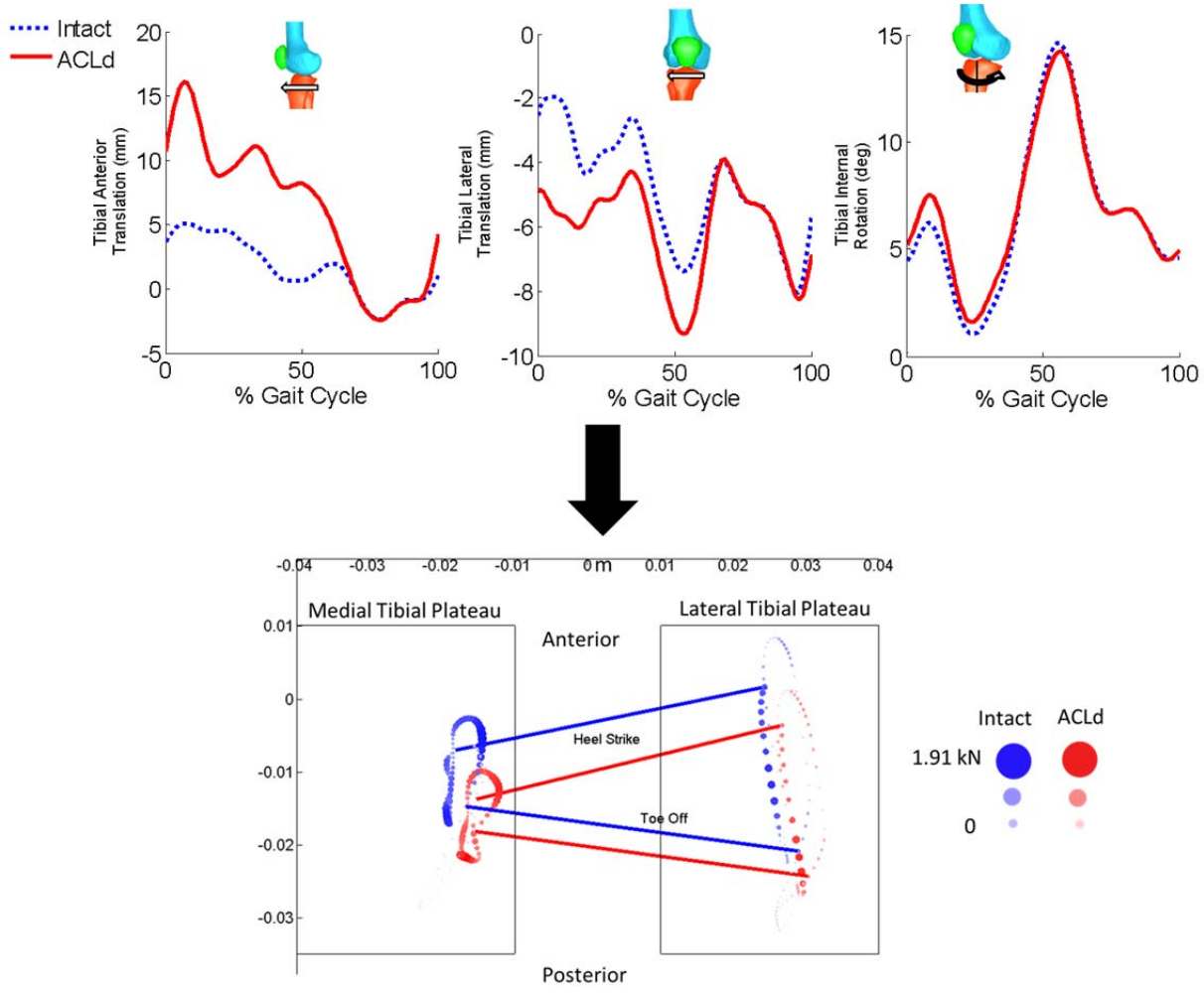


**Figure 49: Shown is the excursion of the center of cartilage contact on the medial and lateral tibia plateau through the stance phase of gait. Increased anterior tibial translation, medial translation, and internal rotation in the ACLd model (top) accompanied this posterior and lateral shift of the cartilage contact location (bottom).**

The model predicted net cartilage loading patterns that compare well to direct *in vivo* measures obtained with instrumented total knee replacements (Figure 50) (Fregly, et al., 2012). In the intact knee, peak loads were 3 times body weight (BW) during load acceptance and late swing phases of gait. Lateral and medial tibia plateau contact peaked at 2 and 2.5 times bodyweight during the load acceptance phase, respectively. Tibia plateau load magnitudes were generally similar in the ACLd knee model, with only a small (0.2BW = 147 N) increase in medial plateau loading in the load acceptance phase of gait.

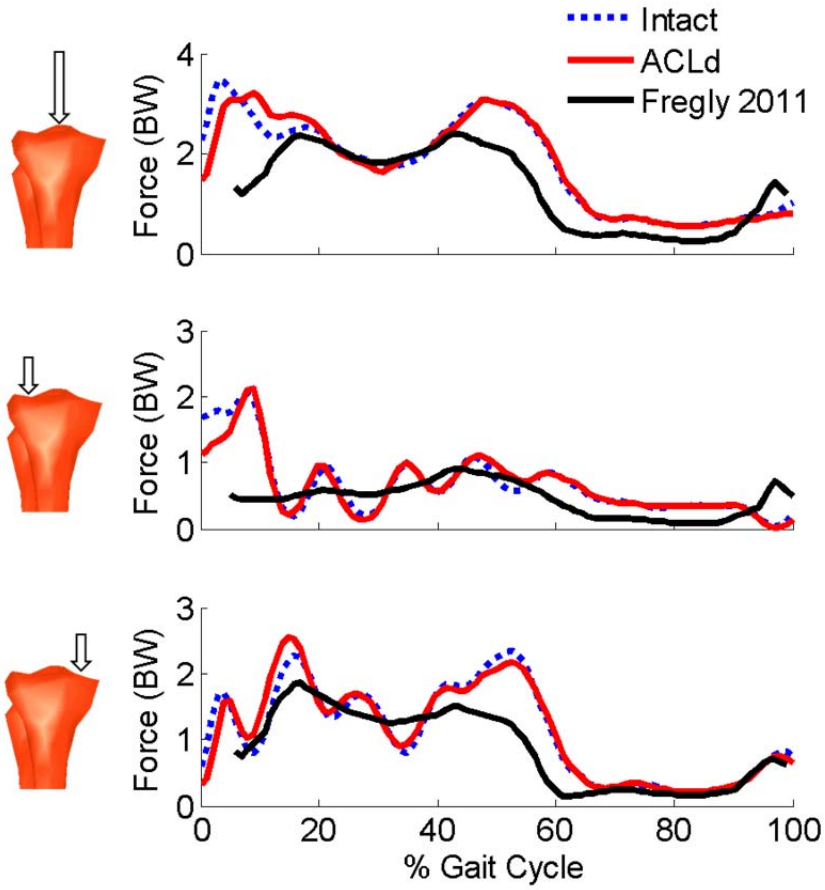


**Figure 50: Shown are model predictions of net cartilage loading (top plot), and the relative loading on the lateral (middle) and medial (bottom) tibia plateau. Model predictions are generally consistent with the medial-lateral load distribution observed in (Fregly, et al., 2012). In the ACLd model, cartilage compressive loading patterns are generally similar with only slight increased lateral compartment loading after heel strike.**

## Discussion

Co-simulation is an important computational tool that can be used to predict soft tissue loading within the context of whole body movement. In this study, we used a co-simulation framework to investigate how normal and pathological joint laxity could affect muscle force and cartilage load predictions during gait. Our results show that a model with normal knee laxity predicts tibiofemoral kinematic patterns that differ markedly from the passive envelope of motion (Blankevoort, et al., 1988), but are generally consistent with direct *in vivo* measures during gait (Lafortune, et al., 1992). We show that these altered tibiofemoral kinematics can diminish the patellar tendon moment arm and hence necessitate an increase in vastii and rectus femoris loading from what would be assumed with traditional gait models. Simulating gait with an ACL deficient knee resulted in substantial changes in tibiofemoral kinematics that moved tibia cartilage contact posteriorly. Hence, the co-simulation modeling framework provides a powerful consistent approach of assessing how neural and mechanical factors can affect knee soft tissue loading, which is important for investigating the causes and treatments of knee injuries.

The models with laxity predicted larger quadriceps forces than the kinematic model. This is due to the change in patellar tendon moment arm between the models. Joint laxity diminished the capacity of the patellar tendon to generate an extension torque, therefore the vastii and rectus femoris forces were increased to compensate and produce the same flexion/extension moment. This highlights the importance of considering the effect of load-dependent changes in knee kinematics on soft tissue loading, which is not considered in gait simulation models that utilize kinematic knees (Fernandez and Pandy, 2006; Shelburne, et al., 2005a).

Compared to the intact model, the ACLd joint exhibited increased anterior translation and internal rotation, which agrees with the literature (Georgoulis, et al., 2003; Masouros, et al., 2010;

Shelburne, et al., 2005a). These kinematic changes resulted in a posterior and lateral shift of the cartilage contact locations in the ACLd knee, which agrees with (Li, et al., 2006). Li highlighted the importance of the lateral shift, suggesting that this may cause contact between the femur and medial tibial spine, a site of osteophyte formation in ACLd patients (Li, et al., 2006). However, the limited tibial geometry used in our model cannot be used to investigate this further.

The ACLd model also showed an increase in hamstring force, which is in agreement with the findings of (Beard, et al., 1996; Berchuck, et al., 1990) using EMG. A slight decrease in vastii loading of the ACLd model was also observed, which is consistent with the idea of quadriceps avoidance (Alkjaer, et al., 2003; Berchuck, et al., 1990). However, the ACLd model predicted a simultaneous increase in rectus femoris force.

Cartilage loading slightly increased in the medial compartment of the ACLd knee, which is consistent with osteoarthritis developing mostly in the medial compartment (Vincent, et al., 2012). However, this is often explained by the knee adduction moment of the ground reaction force (Vincent, et al., 2012). Our framework provides a direct estimation without the need for this surrogate measure and suggests changes in muscle forces after ligament injury may be more important to cartilage loading than previously thought.

Compared to an intact knee, the ACLd knee has been shown to exhibit increased knee flexion angles during gait, which we did not account for in this study (Devita, et al., 1997). We did this to isolate the effect of joint laxity on muscle forces. Chapter 3 and 4 discuss the limitations of the model (i.e. no menisci, planar tibial plateaus). A limitation of the CMC approach is that we only considered one possibility of muscle force distribution and assumed that both populations, the intact and ACLd, used the same cost function.

This is the first the first study to use a modified CMC algorithm to co-simulate soft tissue loads and musculoskeletal dynamics during gait. This study shows that accounting for these knee mechanics is

important when predicting secondary joint kinematics and muscle forces, especially in cases of ligament injury. This framework provides a powerful tool to study how ligament surgeries and injuries lead to long-term complications (e.g. osteoarthritis) and to investigate the effectiveness of treatment strategies.

# Chapter 6: Conclusion

Musculoskeletal simulations of gait are commonly used to estimate soft tissue loads such as muscle forces and ligament strains and stresses. Typically, muscle forces are calculated using a simplified knee joint model that behaves independently of load. These muscle forces are then used as boundary conditions for a more detailed joint model to compute soft tissue loads. However, we have shown *in vivo* knee kinematics and extensor function are load-dependent in physiological loading conditions (Chapter 4). By simultaneously solving for muscle forces and soft tissue loads, we developed a co-simulation framework to predict the load-dependence of knee mechanics as seen *in vivo*.

The co-simulation framework was used to assess how the load-dependent behavior of the knee affects predicted muscle forces during gait simulations. The kinematic joint assumption under predicted quadriceps forces during the weight-acceptance phase of gait (Chapter 5) and cannot predict alterations in muscle forces that arise from varying laxity. This is important to consider clinically. The ACLd model showed a large increase in rectus femoris force from the intact model and a slight increase in medial cartilage contact loading. We also predicted ACL-deficiency to change cartilage loading locations posteriorly and medially. These predictions of cartilage loading are consistent with the initiation of osteoarthritis (Andriacchi, et al., 2004; Chaudhari, et al., 2008; Vincent, et al., 2012).

Overall, we have shown the kinematic joint assumption does not represent *in vivo* behavior and introduces errors into model predictions of muscle force, kinematics, and knee extensor function. To overcome this, we have developed a co-simulation framework that incorporates the load-dependent behavior of the knee while solving for muscle forces. This provides a powerful tool to evaluate the effectiveness of rehabilitation strategies and treatment. For example, what muscle patterns could be used to reduce anterior translation in the ACLd knee and possibly avoid surgery? This framework could also be used to optimize surgical parameters to restore normal joint function after injury. For example, it

provides insight on how to make surgical decisions such as what the best tunnel placement is for a single bundle ACL reconstruction to restore normal cartilage loading. However, before surgery can be simulated, further work should be done to refine the knee model. This would include adding a detailed description of the tibial articular geometry and patellofemoral joint along with ligament wrapping about the bones and incorporation of menisci. Also, it is important to understand how model predictions are influenced by parameters set in the model (e.g. ligament properties, cartilage properties, geometry, etc.). Therefore, it would be useful to use a Monte Carlo analysis to investigate how uncertainties in model parameters propagate to model predictions.

# Appendix A: Ligament Properties

Ligaments have been modeled as nonlinear springs (Figure 51) in mathematical joint models. This appendix summarizes values used for stiffness and reference strains in the literature (Table 8 through Table 12) as well as those measured from *ex vivo* and *in vivo* studies (Table 13 through Table 19). The reference strain is the strain in the ligament when the knee is fully extended.

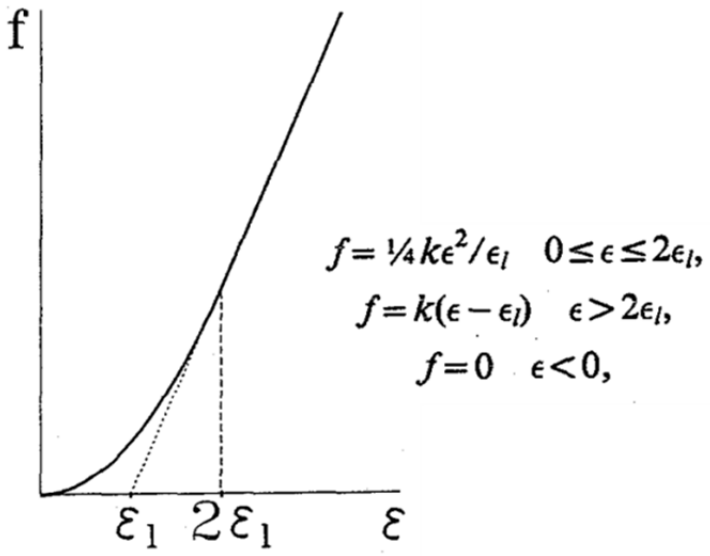


**Figure 51: Figure from (Blankevoort and Huiskes, 1991). Ligaments were modeled with a nonlinear force (f) – strain (ε) curve. $\varepsilon_l$ is the transition strain, ε the current ligament strain calculated from zero-load length and current length, k the ligament stiffness, and f the force.**

Table 8: Review of ACL bundles and properties used in mathematical knee models

| Bundle | Stiffness (N) | Reference Strain (-) |
|---|---|---|
| **aACL** | 1000 (Shelburne, et al., 2011; Shelburne, et al., 2004; Shelburne, et al., 2006)<br>5000 (Amiri, et al., 2006; Blankevoort and Huiskes, 1991; Blankevoort and Huiskes, 1996; Blankevoort, et al., 1991b)<br>1500 (Kim, 1996; Pandy, et al., 1997; Shelburne and Pandy, 1997; Shelburne and Pandy, 2002)<br>3803 (Shin, et al., 2007) | 0.093 (Shelburne, et al., 2011; Shelburne, et al., 2004; Shelburne, et al., 2006)<br>0.06 (Blankevoort and Huiskes, 1991; Blankevoort, et al., 1991b)<br>0.02 (Kim, 1996; Pandy, et al., 1997; Shelburne and Pandy, 1997; Shelburne and Pandy, 2002; Shin, et al., 2007)<br>0.031 (Amiri, et al., 2006)<br>0 (Abdel-Rahman and Hefzy, 1998) |
| **pACL** | 1500 (Shelburne, et al., 2011; Shelburne, et al., 2004; Shelburne, et al., 2006)<br>5000 (Amiri, et al., 2006; Blankevoort and Huiskes, 1991; Blankevoort and Huiskes, 1996; Blankevoort, et al., 1991b)<br>1600 (Kim, 1996; Pandy, et al., 1997; Shelburne and Pandy, 1997; Shelburne and Pandy, 2002)<br>3738 (Shin, et al., 2007) | 0.083 (Shelburne, et al., 2011; Shelburne, et al., 2004; Shelburne, et al., 2006)<br>0.1 (Blankevoort and Huiskes, 1991; Blankevoort, et al., 1991b)<br>0.02 (Kim, 1996; Shelburne and Pandy, 1997; Shelburne and Pandy, 2002; Shin, et al., 2007)<br>0.01 (Pandy, et al., 1997)<br>0.012 (Amiri, et al., 2006)<br>0.051 (Abdel-Rahman and Hefzy, 1998) |
| **1 bundle** | 3041 (Trent, et al., 1976)<br>3000 (Wismans, 1980)<br>7200 (Andriacchi, et al., 1983) | 0.05 (Wismans, et al., 1980) |
| **10 bundles** | 5000 (for each bundle) (Amiri, et al., 2007) | aACL: 0, 0.15, 0, 0 (Amiri, et al., 2007)<br>iACL: 0.15, 0, 0 (Amiri, et al., 2007)<br>pACL: 0.15, 0, 0.15 (Amiri, et al., 2007) |

Table 9: Review of PCL bundles and properties used in mathematical knee models

| Bundle | Stiffness (N) | Reference Strain (-) |
|---|---|---|
| **aPCL** | 2600 (Kim, 1996; Pandy, et al., 1997; Shelburne, et al., 2011; Shelburne and Pandy, 1997; Shelburne and Pandy, 2002; Shelburne, et al., 2004; Shelburne, et al., 2006)<br>9000 (Amiri, et al., 2006; Blankevoort and Huiskes, 1991; Blankevoort and Huiskes, 1996; Blankevoort, et al., 1991b)<br>4348 (Shin, et al., 2007) | -0.39 (Shelburne, et al., 2011; Shelburne, et al., 2004; Shelburne, et al., 2006)<br>-0.24 (Blankevoort and Huiskes, 1991; Blankevoort, et al., 1991b)<br>-0.21 (Kim, 1996; Shelburne and Pandy, 1997; Shelburne and Pandy, 2002)<br>-0.23 (Pandy, et al., 1997)<br>-0.1 (Amiri, et al., 2006; Shin, et al., 2007)<br>0.004 (Abdel-Rahman and Hefzy, 1998) |
| **pPCL** | 1900 (Kim, 1996; Pandy, et al., 1997; Shelburne, et al., 2011; Shelburne and Pandy, 1997; Shelburne and Pandy, 2002; Shelburne, et al., 2004; Shelburne, et al., 2006)<br>9000 (Amiri, et al., 2006; Blankevoort and Huiskes, 1991; Blankevoort and Huiskes, 1996; Blankevoort, et al., 1991b)<br>1580 (Shin, et al., 2007) | -0.12 (Shelburne, et al., 2011; Shelburne, et al., 2004; Shelburne, et al., 2006)<br>-0.03 (Blankevoort and Huiskes, 1991; Blankevoort, et al., 1991b)<br>0.02 (Kim, 1996; Pandy, et al., 1997; Shelburne and Pandy, 1997; Shelburne and Pandy, 2002)<br>-0.1 (Amiri, et al., 2006)<br>0.05 (Abdel-Rahman and Hefzy, 1998)<br>-0.02 (Shin, et al., 2007) |
| **1 bundle** | 4483 (Trent, et al., 1976)<br>4500 (Wismans, 1980)<br>14300 (Andriacchi, et al., 1983) | -0.01 (Wismans, et al., 1980) |
| **9 bundles** | 9000 (for each bundle) (Amiri, et al., 2007) | aPCL: -0.05, -0.05, -0.05 (Amiri, et al., 2007)<br>iPCL: -0.05, -0.057, -0.05 (Amiri, et al., 2007)<br>pPCL: -0.063 -0.237, -0.1 (Amiri, et al., 2007) |

Table 10: Review of MCL bundles and properties used in mathematical knee models

| Bundle | Stiffness (N) | Reference Strain (-) |
|---|---|---|
| **aMCL** | 2500 (Kim, 1996; Pandy, et al., 1997; Shelburne, et al., 2011; Shelburne and Pandy, 1997; Shelburne and Pandy, 2002; Shelburne, et al., 2004; Shelburne, et al., 2006)<br>2750 (Blankevoort and Huiskes, 1991; Blankevoort and Huiskes, 1996; Blankevoort, et al., 1991b) | -0.017 (Shelburne, et al., 2011; Shelburne, et al., 2004; Shelburne, et al., 2006)<br>0.04 (Blankevoort and Huiskes, 1991; Blankevoort, et al., 1991b)<br>0.02 (Shelburne and Pandy, 1997; Shelburne and Pandy, 2002)<br>0.05 (Kim, 1996) |
| **cMCL** | 3000 (Kim, 1996; Pandy, et al., 1997; Shelburne, et al., 2011; Shelburne and Pandy, 1997; Shelburne and Pandy, 2002; Shelburne, et al., 2004; Shelburne, et al., 2006)<br>2750 (Blankevoort and Huiskes, 1991; Blankevoort and Huiskes, 1996; Blankevoort, et al., 1991b) | 0.044 (Shelburne, et al., 2011; Shelburne, et al., 2004; Shelburne, et al., 2006)<br>0.04 (Blankevoort and Huiskes, 1991; Blankevoort, et al., 1991b; Kim, 1996; Pandy, et al., 1997; Shelburne and Pandy, 1997; Shelburne and Pandy, 2002)<br>0.02 (Pandy, et al., 1997) |
| **pMCL** | 2500 (Kim, 1996; Pandy, et al., 1997; Shelburne, et al., 2011; Shelburne and Pandy, 1997; Shelburne and Pandy, 2002; Shelburne, et al., 2004; Shelburne, et al., 2006)<br>2750 (Blankevoort and Huiskes, 1991; Blankevoort and Huiskes, 1996; Blankevoort, et al., 1991b) | 0.049 (Shelburne, et al., 2011; Shelburne, et al., 2004; Shelburne, et al., 2006)<br>0.03 (Blankevoort and Huiskes, 1991; Blankevoort, et al., 1991b)<br>0.02 (Kim, 1996; Pandy, et al., 1997; Shelburne and Pandy, 1997; Shelburne and Pandy, 2002) |
| **aCM** | 2000 (Kim, 1996; Pandy, et al., 1997; Shelburne, et al., 2011; Shelburne and Pandy, 1997; Shelburne and Pandy, 2002; Shelburne, et al., 2004; Shelburne, et al., 2006) | -0.274 (Shelburne, et al., 2011; Shelburne, et al., 2004; Shelburne, et al., 2006)<br>-0.08 (Kim, 1996; Pandy, et al., 1997; Shelburne and Pandy, 1997; Shelburne and Pandy, 2002) |
| **pCM** | 4500 (Kim, 1996; Pandy, et al., 1997; Shelburne, et al., 2011; Shelburne and Pandy, 1997; Shelburne and Pandy, 2002; Shelburne, et al., 2004; Shelburne, et al., 2006) | -0.061 (Shelburne, et al., 2011; Shelburne, et al., 2004; Shelburne, et al., 2006)<br>0.03 (Kim, 1996; Pandy, et al., 1997; Shelburne and Pandy, 1997; Shelburne and Pandy, 2002) |
| **1 bundle** | 5160 (Trent, et al., 1976)<br>8000 (Wismans, 1980)<br>8200 (Andriacchi, et al., 1983) | |

| Bundle | Stiffness (N) | Reference Strain (-) |
|---|---|---|
| **4 bundles** | 2750 (for each bundle) (Amiri, et al., 2006; Amiri, et al., 2007) | aMCL: 0.1 (Amiri, et al., 2007)<br>iMCL: 0.1, 0.1 (Amiri, et al., 2007)<br>pMCL: 0.1 (Amiri, et al., 2007)<br><br>pMCL: 0.05 (Amiri, et al., 2006)<br>aMCL: -0.04 (Amiri, et al., 2006)<br>oMCL: 0.031 (Amiri, et al., 2006)<br>dMCL: 0.049 (Amiri, et al., 2006) |
| **2 bundles** | | AMC: -0.03 (Wismans, et al., 1980)<br>PMC: 0.05 (Wismans, et al., 1980) |
| **3 bundles** | oMCL: 742 (Shin, et al., 2007)<br>aMCL: 1270 (Shin, et al., 2007)<br>dMCL: 4201 (Shin, et al., 2007) | oMCL: 0.031 (Abdel-Rahman and Hefzy, 1998)<br>0.02 (Shin, et al., 2007)<br>aMCL: 0.94 (Abdel-Rahman and Hefzy, 1998)<br>0.02 (Shin, et al., 2007)<br>dMCL: 0.049 (Abdel-Rahman and Hefzy, 1998)<br>0.02 (Shin, et al., 2007) |

Table 11: Review of LCL bundles and properties used in mathematical knee models

| Bundle | Stiffness (N) | Reference Strain (-) |
|---|---|---|
| **1 bundle** | 4000 (Shelburne, et al., 2011; Shelburne, et al., 2004; Shelburne, et al., 2006)<br>2000 (Amiri, et al., 2006; Kim, 1996; Pandy, et al., 1997; Shelburne and Pandy, 1997; Shelburne and Pandy, 2002)<br>3051 (Trent, et al., 1976)<br>3000 (Wismans, 1980)<br>7300 (Andriacchi, et al., 1983) | 0.056 (Shelburne, et al., 2011; Shelburne, et al., 2004; Shelburne, et al., 2006)<br>0.02 (Kim, 1996; Pandy, et al., 1997; Shelburne and Pandy, 1997; Shelburne and Pandy, 2002; Shin, et al., 2007)<br>0.05 (Abdel-Rahman and Hefzy, 1998; Amiri, et al., 2006; Wismans, et al., 1980) |
| **3 bundles** | 2000 for each (Blankevoort and Huiskes, 1991; Blankevoort and Huiskes, 1996; Blankevoort, et al., 1991b) | aLC: -0.25 (Blankevoort and Huiskes, 1991; Blankevoort, et al., 1991b)<br>sLC: -0.05 (Blankevoort and Huiskes, 1991; Blankevoort, et al., 1991b)<br>pLC: 0.08 (Blankevoort and Huiskes, 1991; Blankevoort, et al., 1991b) |
| **4 bundles** | 2000 (for each bundle) (Amiri, et al., 2007) | aLCL: 0.071 (Amiri, et al., 2007)<br>sLCL: 0.064 (Amiri, et al., 2007)<br>pLCL: 0.1 (Amiri, et al., 2007) |

Table 12: Review of posterior capsule bundles and properties used in mathematical knee models

| Bundle | Stiffness (N) | Reference Strain (-) |
|---|---|---|
| **mCap** | 2500 (Shelburne, et al., 2011; Shelburne, et al., 2004; Shelburne, et al., 2006)<br>1500 (Kim, 1996; Pandy, et al., 1997) | 0.077 (Shelburne, et al., 2011; Shelburne, et al., 2004; Shelburne, et al., 2006)<br>0.06 (Kim, 1996; Pandy, et al., 1997)<br>0.05 (Wismans, et al., 1980) |
| **lCap** | 2500 (Shelburne, et al., 2011; Shelburne, et al., 2004; Shelburne, et al., 2006)<br>1500 (Kim, 1996; Pandy, et al., 1997) | 0.064 (Shelburne, et al., 2011; Shelburne, et al., 2004; Shelburne, et al., 2006)<br>0.06 (Kim, 1996; Pandy, et al., 1997)<br>0.05 (Wismans, et al., 1980) |
| **2 anterior/posterior bundles** | 1000 for each (Blankevoort and Huiskes, 1991; Blankevoort and Huiskes, 1996; Blankevoort, et al., 1991b; Wismans, 1980) | aCM: -0.18 (Blankevoort and Huiskes, 1991; Blankevoort, et al., 1991b)<br>pCM: -0.04 (Blankevoort and Huiskes, 1991; Blankevoort, et al., 1991b) |
| **Posteromedial capsule (2 bundles, anterior/posterior)** | 1000 (for each bundle) (Amiri, et al., 2007) | 0.1, 0.1 (Amiri, et al., 2007) |
| **4 bundles** | lPC: 1300 (Amiri, et al., 2006)<br>mPC: 1300 (Amiri, et al., 2006)<br>1oblPC: 2750 (Amiri, et al., 2006)<br>2oblPC: 2750 (Amiri, et al., 2006)<br>mPC: 2009 (Shin, et al., 2007)<br>lPC: 2176 (Shin, et al., 2007)<br>oPC: 1352 (Shin, et al., 2007)<br>aPC: 1293 (Shin, et al., 2007) | lPC: 0.05 (Amiri, et al., 2006)<br>0.08 (Abdel-Rahman and Hefzy, 1998)<br>mPC: 0.05 (Amiri, et al., 2006)<br>0.08 (Abdel-Rahman and Hefzy, 1998)<br>1oblPC: 0.05 (Amiri, et al., 2006)<br>2oblPC: 0.042 (Amiri, et al., 2006)<br>oblPopPC: 0.08 (Abdel-Rahman and Hefzy, 1998)<br>acrPopPC: 0.07 (Abdel-Rahman and Hefzy, 1998)<br>mPC: 0.02 (Shin, et al., 2007)<br>lPC: 0.02 (Shin, et al., 2007)<br>oPC: 0.02 (Shin, et al., 2007)<br>aPC: 0.02 (Shin, et al., 2007) |

Table 13: Review of ligament lengths at extension and slack lengths from ex vivo and in vivo studies

| Ligament | Slack Length (mm) | Length at Extension (mm) |
|---|---|---|
| **Patellar tendon** | 44.5 – 57.8 *ex vivo* (Butler, et al., 1986)<br>41.5 *in vivo* (Hansen, et al., 2006)<br>42.8 – 48.8 *in vivo* (Sheehan and Drace, 2000) | 45 – 52 *ex vivo* (Van Eijden, et al., 1987) |
| **ACL** | 25.4 – 31.7 *ex vivo* (Butler, et al., 1986)<br>22.15 – 36.5 *ex vivo* (Hashemi, et al., 2005) | 32.5 +- 2.8 for amACL *in vivo* (Li, et al., 2004)<br>27.6 +- 5.2 for plACL *in vivo* (Li, et al., 2004) |
| **PCL** | 29.5 – 32 *ex vivo* (Butler, et al., 1986) | 25 – 31 for alPCL *ex vivo* (Ahmad, et al., 2003)<br>27.8 +- 2.1 for alPCL *in vivo* (Li, et al., 2004)<br>32 – 46 for pmPCL *ex vivo* (Ahmad, et al., 2003)<br>28.8 +- 1.9 for pmPCL *in vivo* (Li, et al., 2004) |
| **LCL** | 48.7 – 50.9 *ex vivo* (Butler, et al., 1986) | 59 – 74 *ex vivo* (Meister, et al., 2000)<br>46.5 – 61 *in vivo* (Park, et al., 2005)<br>51.5 – 64 *ex vivo* (Sugita and Amis, 2001) |
| **PFL** | - | 42.6 +- 7.3 *ex vivo* (Sugita and Amis, 2001) |
| **MCL** | - | 61 – 94 in superficial layer *in vivo* (Park, et al., 2005)<br>80 – 112 in middle layer *ex vivo* (Robinson, et al., 2004)<br>29 – 33 in deep layer *ex vivo* (Robinson, et al., 2004)<br>21 – 38 in deep layer *in vivo* (Park, et al., 2005) |
| **Iliotibial Band** | 490 – 540 *ex vivo* (Birnbaum, et al., 2004) | |

**Table 14: Review of patellar tendon stiffness values derived from experimentally measured values**

| Young's Modulus (MPa) | Cross Sectional Area of Specimen ($mm^2$) | Specimen (fascicle, bone-ligament-bone, etc.) | Derived Stiffness (modulus * area), (N) | Stiffness (N/mm) | Specimen Length (mm) | Derived Stiffness (stiffness N/mm * length mm), (N) | Source |
|---|---|---|---|---|---|---|---|
| **1.09e3 +- 0.12**<br>**1.09e3 +- 0.10**<br>**0.91e3 +- 0.07**<br>**0.99e3 +- 0.07** | 163 +- 12 | *In vivo* | 177670<br>177670<br>148330<br>161370 | 4334 +- 562<br>4273 +- 533<br>3725 +- 293<br>4195 +- 369 | 41.5 +- 0.9 (slack length) | 179861<br>177329.5<br>154587.5<br>174092.5 | (Hansen, et al., 2006) |
| **363.3 +- 93.7 (200 N, unconditioned)**<br>**459.3 +- 83.2 (800 N, unconditioned)**<br>**565.9 +- 159.1 (200 N, preconditioned)**<br>**811.7 +- 154.1 (800 N, preconditioned)** | 36.8 +- 5.7 (unconditioned)<br>34.5 +- 4.4 (preconditioned) | Bone-ligament-bone complex | 13369.44<br>16902.24<br>19523.55<br>28003.65 | - | - | - | (Stäubli, et al., 1999) |
| **660 +- 266 (younger group)**<br>**504 +- 222 (older group)** | 14.6 +- 0.3<br>14.8 +- 0.2 | Central third of bone-ligament-bone complex | 9636<br>7459 | - | - | - | (Johnson, et al., 1994) |
| **307 +- 17** | 76 | Bone-ligament-bone complex | 23332 | - | - | - | (Haut and Powlison, 1990) |
| **643 +- 53** | 1.20 +- 0.3<br>1.86 +- 0.3<br>1.65 +- 0.2 | Fascicles | 771.6/fascicle * 5 fascicles = 3858<br>1195.98/fascicle * 8 fascicles = 9567.84<br>1060.95/fascicle * 6 fascicles = 6365.7 | - | 44.5 +- 1.1<br>57.8 +- 1.4<br>55.6 +- 2.4 | - | (Butler, et al., 1986) |
| **305.5 +- 59.0 (central)**<br>**361.1 +- 34.4 (medial)** | 50.5 +- 2.8 (central)<br>49.9 +- 3.8 (medial) | Central or medial third of bone-ligament-bone complex | 15427.75 (central)<br>18010.89 (medial) | - | 48.7 +- 3.8 (central)<br>48.8 +- 2.8 (medial) | - | (Butler, et al., 1984) |
| - | 50.5 +- 2.8 (central)<br>49.9 +- 3.8 (medial) | Bone-ligament-bone complex (divided into 3 portions) | - | 685.2 +- 85.6 (central)<br>650.6 +- 85.4 (medial) | 48.7 +- 3.8 (central)<br>48.8 +- 2.8 (medial) | 33369.24<br>31749.28 | (Noyes, et al., 1984) |

Table 15: Review of ACL stiffness values derived from experimentally measured values

| Young's Modulus (MPa) | Cross Sectional Area of Specimen ($mm^2$) | Specimen (fascicle, bone-ligament-bone, etc.) | Derived Stiffness (modulus * area), (N) | Stiffness (N/mm) | Specimen Length (mm) | Derived Stiffness (stiffness N/mm * length mm), (N) | Source |
|---|---|---|---|---|---|---|---|
| **128 +- 35**<br><br>**99 +- 50** | 72.91 +- 18.90 (male)<br>57.32 +- 15.70 (female) | Bone-ligament-bone complex | 9332.48<br><br>5674.68 | 308 +- 89<br><br>199 +- 88 | 29.61 +- 2.70<br>27.04 +- 2.90 | 9119.88<br><br>5381.96 | (Chandrashekar, et al., 2006) |
| - | - | Bone-ligament-bone complex | - | 167 - 205 | *27 | 4509 - 5535 | (Jones, et al., 1995) |
| **283.1 +- 114.4**<br>**285.9 +- 140.6**<br>**154.9 +- 119.5** | 2.92 +- 1.61<br>1.91 +- 1.02<br>4.57 +- 3.84 | Bundles | 1949.21 | - | 32.5 +- 4.7<br>28.6 +- 5.1<br>24.6 +- 4.5 | - | (Butler, et al., 1992) |
| - | - | Bone-ligament-bone complex | - | 242 +- 28 (young)<br>220 +- 24 (middle)<br>180 +- 25 (older) | *27 | 6534<br><br>5940<br><br>4860 | (Woo, et al., 1991) |
| **275**<br>**350**<br>**325** | 1.29 +- 0.13<br>1.17 +- 0.39<br>1.91 +- 0.09 | Fascicles (3) | 1064.25<br>1228.5<br>1862.25 | - | 25.4 +- 3.7<br>31.7 +- 2.4<br>29.1 +- 3.1 | - | (Butler, et al., 1986) |
| - | **44.4 +- 4.0** | **??** | **-** | **182 +- 33** | **26.9 +- 1.1** | **4895.8** | **(Noyes, et al., 1984)** |
| - | **-** | Bone end-ligament-bone end | **-** | **81 +- 36** | **26 +- 5** | **2106** | **(Marinozzi, et al., 1983)** |
| **65.3 +- 24 (older)**<br>**111 +- 26 (younger)** | 57.5 +- 16.2<br><br>44.4 +- 9.7 | ?? | 3754.75<br><br>4928.4 | 129 +- 39<br><br>182 +- 56 | 27.5 +- 2.8<br><br>26.9 +- 1.5 | 3547.5<br><br>4895.8 | (Noyes and Grood, 1976) |
| - | - | Bone-ligament-bone complex | - | 138.2 | *27 | 3731.4 | (Trent, et al., 1976) |

*Average ACL length used ~27 mm (Noyes, et al., 1984)

Table 16: Review of PCL stiffness values derived from experimentally measured values

| Young's Modulus (MPa) | Cross Sectional Area of Specimen ($mm^2$) | Specimen (fascicle, bone-ligament-bone, etc.) | Derived Stiffness (modulus * area), (N) | Stiffness (N/mm) | Specimen Length (mm) | Derived Stiffness (stiffness N/mm * length mm), (N) | Source |
|---|---|---|---|---|---|---|---|
| **248 +- 119 (aPCL)**<br>**145 +- 69 (pPCL)** | 43.0 +- 11.3<br><br>10.0 +- 1.3 | Bone-ligament-bone complex | 10664<br><br>1450 | 347 +- 140<br><br>77 +- 32 | 35.3 +- 3.4<br><br>33.8 +- 3.2 | 12249.1<br><br>2602.6 | (Race and Amis, 1994) |
| **375**<br>**450**<br>**280** | 1.91 +- 0.24<br>1.12 +- 0.45<br>2.40 +- 0.24 | Fascicles (3)<br>Fascicles (2)<br>Fascicles (3) | 2148.75<br>1008<br>2016 | - | 32.0 +- 4.5<br>31.4 +- 0.3<br>29.5 +- 2.7 | - | (Butler, et al., 1986) |
| - | - | Bone end-ligament-bone end | - | 145 +- 66 | 25 +- 4 | 3625 | (Marinozzi, et al., 1983) |
| - | - | Bone-ligament-bone complex | - | 179.5 | *31 | 5564.5 | (Trent, et al., 1976) |

*Average PCL length used ~31 mm.

Table 17: Review of LCL and PFL stiffness values derived from experimentally measured values

| Young's Modulus (MPa) | Cross Sectional Area of Specimen ($mm^2$) | Specimen (fascicle, bone-ligament-bone, etc.) | Derived Stiffness (modulus * area), (N) | Stiffness (N/mm) | Specimen Length (mm) | Derived Stiffness (stiffness N/mm * length mm), (N) | Source |
|---|---|---|---|---|---|---|---|
| - | - | Bone-ligament-bone complex | - | 58.1 +- 22.8<br>43.6 +- 14.8 | 59.2 +- 4.3 (LCL)<br>42.6 +- 7.3 (PFL) | 3439.52<br>1857.36 | (Sugita and Amis, 2001) |
| **430**<br>**370**<br>**360** | 1.54 +- 0.21<br>2.98 +- 0.07<br>3.73 +- 0.23 | Fascicles (2) | 1324.4<br>2205.2<br>2686.6 | - | 50.9 +- 2.4<br>52.9 +- 1.9<br>48.7 +- 0.6 | - | (Butler, et al., 1986) |
| - | - | Bone end-ligament-bone end | - | 60 +- 22 (LCL) | 56 +- 10 | 3360 | (Marinozzi, et al., 1983) |
| - | - | Bone-ligament-bone complex | - | 59.8 (LCL) | *50 | 2990 | (Trent, et al., 1976) |

*Average LCL length used ~50 mm.

Table 18: Review of MCL stiffness values derived from experimentally measured values

| Young's Modulus (MPa) | Cross Sectional Area of Specimen ($mm^2$) | Specimen (fascicle, bone-ligament-bone, etc.) | Derived Stiffness (modulus * area), (N) | Stiffness (N/mm) | Specimen Length (mm) | Derived Stiffness (stiffness N/mm * length mm), (N) | Source |
|---|---|---|---|---|---|---|---|
| **332.2 +- 58.3** | 2.7475 | Dog bone shaped specimens | 912.7 | - | 15.07 +- 2.46 | - | (Quapp and Weiss, 1998) |
| - | - | Bone end-ligament-bone end | - | 60 +- 22 | 104 +- 4 | 6240 | (Marinozzi, et al., 1983) |
| - | - | Bone-ligament-bone complex | - | 70.6 | *100 | 7060 | (Trent, et al., 1976) |

*Average MCL length used ~100 mm.

Table 19: Review of Iliotibial band stiffness values derived from experimentally measured values

| Young's Modulus (MPa) | Cross Sectional Area of Specimen ($mm^2$) | Specimen (fascicle, bone-ligament-bone, etc.) | Derived Stiffness (modulus * area), (N) | Stiffness (N/mm) | Specimen Length (mm) | Derived Stiffness (stiffness N/mm * length mm), (N) | Source |
|---|---|---|---|---|---|---|---|
| **564.7 +- 193.8** | 8.46 | Tissue sample | 4777.36 | - | - | - | (Steinke, et al., 2012) |
| - | - | Entire tissue | - | 17 | 510 | 8670 | (Birnbaum, et al., 2004) |

# Appendix B: Lower Extremity Model

## Introduction

A model of the lower extremity was used within forward dynamic simulations to compute simulated kinematics resulting from muscle excitations (Figure 52).

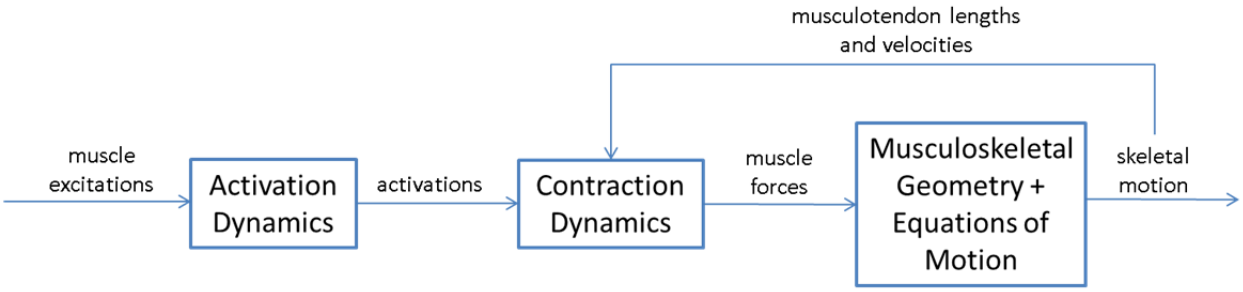


**Figure 52: Schematic of a forward dynamic simulation. Figure adapted from (Pandy, 2001).**

## Anthropometry

A generic model of the lower extremity was created using the SIMM Dynamics Pipeline (MusculoGraphics, Evanston, IL, USA). The geometry included rigid models of the pelvis, femur, tibia, fibula, patella, talus, calcaneus, metatarsals, and phalanges digitized from a male cadaver, dimensions of which were consistent with a 170 cm tall male (Arnold, et al., 2010; Gordon, 1989) and mass properties of a 75 kg male (Table 20) (de Leva, 1996a).

Table 20: Inertia properties of body segments

| Segment | Mass (kg) | Moment of Inertia about segment center of mass (kg*m$^2$) |
|---|---|---|
| **Pelvis** | 8.38 | Ixx = 0.0540<br>Iyy = 0.0613<br>Izz = 0.0673 |
| **Femur** | 10.1 | Ixx = 0.172<br>Iyy = 0.0353<br>Izz = 0.172 |
| **Tibia** | 3.25 | Ixx = 0.030<br>Iyy = 0.00516<br>Izz = 0.0312 |
| **Patella** | 0.488 | Ixx = 0.0001<br>Iyy = 0.0001<br>Izz = 0.0001 |
| **Talus** | 0.045 | Ixx = 0.000003<br>Iyy = 0.000001<br>Izz = 0.000003 |
| **Calcaneus** | 1.24 | Ixx = 0.00127<br>Iyy = 0.00323<br>Izz = 0.00374 |
| **Toes (metatarsals and phalanges)** | 0.198 | Ixx = 0.000202<br>Iyy = 0.000517<br>Izz = 0.000595 |

Bone embedded reference frames (Figure 53) were adapted from (Arnold, et al., 2010). Each coordinate system was oriented so that in anatomical position, x-axis pointed anteriorly, y-axis superiorly, and the z-axis to the right. These were also aligned with the inertial axes of each bone. The origin of the pelvis frame was positioned at the midpoint of a line connecting the left and right anterior superior iliac spines (ASIS). The ASIS and pubic tubercles formed the yz plane. The femur origin was placed at the center of the femoral head. The y-axis was placed along a line connecting the femoral head and the center of the femoral condyles. The patella origin was located at the proximal pole of the patella. The tibia origin was placed at the midpoint of the femoral condyles with the knee in full extension. The talus origin was positioned at the midpoint of a line between the apices of the medial

and lateral malleoli. The toe origin was located at the distal end of the second metatarsal. The calcaneus origin was positioned on the most inferior, lateral point on the posterior surface of the calcaneus.

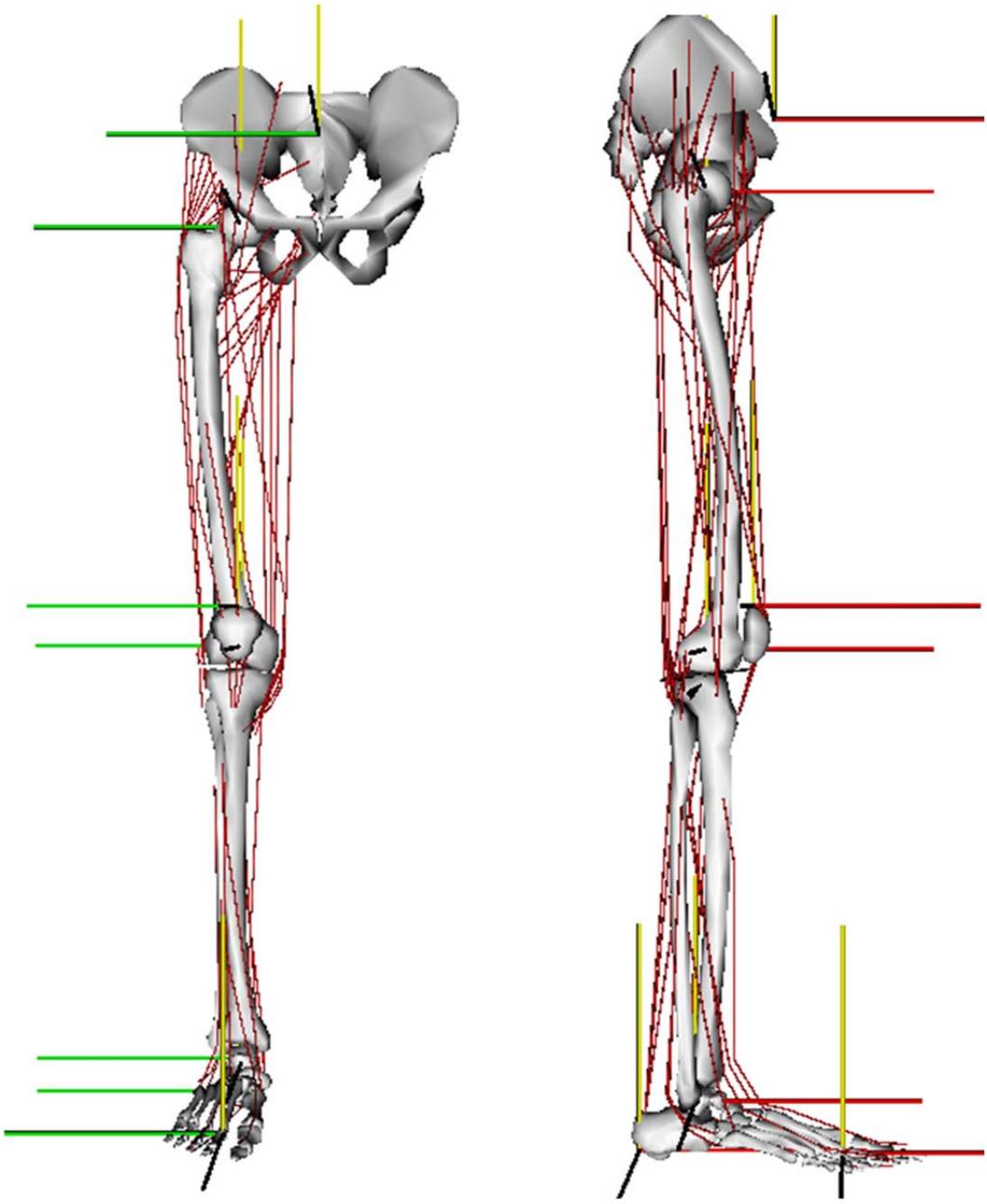

**Figure 53: Bone embedded frames of the lower extremity model, adapted from (Arnold, et al., 2010).**

The segments were connected via joints using the definitions of SD/Fast (Symbolic Dynamics, Mountainview CA, USA). The generalized coordinates of each joint described the motion of the 'body' with respect to the 'inboard body' (Figure 54). For example, knee motion was described as the motion of the tibia relative to the femur. The joint location was placed at segment origins and defined relative to the segment's center of mass (Figure 54 and Table 21).

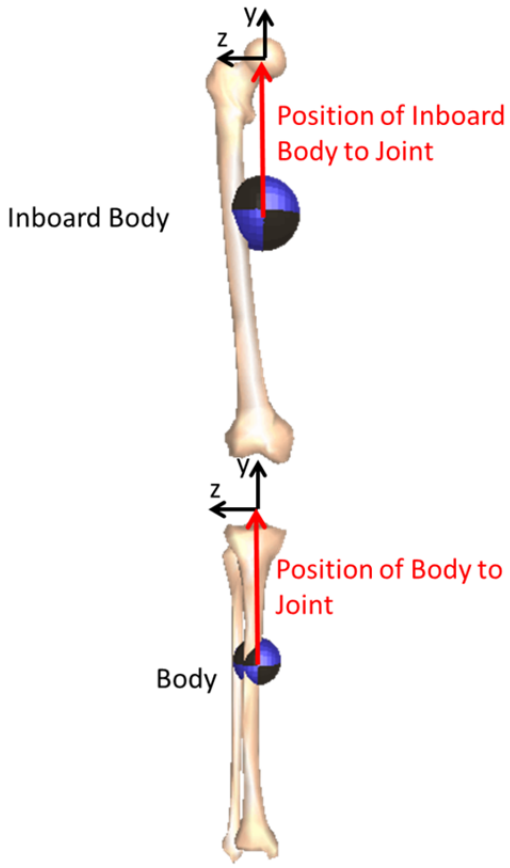


**Figure 54: Joint location at the segment origin was defined relative to each segment's center of mass when the segment axes were aligned.**

**Table 21: Joint parameters**

| Joint | Body | Inboard Body | Body to Joint | Inboard Body to Joint |
|---|---|---|---|---|
| **Pelvis/ground** | Pelvis | Ground | (0.0893, 0.0258, 0) | (0, 0, 0) |
| **Hip** | Femur | Pelvis | (0, 0.162, 0) | (0.0330, -0.0527, 0.0773) |
| **Tibiofemoral** | Tibia | Femur | (0, 0.172, 0) | (0, 0.162, 0) |
| **Patellofemoral** | Patella | Femur | (0, 0, 0) | (0, 0.162, 0) |
| **Ankle** | Talus | Tibia | (-0.0055, -0.0023, 0) | (-0.01, -0.228, 0) |
| **Subtalar** | Calcaneus | Talus | (-0.102, -0.0156, 0) | (-0.0543, -0.0443, 0.00792) |
| **Metatarsophalangeal** | Toes | Calcaneus | (-0.0307, 0.0026, -0.0105) | (0.0769, 0.0176, 0.00108) |

The pelvis was connected to the ground with a bushing joint, which consisted of three translational and three rotational (body fixed 3-1-2 rotation) degrees of freedom. The hip was modeled as a gimbal joint (i.e. ball and socket joint) with three rotational (body fixed 3-1-2 rotation) degrees of freedom. The knee was represented with a six degree of freedom tibiofemoral joint and a patellofemoral joint that was defined as a planar joint with two translational and one rotational degree of freedom (Chapter 3). The ankle joint was modeled as a pin joint, one rotational degree of freedom, about a vector defined as -0.105**x** - 0.174**y** + 0.979**z** in the tibial reference frame. The subtalar joint was also defined as a pin joint about a vector 0.787**x** + 0.605**y** - 0.121**z** defined in the talus frame and the metatarsophalangeal a pin joint about a vector 0.581**x** - 0.814**z** defined in the calcaneal frame. The orientation of the rotation axes for the ankle complex was based on (Delp, 1990; Inman, 1976).

## Muscles

Adapted from (Arnold, et al., 2010), the model included 44 muscles of the right lower limb, where the musculotendon path from origin to insertion was approximated as line segments for each muscle (Figure 53). Wrapping surfaces were included to avoid penetration with bones and deeper soft tissues (Table 22 through Table 24).

Table 22: Wrapping objects located in the pelvis

| | Wrapping Object | Geometry | Orientation and Location in Bone Reference Frame |
|---|---|---|---|
| 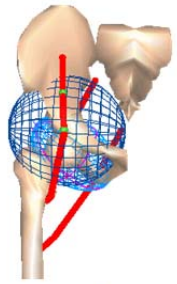 | Iliacus | Ellipsoid with radius (0.0549, 0.0665, 0.071) | Translated (-0.0685, -0.0557, 0.0756) in pelvis |
| 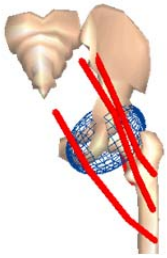 | Glueteus maximus superior, middle, and inferior | Ellipsoid with radius (0.04, 0.04, 0.06) | XYZ body rotated by (-36.5, 21.98, -39.24) and translated (-0.0795, -0.0825, 0.0665) in pelvis |

Table 23: Wrapping objects located in the femur

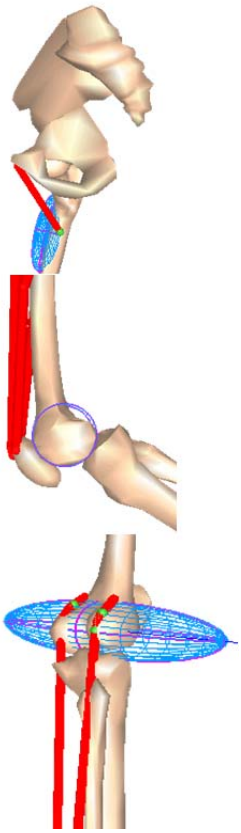

| Wrapping Object | Geometry | Orientation and Location in Bone Reference Frame |
|---|---|---|
| Pectineus | Ellipsoid with radius (0.0166, 0.05, 0.0131) | XYZ body rotated by (6.4, 0, 12.1) and translated (0.00762, -0.0853, 0.0290) |
| Vastii (intermedius, lateralis, medialis) and rectus femoris | Cylinder with radius 0.025 | XYZ body rotated by (-3.572, 2.908, -51.138) and translated (0.00359, -0.403, 0.00209) in femur |
| Gastrocnemius lateral and medial head | Ellipsoid with radius (0.03, 0.025, 0.15) | XYZ body rotated by (3.38, -5, 1.33) and translated (0.01, -0.408, 0.0003) in femur |

Table 24: Wrapping objects located in the tibia

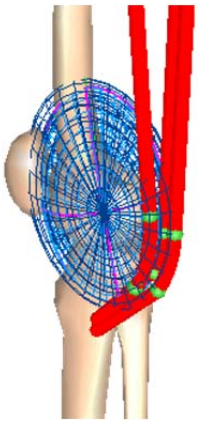

| Wrapping Object | Geometry | Orientation and Location in Bone Reference Frame |
|---|---|---|
| Gracilis | Ellipsoid with radius (0.036, 0.0635, 0.0533) | XYZ body rotated by (0, 0, -10.5) and translated (0, 0, 0) |
| Semimembranosus | Ellipsoid with radius (0.0352, 0.0602, 0.0489) | XYZ body rotated by (0, 0, -17) and translated (0, 0, 0) |
| Semitendinosus | Ellipsoid with radius (0.0425, 0.069, 0.0572) | XYZ body rotated by (0, 0, -15.5) and translated (0, 0, 0) |

The muscles were modeled using a lumped-parameter model (Figure 55) where the distributed properties of all the fibers in a muscle are lumped into a single ideal fiber (Zajac, 1989). The tendon was modeled as a nonlinear spring in series with a contractile element and passive spring component. This lumped-parameter model assumed that all fibers were the same length, same pennation angle, etc. and muscle strength was the summed strength of the individual fibers.

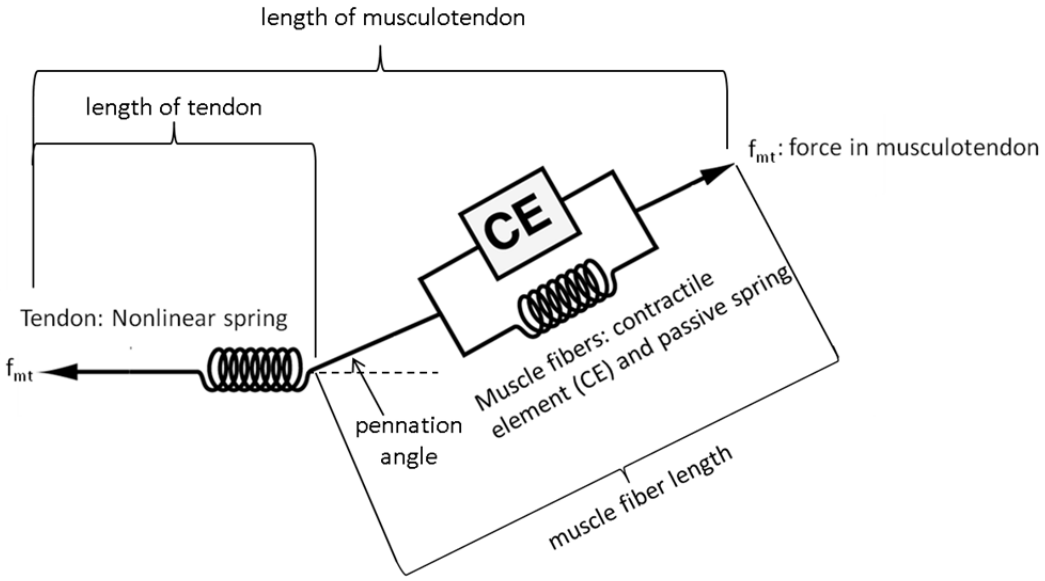


**Figure 55: Hill lumped-parameter model of muscle.**

Muscle dynamics were composed of two parts: the activation dynamics and contraction dynamics (Thelen, 2003). The activation dynamics were governed by a non-linear first-order differential equation (Eq 9) where the motor unit excitation, u, was the input for each of the muscles.

$$\dot{a}=\frac{u-a}{\tau_a(a,u)} \qquad \text{Eq 9}$$

In Eq 9, a is the muscle activation and $\tau_a$ a time constant defined by Eq 10.

$$\tau_a(a,u)=\begin{cases}\tau_{act}(0.5+1.5a); & u>a\\ \frac{\tau_{deact}}{0.5+1.5a}; & u\leq a\end{cases} \qquad \text{Eq 10}$$

where $\tau_{act}$ is the activation time constant and $\tau_{deact}$ the deactivation time constant. The activation and deactivation time constants were set at 0.015 and 0.05 sec, respectively. The motor unit excitation and

muscle activation were constrained between 0 and 1, inclusive. Time constants are needed because a muscle cannot generate force or relax immediately. To generate force, the excitation of motor units induces action potentials in the muscle fibers and causes the release of calcium ions into the muscle cells. These ions initiate cross bridge formation, the force producing mechanism of the muscle **(Guyton, 1986)**. The muscle relaxes with the reuptake of the calcium ions.

The passive force-length properties of muscles were described using an exponential equation (Eq 11).

$$\overline{F^{PE}} = \frac{e^{k^{PE}(\overline{L^M}-1)/\varepsilon_0^M}-1}{e^{k^{PE}}-1} \quad \text{Eq 11}$$

where $\overline{F^{PE}}$ is the force in the passive element normalized by maximum isometric force, $k^{PE}$ is a shape factor, $\varepsilon_0^M$ is the passive muscle strain at the maximum isometric force, and $\overline{L^M}$ the muscle fiber length normalized by the optimal fiber length. The passive muscle strain at maximum isometric force, $\varepsilon_0^M$, was set to 0.6 for all muscles except for the rectus femoris and vastii, which were set at 1.0. The shape factor, $k^{PE}$, was 4.0 for all muscles but 10.0 for the vastii.

The force in the contractile element of the muscle was related to muscle fiber length by Eq 12.

$$f = e^{-(\overline{L^M}-1)^2/\gamma} \quad \text{Eq 12}$$

where f is a scale factor and $\gamma$ a shape factor. The shape factor was set at 0.35 for all muscles.

The force generating property of the tendon was represented by a non-linear toe region, followed by a linear force-strain relationship (Eq 13).

$$\overline{F^T} = \begin{cases} \dfrac{\overline{F_{toe}^T}}{e^{k_{toe}}-1}\left(e^{\frac{k_{toe}\varepsilon^T}{\varepsilon_{toe}^T}}-1\right); & \varepsilon^T \le \varepsilon_{toe}^T \\ k_{lin}(\varepsilon^T-\varepsilon_{toe}^T)+\overline{F_{toe}^T}; & \varepsilon^T > \varepsilon_{toe}^T \end{cases} \quad \text{Eq 13}$$

where $\overline{F^T}$ is the force in the tendon normalized by maximum isometric force, $k_{toe}$ a shape factor (set at 2.0), $\overline{F_{toe}^T}$ normalized force at which the curve reaches the toe strain $\varepsilon_{toe}^T$, $k_{lin}$ a scale factor, and $\varepsilon^T$ tendon strain. The transition from the toe to linear region was set at a normalized tendon force 0.33.

The strain at which the tendon reached maximum isometric force, $\varepsilon_0^T$, was 0.05. To avoid discontinuities at the transition, $\varepsilon_{toe}^T = 0.609\varepsilon_0^T$ and $k_{lin} = 1.712/\varepsilon_0^T$.

Contraction dynamics of the musculotendon unit, which incorporates the interaction of the contractile-passive element with the tendon, was represented by Eq 14.

$$V^M = (0.25 + 0.75a) V_{max}^M \frac{\overline{F^M} - af}{b} \quad \text{Eq 14}$$

Where $V^M$ is the muscle fiber velocity, $V_{max}^M$ is the maximum contraction velocity (set at 10.0), $\overline{F^M}$ the active muscle force normalized by maximum isometric force, and b computed using Eq 15.

$$b = \begin{cases} af + \frac{\overline{F^M}}{A_f}; & \overline{F^M} \leq af \\ \frac{(2 + \frac{2}{A_f})(af\overline{F_{len}^M} - \overline{F^M})}{\overline{F_{len}^M} - 1}; & \overline{F^M} > af \end{cases} \quad \text{Eq 15}$$

where $\overline{F_{len}^M}$ is the maximum normalized muscle force possible when the fiber is lengthening (set to 1.5) and $A_f$ is a shape factor (set to 0.3).

Muscle specific parameters were adapted from (Arnold, et al., 2010) (Table 25).

**Table 25: Muscle properties**

| Muscle | Maximum Isometric Muscle Force (N) | Optimal fiber length (cm) | Tendon slack length (cm) | Pennation angle (deg) | Locations of attachments in segment reference frames (m) |
|---|---|---|---|---|---|
| **Adductor brevis** | 607.4 | 10.3 | 3.6 | 6.1 | (-0.0191, -0.094, 0.0154) pelvis<br>(-0.002, -0.118, 0.0249) femur |
| **Adductor longus** | 799.4 | 10.8 | 13.0 | 7.1 | (-0.00758, -0.0889, 0.0189) pelvis<br>(0.0113, -0.239, 0.0158) femur |
| **Adductor magnus distal** | 648.4 | 17.7 | 9.0 | 13.8 | (-0.0740, -0.128, 0.0398) pelvis<br>(0.0113, -0.263, 0.0193) femur |
| **Adductor magnus ischial** | 648.4 | 15.6 | 22.1 | 11.9 | (-0.0896, -0.130, 0.0417) pelvis<br>(0.00481, -0.388, -0.0327) femur |

| Muscle | Maximum Isometric Muscle Force (N) | Optimal fiber length (cm) | Tendon slack length (cm) | Pennation angle (deg) | Locations of attachments in segment reference frames (m) |
|---|---|---|---|---|---|
| **Adductor magnus middle** | 648.4 | 13.8 | 4.8 | 14.7 | (-0.0527, -0.121, 0.0285) pelvis<br>(0.00242, -0.162, 0.0292) femur |
| **Adductor magnus proximal** | 648.4 | 10.6 | 4.3 | 22.2 | (-0.0310, -0.108, 0.0137) pelvis<br>(-0.0153, -0.0789, 0.0320) femur |
| **Biceps femoris long head** | 1410.4 | 9.8 | 32.2 | 11.6 | (-0.104, -0.119, 0.0586) pelvis<br>(-0.0317, -0.0425, 0.0333) tibia |
| **Biceps femoris short head** | 631.6 | 11.0 | 10.4 | 12.3 | (0.005, -0.211, 0.0234) femur<br>(-0.0301, -0.0419, 0.0318) tibia |
| **Extensor digitorum longus** | 690.8 | 6.9 | 36.7 | 10.8 | (-0.016, -0.116, 0.0205) tibia<br>(0.0164, -0.376, 0.0112) tibia<br>(0.0919, 0.036, 0.0008) calcaneus<br>(0.162, 0.0055, 0.013) calcaneus<br>(0.0003, 0.0047, 0.0153) toes<br>(0.0443, -0.0004, 0.025) toes |
| **Extensor hallucis longus** | 330.0 | 7.5 | 33.2 | 9.4 | (-0.014, -0.155, 0.0189) tibia<br>(0.007, -0.291, 0.0164) tibia<br>(0.02, -0.369, -0.0028) tibia<br>(0.097, 0.0389, -0.0211) calcaneus<br>(0.173, 0.0139, -0.028) calcaneus<br>(0.0298, 0.0041, -0.0245) toes<br>(0.0563, 0.0034, -0.0186) toes |
| **Flexor digitorum longus** | 548.8 | 4.5 | 37.8 | 13.6 | (-0.0023, -0.183, -0.0018) tibia<br>(-0.0176, -0.365, -0.0124) tibia<br>(0.0436, 0.0315, -0.028) calcaneus<br>(0.166, -0.0081, 0.0116) calcaneus<br>(-0.0019, -0.0078, 0.0215) toes<br>(0.0441, -0.006, 0.0242) toes |

| Muscle | Maximum Isometric Muscle Force (N) | Optimal fiber length (cm) | Tendon slack length (cm) | Pennation angle (deg) | Locations of attachments in segment reference frames (m) |
|---|---|---|---|---|---|
| **Flexor hallucis longus** | 873.6 | 5.3 | 35.6 | 16.9 | (-0.031, -0.216, 0.02) tibia<br>(-0.0242, -0.367, -0.0076) tibia<br>(0.0374, 0.0276, -0.0241) calcaneus<br>(0.104, 0.0068, -0.0256) calcaneus<br>(0.173, -0.0053, -0.0269) calcaneus<br>(0.0155, -0.0064, -0.0265) toes<br>(0.0562, -0.0102, -0.0181) toes |
| **Gastrocnemius lateral head** | 1212.8 | 5.9 | 36.9 | 12.0 | (-0.003, -0.381, 0.0277) femur<br>(0.0044, 0.031, -0.0053) calcaneus |
| **Gastrocnemius medial head** | 2616.0 | 5.1 | 38.9 | 9.9 | (0.008, -0.379, -0.0208) femur<br>(0.0044, 0.031, -0.0053) calcaneus |
| **Gemelli** | 218.0 | 2.4 | 3.9 | 0.0 | (-0.104, -0.0764, 0.0671) pelvis<br>(-0.0142, -0.0033, 0.0443) femur |
| **Gluteus maximus superior** | 1092.2 | 14.7 | 5.0 | 21.9 | (-0.123, 0.0345, 0.0563) pelvis<br>(-0.126, -0.0242, 0.0779) pelvis<br>(-0.0444, -0.0326, 0.0302) femur<br>(-0.0277, -0.0566, 0.047) femur |
| **Gluteus maximus middle** | 1561.0 | 15.7 | 7.3 | 21.9 | (-0.132, 0.0087, 0.0462) pelvis<br>(-0.134, -0.0609, 0.0813) pelvis<br>(-0.045, -0.0584, 0.0252) femur<br>(-0.0156, -0.102, 0.0419) femur |
| **Gluteus maximus inferior** | 1052.2 | 16.7 | 7.0 | 21.9 | (-0.13, -0.0525, 0.009) pelvis<br>(-0.127, -0.126, 0.0435) pelvis<br>(-0.0281, -0.113, 0.0094) femur<br>(-0.006, -0.142, 0.0411) femur |
| **Gluteus medius anterior** | 1762.2 | 7.3 | 5.7 | 20.5 | (-0.0445, 0.0245, 0.117) pelvis<br>(-0.0218, -0.0117, 0.0555) femur |

| Muscle | Maximum Isometric Muscle Force (N) | Optimal fiber length (cm) | Tendon slack length (cm) | Pennation angle (deg) | Locations of attachments in segment reference frames (m) |
|---|---|---|---|---|---|
| **Gluteus medius middle** | 1233.0 | 7.3 | 6.6 | 20.5 | (-0.085, 0.0316, 0.0675) pelvis<br>(-0.0258, -0.0058, 0.0527) femur |
| **Gluteus medius posterior** | 1404 | 7.3 | 4.6 | 20.5 | (-0.115, -0.0073, 0.0526) pelvis<br>(-0.0309, -0.0047, 0.0518) femur |
| **Gluteus minimus anterior** | 360.0 | 6.8 | 1.6 | 10.0 | (-0.0464, -0.0149, 0.104) pelvis<br>(-0.0072, -0.0104, 0.056) femur |
| **Gluteus minimus middle** | 380.0 | 5.6 | 2.6 | 0.0 | (-0.0616, -0.0142, 0.0971) pelvis<br>(-0.0096, -0.0104, 0.056) femur |
| **Gluteus minimus posterior** | 430.0 | 3.8 | 5.1 | 1.0 | (-0.0789, -0.0155, 0.0798) pelvis<br>(-0.0135, -0.0083, 0.055) femur |
| **Gracilis** | 274.6 | 22.8 | 16.9 | 8.2 | (-0.0474, -0.129, 0.0246) pelvis<br>(-0.0184, -0.0475, -0.0296) tibia<br>(0.00178, -0.0696, -0.0157) tibia |
| **Iliacus** | 1243.8 | 10.7 | 9.4 | 14.3 | (-0.0605, 0.0309, 0.0843) pelvis<br>(-0.0135, -0.0557, 0.0756) pelvis<br>(-0.0023, -0.0565, 0.0139) femur<br>(-0.0122, -0.0636, 0.0196) femur |
| **Pectineus** | 354 | 10.0 | 3.3 | 0.0 | (-0.0232, -0.0833, 0.0453) pelvis<br>(-0.00797, -0.0852, 0.0240) femur |
| **Peroneus brevis** | 611.8 | 4.5 | 14.8 | 11.5 | (-0.0243, -0.253, 0.0251) tibia<br>(-0.0339, -0.389, 0.0249) tibia<br>(-0.0285, -0.400, 0.0255) tibia<br>(0.0471, 0.027, 0.0233) calcaneus<br>(0.0677, 0.0219, 0.0343) calcaneus |

| Muscle | Maximum Isometric Muscle Force (N) | Optimal fiber length (cm) | Tendon slack length (cm) | Pennation angle (deg) | Locations of attachments in segment reference frames (m) |
|---|---|---|---|---|---|
| **Peroneus longus** | 1306.6 | 5.1 | 33.3 | 14.1 | (-0.02, -0.137, 0.0282) tibia<br>(-0.0317, -0.39, 0.0237) tibia<br>(-0.0272, -0.401, 0.024) tibia<br>(0.0438, 0.023, 0.0221) calcaneus<br>(0.0681, 0.0106, 0.0284) calcaneus<br>(0.0852, 0.0069, 0.0118) calcaneus<br>(0.120, 0.0085, -0.0184) calcaneus |
| **Peroneus tertius** | 180.0 | 7.9 | 10.0 | 13.0 | (-0.0149, -0.249, 0.0222) tibia<br>(0.0108, -0.382, 0.0225) tibia<br>(0.0857, 0.0228, 0.0299) calcaneus |
| **Piriformis** | 592.0 | 2.6 | 11.5 | 10.0 | (-0.102, -0.00653, 0.0135) pelvis<br>(-0.102, -0.0307, 0.0609) pelvis<br>(-0.0148, -0.0036, 0.0437) femur |
| **Psoas** | 959.4 | 11.7 | 9.7 | 10.7 | (-0.0606, 0.0619, 0.039) pelvis<br>(-0.0205, -0.0654, 0.0656) pelvis<br>(-0.0132, -0.0467, 0.0046) femur<br>(-0.0235, -0.0524, 0.0088) femur |
| **Quadratus femoris** | 508.0 | 5.4 | 2.4 | 0.0 | (-0.112, -0.115, 0.0517) pelvis<br>(-0.0358, -0.0355, 0.0361) femur |
| **Rectus femoris** | 1697.6 | 7.6 | 34.6 | 13.9 | (-0.024, -0.0388, 0.0933) pelvis<br>(0.01, -0.0035, 0.0007) patella<br>(0.0121, -0.0088, -0.001) patella |
| **Sartorius** | 227 | 40.3 | 11.0 | 1.3 | (-0.0195, -0.0156, 0.106) pelvis<br>(-0.003, -0.357, -0.0421) femur<br>(-0.0251, -0.0401, -0.0365) tibia<br>(-0.0159, -0.0599, -0.0264) tibia<br>(0.0136, -0.081, -0.0026) tibia |
| **Semimembranosus** | 2325.4 | 6.9 | 37.8 | 15.1 | (-0.0987, -0.114, 0.0614) pelvis<br>(-0.029, -0.0417, -0.0196) tibia |

| Muscle | Maximum Isometric Muscle Force (N) | Optimal fiber length (cm) | Tendon slack length (cm) | Pennation angle (deg) | Locations of attachments in segment reference frames (m) |
|---|---|---|---|---|---|
| **Semitendinosus** | 603.8 | 19.3 | 24.5 | 12.9 | (-0.104, -0.125, 0.0515) pelvis<br>(-0.0312, -0.0598, -0.0229) tibia<br>(0.0019, -0.0773, -0.0117) tibia |
| **Soleus** | 7171.8 | 4.4 | 28.2 | 28.3 | (-0.0076, -0.0916, 0.0098) tibia<br>(0.0044, 0.031, -0.0053) calcaneus |
| **Tensor fascia latae** | 310.0 | 9.5 | 45.0 | 3.0 | (-0.0311, 0.0214, 0.124) pelvis<br>(0.0294, -0.0995, 0.0597) femur<br>(0.0108, -0.041, 0.0346) tibia |
| **Tibialis anterior** | 1347.4 | 6.8 | 24.1 | 9.6 | (0.0154, -0.131, 0.0162) tibia<br>(0.0251, -0.191, 0.0128) tibia<br>(0.0233, -0.366, -0.0132) tibia<br>(0.117, 0.0178, -0.0305) calcaneus |
| **Tibialis posterior** | 1811.2 | 3.8 | 28.2 | 13.7 | (-0.0041, -0.130, 0.0103) tibia<br>(-0.0164, -0.366, -0.0175) tibia<br>(0.0417, 0.0334, -0.0286) calcaneus<br>(0.0772, 0.0159, -0.0281) calcaneus |
| **Vastus intermedius** | 2048.4 | 9.9 | 10.6 | 4.5 | (0.029, -0.192, 0.031) femur<br>(0.0335, -0.208, 0.0285) femur<br>(0.0058, -0.0045, -0.0006) patella |
| **Vastus lateralis** | 4510.8 | 9.9 | 13 | 18.4 | (0.0048, -0.185, 0.0349) femur<br>(0.0269, -0.259, 0.0409) femur<br>(0.0103, -0.0102, 0.0141) patella |
| **Vastus medialis** | 2887.4 | 9.7 | 11.2 | 29.6 | (0.014, -0.210, 0.0188) femur<br>(0.0356, -0.277, 0.0009) femur<br>(0.0063, -0.008, -0.017) patella |

# Appendix C: Computed Muscle Control

## Musculoskeletal Dynamics

The equations of motion for a system of bodies can be written as a second-order equation that involve matrices and vectors (Eq 16) (Thelen, Anderson et al. 2003; Erdemir, McLean et al. 2007):

$$\ddot{\vec{q}}=\vec{M}^{-1}(\vec{q})\,[\vec{G}(\vec{q})+\vec{C}(\vec{q},\dot{\vec{q}})+\vec{R}(\vec{q})*\vec{f}_{mt}+\vec{E}(\vec{q},\dot{\vec{q}})] \qquad \text{Eq 16}$$

where $\ddot{\vec{q}}$ are generalized accelerations, $\dot{\vec{q}}$ generalized velocities, , $\vec{q}$ generalized coordinates, $\vec{M}$ the mass matrix, $\vec{G}$ generalized forces from gravity, $\vec{C}$ generalized forces due to Coriolis and centripetal effects, $\vec{R}$ muscle moment arms, $\vec{f}_{mt}$ musculotendon forces, and $\vec{E}$ generalized forces from the external environment (e.g. force of the ground on the feet).

## CMC Basics

Computed muscle control (CMC) is an algorithm used to calculate a set of muscle excitation waveforms that will drive a musculoskeletal model to track a set of experimental kinematics. The algorithm consists of three general steps (Figure 56).

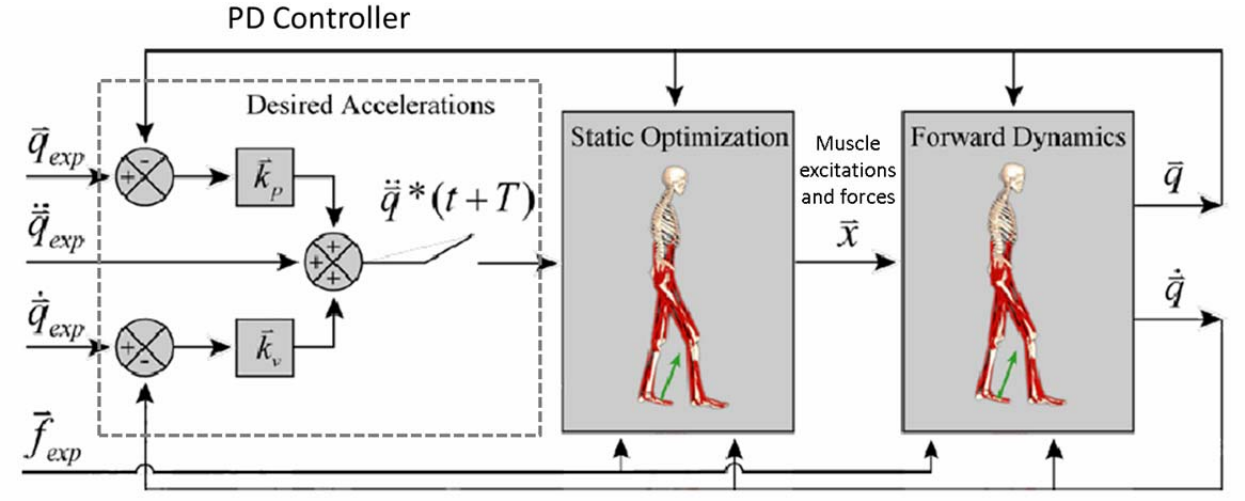


Figure 56: Schematic of computed muscle control adapted from (Thelen and Anderson, 2006b).

First, a controller is used to compute the desired accelerations needed to drive the model coordinates toward the given experimental coordinates. At time t in the simulation, the current simulated segment positions ($\vec{q}$) and velocities ($\dot{\vec{q}}$) are used in conjunction with the experimental segment positions ($\vec{q}_{exp}$), velocities ($\dot{\vec{q}}_{exp}$), and accelerations ($\ddot{\vec{q}}_{exp}$) to calculate desired segment accelerations ($\ddot{\vec{q}}^*$) that should be achieved a short amount of time later, t + T, to track the desired experimental motion (Eq 17), where $\vec{k}_v$ and $\vec{k}_p$ are feedback gains.

$$\ddot{\vec{q}}^{*}(t+T) = \ddot{\vec{q}}_{exp}(t+T) + \vec{k}_v\left[\dot{\vec{q}}_{exp}(t) - \dot{\vec{q}}(t)\right] + \vec{k}_p[\vec{q}_{exp}(t) - \vec{q}(t)] \quad \text{Eq 17}$$

Second, static optimization is used to compute actuator controls (e.g. muscle excitations), x in Figure 56, that will achieve the desired accelerations. Since there is muscle redundancy, there is not a unique set of controls that produces the desired accelerations. Thus, an optimization algorithm is implemented to find a set of muscle excitations that minimizes the sum of volume weighted squared activations (Thelen and Anderson, 2006b). The optimization is referred to as static because the cost function is based on measures that are evaluated at every instant in time. An example of a non-static measure would be maximum jump height found from evaluating kinematics measured over a finite time period. Third, a forward dynamics model is used to integrate forward in time to calculate the new model states. During the optimization step, CMC calculates the capacity of each muscle to accelerate the segments.

## Acceleration Capacity of Muscles

CMC was developed based on musculoskeletal models with kinematic joints. In such cases, the capacity of a muscle to induce accelerations can be directly computed at an instant in time by solving the whole body equations of motion (Eq 16).

This is no longer true when using a knee joint model with ligamentous constrains and cartilage contact loading. In our case, we use a discrete element cartilage contact model which determines contact loads based on the degree of overlap between cartilage surfaces (Anderson, et al., 2010c;

Blankevoort and Huiskes, 1991; Blankevoort, et al., 1991b; Caruntu and Hefzy, 2004; Kim, 1996; Pandy, et al., 1997; Shelburne, et al., 2004). The ligaments are described by nonlinear springs which must change length before loading changes. Hence, a change in kinematics is needed before the joint cartilage or ligament loads will change. For example, a change in vastii force will not affect patellar tendon loading instantaneously, since the ligament must first change length. For example, in the knee, a change in vastii force will instantly accelerate the patella. If there is a kinematic constraint between the patella and tibia, the tibia will also instantly accelerate. In a non-kinematic joint, the patellar tendon must stretch before inducing acceleration of the tibia. Therefore, the CMC algorithm for computing the acceleration capacity of muscles was modified by temporarily imposing kinematic constraints for the non-kinematic knee model.

## Example

Consider an example of a pendulum attached to a pivot by a spring and damper, where the spring and damper are also attached by a pivot to the mass (Figure 57). Computed muscle control can be used to calculate the required torque, T, and secondary kinematics (translations in the x and y direction) for a prescribed angle, θ.

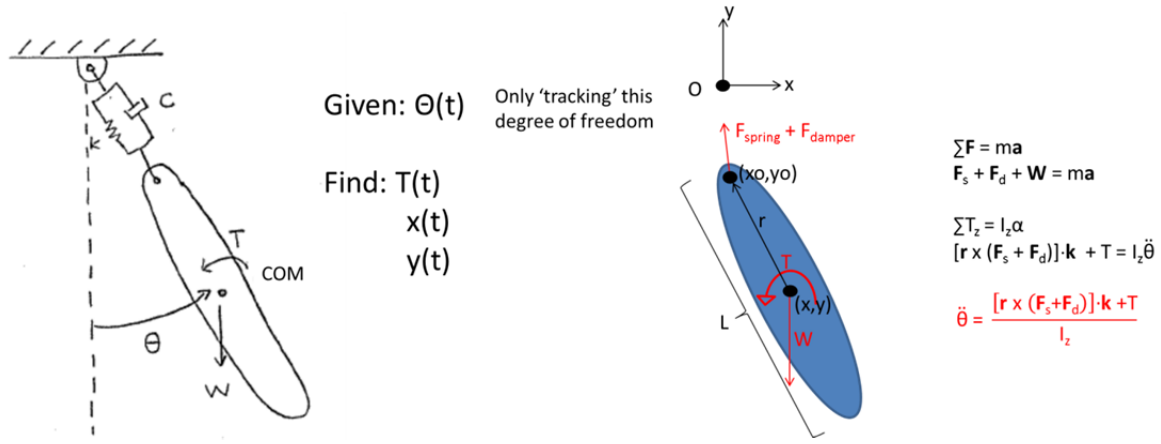


Figure 57: (left) Schematic of problem. (right) Free body diagram.

For every time in the simulation, the controller law (Eq 17) was used to compute the desired accelerations needed to drive the model coordinates to the given experimental coordinates (step 1 of CMC). Note this was only done for θ (i.e. q = θ in Eq 17), since this was the only degree of freedom being tracked. The torque needed to bring the current model θ back to the experimental θ was calculated (Figure 58). The time to bring the model back to the experimental configuration depends on the values used for the feedback gains. This is where optimization would be used if there were more than one actuator (step 2 of CMC). Then the torque was applied to the pendulum and the equations of motion integrated forward a small amount of time to get to a new configuration (step 3 of CMC).

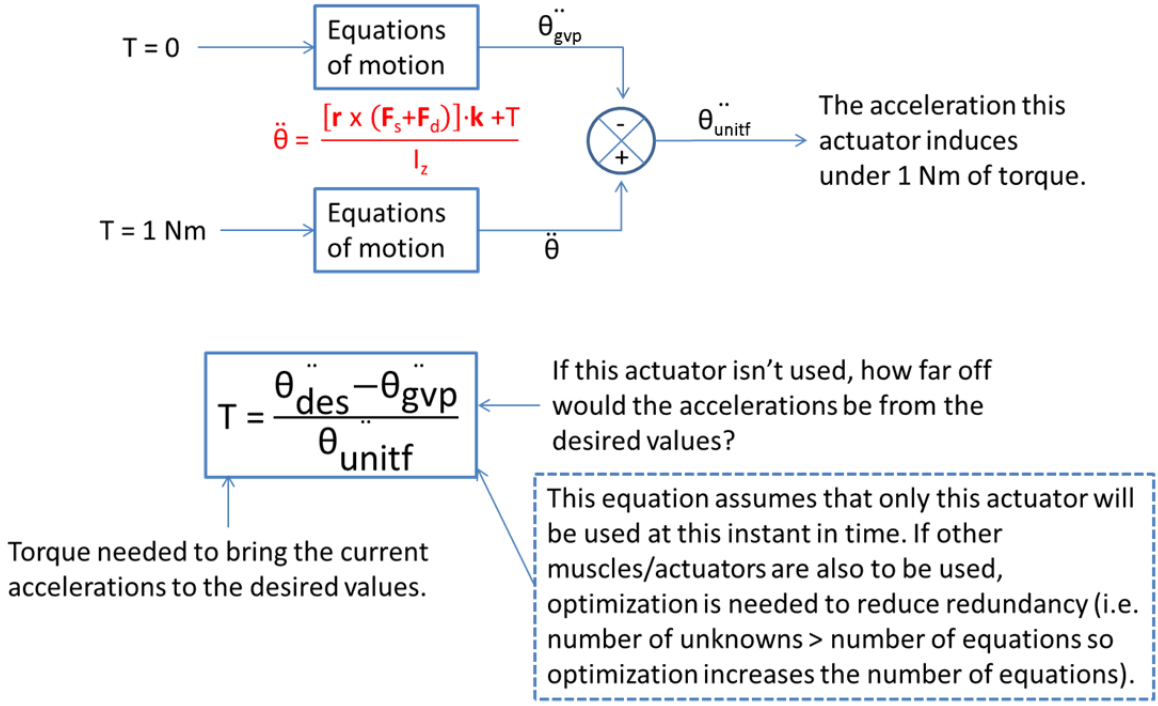


Figure 58: Calculating the required torque, T, to drive the pendulum to the prescribed motion.

# References

Aagaard, H. and Verdonk, R. 1999. Function of the normal meniscus and consequences of meniscal resection. Scand J Med and Sci in Sports 9, 134-140.

Abdel-Rahman, E. M. and Hefzy, M. 1998. Three-dimensional dynamic behaviour of the human knee joint under impact loading. Med Engr and Physics 20, 276-290.

Ahmad, C. S., Cohen, Z. A., Levine, W. N., Gardner, T. R., Ateshian, G. A. and Mow, V. C. 2003. Codominance of the Individual Posterior Cruciate Ligament Bundles. Am J Sports Med 31, 221.

Akbarshahi, M., Schache, A. G., Fernandez, J. W., Baker, R., Banks, S. and Pandy, M. G. 2010. Non-invasive assessment of soft-tissue artifact and its effect on knee joint kinematics during functional activity. J Biomech 43, 1292.

Alkjaer, T., Simonsen, E. B., Jørgensen, U. and Dyhre-Poulsen, P. 2003. Evaluation of the walking pattern in two types of patients with anterior cruciate ligament deficiency: copers and non-copers. Eur J App Physiol 89, 301-308.

Allen, A. A. and Caldwell, G. L. 1995. Anatomy and biomechanics of the meniscus. Op Tech in Orthop 5, 2-9.

Allen, C. R., Wong, E. K., Livesay, G., Sakane, M., Fu, F. H. and Woo, S. L. Y. 2000. Importance of the Medial Meniscus in the Anterior Cruciate Ligament-deficient Knee. J Orthop Research 18, 109-115.

Amiri, S., Cooke, D., Kim, I. Y. and Wyss, U. 2006. Mechanics of the passive knee joint. Part 1: the role of the tibial articular surfaces in guiding the passive motion. Proc of IMechEngr, Part H: J Engr in Med 220, 813-822.

Amiri, S., Cooke, D., Kim, I. Y. and Wyss, U. 2007. Mechanics of the passive knee joint. Part 2: interaction between the ligaments and the articular surfaces in guiding the joint motion. Proc of IMechEngr, Part H: J Engr in Med 221, 821-832.

Anderson, C. J., Westerhaus, B. D., Pietrini, S. D., Ziegler, C. G., Wijdicks, C. A., Johansen, S., Engebretsen, L. and LaPrade, R. F. 2010a. Kinematic Impact of Anteromedial and Posterolateral Bundle Graft Fixation Angles on Double-Bundle Anterior Cruciate Ligament Reconstructions. Am J Sports Med 38, 1575-1583.

Anderson, C. J., Westerhaus, B. D., Pietrini, S. D., Ziegler, C. G., Wijdicks, C. A., Johansen, S., Engebretsen, L. and LaPrade, R. F. 2010b. Kinematic Impact of Anteromedial and Posterolateral Bundle Graft Fixation

Angles on Double-Bundle Anterior Cruciate Ligament Reconstructions. The American Journal of Sports Medicine 38, 1575.

Anderson, D. D., Iyer, K. S., Segal, N. A., Lynch, J. A. and Brown, T. D. 2010c. Implementation of discrete element analysis for subject-specific, population-wide investigations of habitual contact stress exposure. J Appl Biomech 26, 215.

Anderson, F. C. and Pandy, M. G. 1999. A dynamic optimization solution for vertical jumping in three dimensions. Comp Meth in Biomech and BME 2, 201-231.

Anderson, F. C. and Pandy, M. G. 2001. Dynamic optimization of human walking. J Biomech Engr 123, 381-390.

Anderson, F. C. and Pandy, M. G. 2003. Individual muscle contributions to support in normal walking. Gait & posture 17, 159-169.

Andriacchi, T. P., Briant, P. L., Bevill, S. L. and Koo, S. 2006. Rotational Changes at the Knee after ACL Injury Cause Cartilage Thinning. Clin Orthop Relat Res 442, 39-44.

Andriacchi, T. P. and Dyrby, C. O. 2005. Interactions between kinematics and loading during walking for the normal and ACL deficient knee. Knee Mech: Update of Theor and Exp Anal 38, 293-298.

Andriacchi, T. P., Mikosz, R. P., Hampton, S. J. and Galante, J. O. 1983. Model studies of the stiffness characteristics of the human knee joint. J Biomech 16, 23-29.

Andriacchi, T. P., Mundermann, A., Smith, R. L., Alexander, E. J., Dyrby, C. O. and Koo, S. 2004. A Framework for the in Vivo Pathomechanics of Osteoarthritis at the Knee. Ann Biomed Eng 32, 447-457.

Arnold, A. S., Asakawa, D. J. and Delp, S. L. 2000. Do the hamstrings and adductors contribute to excessive internal rotation of the hip in persons with cerebral palsy? Gait & Posture 11, 181-190.

Arnold, E. M., Ward, S. R., Lieber, R. L. and Delp, S. L. 2010. A Model of the Lower Limb for Analysis of Human Movement. Ann Biomed Eng 38, 269-279.

Asano, T., Akagi, M. and Nakamura, T. 2005. The Functional Flexion-Extension Axis of the Knee Corresponds to the Surgical Epicondylar Axis: In Vivo Analysis Using a Biplanar Image-Matching Technique. J Arthro 20, 1060-1067.

Bargar, W. L., Moreland, J. R., Markolf, K. L., Shoemaker, S. C., Amstutz, H. C. and Grant, T. T. 1980. In Vivo Stability Testing of Post-Meniscectomy Knees. Clin Orthop Relat Res 150, 247-252.

Barrance, P. J. P., Williams, G. N. P., Snyder-Mackler, L. S. and Buchanan, T. S. P. 2007. Do ACL-injured Copers Exhibit Differences in Knee Kinematics?: An MRI Study. Clin Orthop Relat Res 454, 74-80.

Beard, D., Soundarapandian, R., O'Connor, J. and Dodd, C. 1996. Gait and electromyographic analysis of anterior cruciate ligament deficient subjects. Gait & Posture 4, 83-88.

Berchuck, M., Andriacchi, T., Bach, B. and Reider, B. 1990. Gait adaptations by patients who have a deficient ACL. J Bone Joint Surg Am 72, 871-877.

Berme, N., Cappozzo, A. and Meglan, J. 1990. Rigid body mechanics as applied to human movement studies. Biomech of Human Move: Appl in Rehab, Sports, and Ergo 89-107.

Besier, T. F., Fredericson, M., Gold, G. E., Beaupré, G. S. and Delp, S. L. 2009. Knee muscle forces during walking and running in patellofemoral pain patients and pain-free controls. J Biomech 42, 898-905.

Besier, T. F., Gold, G. E., Beaupre, G. S. and Delp, S. L. 2005. A modeling framework to estimate patellofemoral joint cartilage stress in vivo. Med Sci Sports Exerc 37, 1924-30.

Birnbaum, K., Siebert, C., Pandorf, T., Schopphoff, E., Prescher, A. and Niethard, F. 2004. Anatomical and biomechanical investigations of the iliotibial tract. Surg and Radio Anat 26, 433-446.

Blankevoort, L. and Huiskes, R. 1991. Ligament-Bone Interaction in a Three-Dimensional Model of the Knee. J Biomech Engr 113, 263-269.

Blankevoort, L. and Huiskes, R. 1996. Validation of a three-dimensional model of the knee. J Biomech 29, 955-961.

Blankevoort, L., Huiskes, R. and de Lange, A. 1991a. Recruitment of Knee Joint Ligaments. J Biomech Engr 113, 94-103.

Blankevoort, L., Huiskes, R. and DeLange, A. 1988. The envelope of passive knee joint motion. J Biomech 21, 705-720.

Blankevoort, L., Kuiper, J. H., Huiskes, R. and Grootenboer, H. J. 1991b. Articular contact in a three-dimensional model of the knee. J Biomech 24, 1019-1031.

Bonnin, M., Carret, J. P., Dimnet, J. and Dejour, H. 1996. The weight-bearing knee after anterior cruciate ligament rupture. Knee Surgery, Sports Traumatology, Arthroscopy 3, 245-251.

Bowman Jr, K. F. and Sekiya, J. K. 2010. Anatomy and Biomechanics of the Posterior Cruciate Ligament, Medial and Lateral Sides of the Knee. Sports Med and Arthro Review 18, 222.

Bradford, R. G. 2011. Functional bilateral kinematic symmetry of the healthy human knee measured by dynamic magnetic resonance imaging.

Brantigan, O. C. and Voshell, A. F. 1941. The Mechanics of the Ligaments and Menisci of the Knee Joint. J Bone Joint Surg Am 23, 44-66.

Buchanan, T. S., Lloyd, D. G., Manal, K. and Besier, T. F. 2005. Estimation of muscle forces and joint moments using a forward-inverse dynamics model. Med Sci Sports Exerc 37, 1911.

Butler, D. L., Grood, E. S., Noyes, F. R., Zernicke, R. F. and Brackett, K. 1984. Effects of structure and strain measurement technique on the material properties of young human tendons and fascia. J Biomech 17, 579-596.

Butler, D. L., Guan, Y., Kay, M. D., Cummings, J. F., Feder, S. M. and Levy, M. S. 1992. Location-dependent variations in the material properties of the anterior cruciate ligament. J Biomech 25, 511-518.

Butler, D. L., Kay, M. D. and Stouffer, D. C. 1986. Comparison of Material Properties in Fascicle-Bone Units from Human Patellar Tendon and Knee Ligaments. J Biomech 19, 425-432.

Butler, D. L., Noyes, F. and Grood, E. S. 1980. Ligamentous restraints to anterior-posterior drawer in the human knee. J Bone Joint Surg Am 62A, 259-270.

Caruntu, D. and Hefzy, M. 2004. 3-D Anatomically Based Dynamic Modeling of the Human Knee to Include Tibio-Femoral and Patello-Femoral Joints. J Biomech Engr 126, 44-53.

Chandrashekar, N., Mansouri, H., Slauterbeck, J. and Hashemi, J. 2006. Sex-based differences in the tensile properties of the human anterior cruciate ligament. J Biomech 39, 2943-2950.

Chaudhari, A. M. W., Briant, P. L., Bevill, S. L., Koo, S. and Andriacchi, T. P. 2008. Knee Kinematics, Cartilage Morphology, and Osteoarthritis after ACL Injury. Med Sci Sports Exerc 40, 215-222.

Coobs, B. R., LaPrade, R. F., Griffith, C. J. and Nelson, B. J. 2007. Biomechanical analysis of an isolated fibular (lateral) collateral ligament reconstruction using an autogenous semitendinosus graft. Am J Sports Med 35, 1521-1527.

Coobs, B. R., Wijdicks, C. A., Armitage, B. M., Spiridonov, S. I., Westerhaus, B. D., Johansen, S., Engebretsen, L. and LaPrade, R. F. 2010. An in vitro analysis of an anatomical medial knee reconstruction. Am J Sports Med 38, 339-347.

Costigan, P. A., Deluzio, K. J. and Wyss, U. P. 2002. Knee and hip kinetics during normal stair climbing. Gait & Posture 16, 31-37.

Dargel, J., Michael, J. W. P., Feiser, J., Ivo, R. and Koebke, J. 2010. Human knee joint anatomy revisited: morphometry in the light of sex-specific total knee arthroplasty. J Arthro 26, 346-353.

Davies, H., Unwin, A. and Aichroth, P. 2004. The posterolateral corner of the knee: Anatomy, biomechanics and management of injuries. Injury 35, 68-75.

de Leva, P. 1996a. Adjustments to Zatsiorsky-Seluyanov's segment inertia parameters. J Biomech 29, 1223-1230.

de Leva, P. 1996b. Adjustments to Zatsiorsky-Seluyanov's segment inertia parameters. J Biomech 29, 1223-30.

Delp, S. L. 1990. Surgery simulation: a computer graphics system to analyze and design musculoskeletal reconstructions of the lower limb. PhD Dissertation, Stanford University.

Delp, S. L., Loan, J. P., Hoy, M. G., Zajac, F. E., Topp, E. L. and Rosen, J. M. 1990. An interactive graphics-based model of the lower extremity to study orthopaedic surgical procedures. IEEE Trans BME 37, 757-767.

Devita, P., Hortobagyi, T., Barrier, J., Torry, M., Glover, K. L., Speroni, D. L., Money, J. and Mahar, M. T. 1997. Gait adaptations before and after anterior cruciate ligament reconstruction surgery. Med Sci Sports Exerc 29, 853-859.

Dhaher, Y. and Kahn, L. 2002. The Effect of Vastus Medialis Forces on Patello-femoral Contact: A Model-based Study. J Biomech Engr 124, 758-767.

Dhaher, Y. Y., Kwon, T. H. and Barry, M. 2010. The effect of connective tissue material uncertainties on knee joint mechanics under isolated loading conditions. J Biomech 43, 3118-3125.

Draper, C. E., Besier, T. F., Santos, J. M., Jennings, F., Fredericson, M., Gold, G. E., Beaupre, G. S. and Delp, S. L. 2008. Using real time MRI to quantify altered joint kinematics in subjects with patellofemoral pain and to evaluate the effects of a patellar brace or sleeve on joint motion. J Orthop Research 27, 571-577.

Dunkin, M. A. 2009. Handout on Health: Sports Injuries.

Dyrby, C. O. and Andriacchi, T. P. 2004. Secondary motions of the knee during weight bearing and non-weight bearing activities. J Orthop Research 22, 794-800.

Edwards, A., Bull, A. M. and Amis, A. A. 2007. The Attachments of the Fiber Bundles of the Posterior Cruciate Ligament: An Anatomic Study. Arthro: J Arthro and Rel Surg 23, 284-290.

Elsevier, C. L. 2008. Gray's Anatomy The Anatomical Basis of Clinical Practice.

Fernandez, J. W. and Pandy, M. G. 2006. Integrating modelling and experiments to assess dynamic musculoskeletal function in humans. Exper Physiol 91, 371-382.

Fregly, B. J., Besier, T. F., Lloyd, D. G., Delp, S. L., Banks, S. A., Pandy, M. G. and D'Lima, D. D. 2012. Grand challenge competition to predict in vivo knee loads. J Orthop Research 30, 503-513

Fu, F. H., Harner, C. D., Johnson, D. L., Miller, M. D. and Woo, S. L. Y. 1993. Biomechanics of Knee Ligaments: Basic Concepts and Clinical Application. J Bone Joint Surg Am 75, 1716-1727.

Fukubayashi, T., Torzilli, P. A., Sherman, M. F. and Warren, R. F. 1982. An in vitro biomechanical evaluation of anterior-posterior motion of the knee. Tibial displacement, rotation, and torque. J Bone Joint Surg Am 64, 258-264.

Garg, A. and Walker, P. S. 1990. Prediction of total knee motion using a three-dimensional computer-graphics model. J Biomech 23, 45-53, 55-58.

Georgoulis, A. D., Papadonikolakis, A., Papageorgiou, C. D., Mitsou, A. and Stergiou, N. 2003. Three-Dimensional Tibiofemoral Kinematics of the Anterior Cruciate Ligament-Deficient and Reconstructed Knee during Walking. Am J Sports Med 31, 75-79

Gering, D., Nabavi, A., Kikinis, R., Grimson, W., Hata, N., Everett, P., Jolesz, F. and Wells, W. 1999. An integrated visualization system for surgical planning and guidance using image fusion and interventional imaging. Medical Image Computing and Computer-Assisted Intervention–MICCAI'99.

Girgis, F. G., Marshall, J. L. and Monajem, A. R. S. 1975. The Cruciate Ligaments of the Knee Joint: Anatomical, Functional and Experimental Analysis. Clin Orthop Relat Res 106, 216-231.

Gollehon, D. L., Torzilli, P. A. and Warren, R. F. 1987. The role of the posterolateral and cruciate ligaments in the stability of the human knee. A biomechanical study. J Bone Joint Surg Am 69, 233-242.

Gordon, C. C. 1989. Anthropometric Survey of US Army Personnel: Methods and Summary Statistics 1988. DTIC Document,

Gray, H. 1918. Anatomy of the human body. Lea & Febiger,

Griffin, F. M., Math, K., Scuderi, G. R., Insall, J. N. and Poilvache, P. L. 2000. Anatomy of the epicondyles of the distal femur:: MRI analysis of normal knees. J Arthro 15, 354-359.

Griffith, C. J., LaPrade, R. F., Johansen, S., Armitage, B. M., Wijdicks, C. and Engebretsen, L. 2009. Medial knee injury: part 1, static function of the individual components of the main medial knee structures. Am J Sports Med 37, 1762-1770.

Grood, E. S., Noyes, F. R., Butler, D. L. and Suntay, W. J. 1981. Ligamentous and capsular restraints preventing straight medial and lateral laxity in intact human cadaver knees. J Bone Joint Surg Am 63, 1257-1269.

Grood, E. S., Stowers, S. F. and Noyes, F. R. 1988. Limits of movement in the human knee. Effect of sectioning the posterior cruciate ligament and posterolateral structures. J Bone Joint Surg Am 70, 88-97.

Grood, E. S. and Suntay, W. J. 1983. A joint coordinate system for the clinical description of three-dimensional motions: application to the knee. J Biomech Engr 105, 136.

Guyton, A. C. 1986. Ch. 11 Contraction of Skeletal Muscle. *Textbook of medical physiology,* W.B. Saunders Co.,

Haimes, J. L., Wroble, R. R., Grood, E. S. and Noyes, F. R. 1994. Role of the medial structures in the intact and anterior cruciate ligament-deficient knee. Limits of motion in the human knee. Am J Sports Med 22, 402-409.

Halloran, J. P., Erdemir, A. and van den Bogert, A. J. 2009. Adaptive Surrogate Modeling for Efficient Coupling of Musculoskeletal Control and Tissue Deformation Models. J Biomech Engr 131, 011014-7.

Hansen, P., Bojsen-Moller, J., Aagaard, P., Kjaer, M. and Magnusson, S. P. 2006. Mechanical properties of the human patellar tendon, in vivo. Clin Biomech 21, 54-58.

Happee, R. 1994. Inverse dynamic optimization including muscular dynamics, a new simulation method applied to goal directed movements. J Biomech 27, 953-960.

Hashemi, J., Chandrashekar, N., Cowden, C. and Slauterbeck, J. 2005. An alternative method of anthropometry of anterior cruciate ligament through 3-D digital image reconstruction. J Biomech 38, 551-555.

Haut, R. C. and Powlison, A. C. 1990. The effects of test environment and cyclic stretching on the failure properties of human patellar tendons. J Orthop Research 8, 532-540.

Hirokawa, S., Solomonow, M., Lu, Y., Lou, Z. P. and D'Ambrosia, R. 1992. Anterior-posterior and rotational displacement of the tibia elicited by quadriceps contraction. Am J Sports Med 20, 299-306.

Hsieh, H. H. and Walker, P. S. 1976. Stabilizing mechanisms of the loaded and unloaded knee joint. J Bone Joint Surg Am 58, 87-93.

Inman, V. T. 1976. The joints of the ankle. Williams & Wilkins Baltimore,

Johnson, G. A., Tramaglini, D. M., Levine, R. E., Ohno, K. and Choi, N. Y. 1994. Tensile and viscoelastic properties of human patellar tendon. J Orthop Research 12, 796-803.

Jones, R. S., Nawana, N. S., Pearcy, M. J., Learmonth, D. J. A., Bickerstaff, D. R., Costi, J. J. and Paterson, R. S. 1995. Mechanical properties of the human anterior cruciate ligament. Clin Biomech 10, 339-344.

Kanamori, A., Woo, S. L. Y., Ma, B., Zeminski, J., Rudy, T. W., Li, G. and Livesay, G. 2000. The forces in the anterior cruciate ligament and knee kinematics during a simulated pivot shift test: A human cadaveric study using robotic technology. Arthro: J Arthro and Rel Surg 16, 633-639.

Kersh, M. 2010. Virtual Biomechanical Knee: A Finite Element Ligament Model with Experimental Validation. Unviersity of Wisconsin-Madison.

Kim, H. J., Fernandez, J. W., Akbarshahi, M., Walter, J. P., Fregly, B. J. and Pandy, M. G. 2009. Evaluation of predicted knee joint muscle forces during gait using an instrumented knee implant. J Orthop Research 27, 1326-1331.

Kim, S. 1996. A three-dimensional dynamic musculoskeletal model of the human knee joint. University of Texas at Austin.

Kopf, S., Musahl, V., Tashman, S., Szczodry, M., Shen, W. and Fu, F. H. 2009. A systematic review of the femoral origin and tibial insertion morphology of the ACL. Knee Surg, Sports Traumatol, Artho 17, 213-219.

Krevolin, J. L., Pandy, M. G. and Pearce, J. C. 2004. Moment arm of the patellar tendon in the human knee. J Biomech 37, 785-788.

Kuster, M. S., Wood, G. A., Stachowiak, G. W. and Gachter, A. 1997. Joint load considerations in total knee replacement. J Bone Joint Surg Br 79, 109.

Lafortune, M. A., Cavanagh, P. R., Sommer Iii, H. J. and Kalenak, A. 1992. Three-dimensional kinematics of the human knee during walking. J Biomech 25, 347-357.

LaPrade, R. F., Bollom, T. S., Wentorf, F. A., Wills, N. J. and Meister, K. 2005. Mechanical properties of the posterolateral structures of the knee. Am J Sports Med 33, 1386-1391.

Levy, I. M., Torzilli, P. A., Gould, J. D. and Warren, R. F. 1989. The effect of lateral meniscectomy on motion of the knee. J Bone Joint Surg Am 71, 401-406.

Levy, I. M., Torzilli, P. A. and Warren, R. F. 1982. The effect of medial meniscectomy on anterior-posterior motion of the knee. J Bone Joint Surg Am 64, 883-888.

Li, G., DeFrate, L. E., Sun, H. and Gill, T. J. 2004. In vivo elongation of the anterior cruciate ligament and posterior cruciate ligament during knee flexion. Am J Sports Med 32, 1415.

Li, G., Moses, J. M., Papannagari, R., Pathare, N. P., DeFrate, L. E. and Gill, T. J. 2006. Anterior Cruciate Ligament Deficiency Alters the In Vivo Motion of the Tibiofemoral Cartilage Contact Points in Both the Anteroposterior and Mediolateral Directions. J Bone Joint Surg Am 88, 1826-1834.

Li, G., Park, S. E., DeFrate, L. E., Schutzer, M. E., Ji, L., Gill, T. J. and Rubash, H. E. 2005. The cartilage thickness distribution in the tibiofemoral joint and its correlation with cartilage-to-cartilage contact. Clin Biomech 20, 736-744.

Li, G., Rudy, T. W., Sakane, M., Kanamori, A., Ma, C. B. and Woo, S. L. Y. 1999. The importance of quadriceps and hamstring muscle loading on knee kinematics and in-situ forces in the ACL. J Biomech 32, 395-400.

Lin, Y. C., Walter, J. P., Banks, S. A., Pandy, M. G. and Fregly, B. J. 2010. Simultaneous prediction of muscle and contact forces in the knee during gait. J Biomech 43, 945-952.

Lloyd, D. G. and Besier, T. F. 2003. An EMG-driven musculoskeletal model to estimate muscle forces and knee joint moments in vivo. J Biomech 36, 765-776.

Lohmander, L. S., Englund, P. M., Dahl, L. L. and Roos, E. M. 2007. The Long-term Consequence of Anterior Cruciate Ligament and Meniscus Injuries: Osteoarthritis. Am J Sports Med 35, 1756-1769.

Manal, K., Davis, I. M. C., Galinat, B. and Stanhope, S. 2003. The accuracy of estimating proximal tibial translation during natural cadence walking: bone vs. skin mounted targets. Clin Biomech 18, 126-131.

Marinozzi, G., Pappalardo, S. and Steindler, R. 1983. Human knee ligaments: mechanical tests and ultrastructural observations. J Ortho and Traum (It) 9, 231.

Markolf, K. L., Bargar, W. L., Shoemaker, S. C. and Amstutz, H. C. 1981. The role of joint load in knee stability. J Bone Joint Surg Am 63, 570-585.

Markolf, K. L., Kochan, A. and Amstutz, H. C. 1984. Measurement of knee stiffness and laxity in patients with documented absence of the anterior cruciate ligament. J Bone Joint Surg Am 66, 242-252.

Markolf, K. L., Mensch, J. S. and Amstutz, H. C. 1976. Stiffness and laxity of the knee--the contributions of the supporting structures. A quantitative in vitro study. J Bone Joint Surg Am 58, 583-594.

Masouros, S. D., Bull, A. M. and Amis, A. A. 2010. (i) Biomechanics of the knee joint. Orthop and Traum 24, 84-91.

McDermott, I. and Amis, A. 2006. The consequences of meniscectomy. J Bone Joint Surg Br 88, 1549.

McLean, S. G., Su, A. and van den Bogert, A. J. 2003. Development and validation of a 3-D model to predict knee joint loading during dynamic movement. J Biomech Engr 125, 864.

Meister, B. R., Michael, S. P., Moyer, R. A., Kelly, J. D. and Schneck, C. D. 2000. Anatomy and kinematics of the lateral collateral ligament of the knee. Am J Sports Med 28, 869.

Mensch, J. and Amstutz, H. 1975. Knee morphology as a guide to knee replacement. Clin Orthop Relat Res 231.

Messner, K. and Gao, J. 1998. The menisci of the knee joint. Anatomical and functional characteristics, and a rationale for clinical treatment. J Anat 193, 161-178.

Neptune, R. and Kautz, S. 2000. Knee joint loading in forward versus backward pedaling: implications for rehabilitation strategies. Clin Biomech 15, 528-535.

Noyes, F., Butler, D., Grood, E., Zernicke, R. and Hefzy, M. 1984. Biomechanical analysis of human ligament grafts used in knee-ligament repairs and reconstructions. J Bone Joint Surg 66, 344.

Noyes, F. R. and Grood, E. S. 1976. The strength of the anterior cruciate ligament in humans and Rhesus monkeys. J Bone Joint Surg 58, 1074.

Oliveria, S. A., Felson, D. T., Reed, J. I., Cirillo, P. A. and Walker, A. M. 2005. Incidence of symptomatic hand, hip, and knee osteoarthritis among patients in a health maintenance organization. Arth and Rheu 38, 1134-1141.

Pandy, M. G. 1999. Moment Arm of a Muscle Force. Exerc and Sports Sci Rev 27, 79-118.

Pandy, M. G. 2001. Computer Modeling and Simulation of Human Movement. Ann Rev in Biomed Engr 3, 245-273.

Pandy, M. G. and Andriacchi, T. P. 2010. Muscle and Joint Function in Human Locomotion. Ann Rev of Biomed Engr 12, 401-433.

Pandy, M. G. and Sasaki, K. 1998. A three-dimensional musculoskeletal model of the human knee joint. Part 2: analysis of ligament function. Comp Meth in Biomech and BME 1, 265-283.

Pandy, M. G., Sasaki, K. and Kim, S. 1997. A Three-Dimensional Musculoskeletal Model of the Human Knee Joint. Part 1: Theoretical Construction. Comp Meth in Biomech and BME 1, 87 - 108.

Park, S. E., DeFrate, L. E., Suggs, J. F., Gill, T. J., Rubash, H. E. and Li, G. 2005. The change in length of the medial and lateral collateral ligaments during in vivo knee flexion. Knee 12, 377.

Pelc, N., Drangova, M., Pelc, L. R., Zhu, Y., Noll, D. C., Bowman, B. S. and Herfkens, R. J. 1995. Tracking of cyclic motion with phase-contrast cine MR velocity data. J MRI 5, 339-345.

Petersen, W. M. D. and Zantop, T. M. D. 2007. Anatomy of the Anterior Cruciate Ligament with Regard to Its Two Bundles. Clin Orthop Relat Res 454, 35-47

Pieper, S., Halle, M. and Kikinis, R. 2005. 3D Slicer. IEEE International Symposium on Biomedical Imaging: Nano to Macro.

Pieper, S., Lorensen, B., Schroeder, W. and Kikinis, R. 2006. The na-mic kit: Itk, vtk, pipelines, grids and 3d slicer as an open platform for the medical image computing community. 3rd IEEE International Symposium on Biomedical Imaging: Nano to Macro.

Quapp, K. and Weiss, J. 1998. Material characterization of human medial collateral ligament. J Biomech Engr 120, 757.

Race, A. and Amis, A. A. 1994. The mechanical properties of the two bundles of the human posterior cruciate ligament. J Biomech 27, 13-24.

Reeder, S. B., McKenzie, C. A., Pineda, A. R., Yu, H., Shimakawa, A., Brau, A. C., Hargreaves, B. A., Gold, G. E. and Brittain, J. H. 2007. Water–fat separation with IDEAL gradient echo imaging. J MRI 25, 644-652.

Reinbolt, J. A., Schutte, J. F., Fregly, B. J., Koh, B. I., Haftka, R. T., George, A. D. and Mitchell, K. H. 2005. Determination of patient-specific multi-joint kinematic models through two-level optimization. J Biomech 38, 621-626.

Robinson, J. R., Sanchez-Ballester, J., Bull, A. M. J., Thomas, R. and Amis, A. A. 2004. The posteromedial corner revisited: an anatomical description of the passive restraining structures of the medial aspect of the human knee. J Bone Joint Surg Br 86, 674.

Röstlund, T., Carlsson, L., Albrektsson, B. and Albrektsson, T. 1989. Morphometrical studies of human femoral condyles. J Biomed Engr 11, 442-448.

Sakane, M., Livesay, G., Fox, R. J., Rudy, T. W., Runco, T. J. and Woo, S. L. Y. 1999. Relative contribution of the ACL, MCL, and bony contact to the anterior stability of the knee. Knee Surg, Sports Traumatol, Artho 7, 93-97.

Seale, K. S., Haynes, D. W., Nelson, C. L., McLeod, P. C. and Gerdes, M. H. 1981. The Effect of Meniscectomy on Knee Stability. Transactions of the annual meeting of ORS.

Seedhom, B., Longton, E., Wright, V. and Dowson, D. 1972. Dimensions of the knee. Radiographic and autopsy study of sizes required by a knee prosthesis. Ann of Rheu Diseases 31, 54.

Seedhom, B. B. 1979. Transmission of the load in the knee joint with special reference to the role of the menisci Part I: anatomy, analysis and apparatus. Arch Engr in Med 8, 207-219.

Seering, W., Piziali, R., Nagel, D. and Schurman, D. 1980. The function of the primary ligaments of the knee in varus-valgus and axial rotation. J Biomech 13, 785-794.

Seisler, A. R. and Sheehan, F. T. 2007. Normative Three-Dimensional Patellofemoral and Tibiofemoral Kinematics: A Dynamic, in vivo study. IEEE Trans BME 54, 1333-1341.

Sheehan, F. 2007a. The 3D patellar tendon moment arm: quantified in vivo during volitional activity. J Biomech 40, 1968-1974.

Sheehan, F. 2007b. The finite helical axis of the knee joint (a non-invasive in vivo study using fast-PC MRI). J Biomech 40, 1038-1047.

Sheehan, F. and Drace, J. E. 2000. Human patellar tendon strain. A noninvasive, in vivo study. Clin Orthop 370, 201-207.

Sheehan, F., Zajac, F. E. and Drace, J. E. 1999. In vivo tracking of the human patella using cine phase contrast magnetic resonance imaging. J Biomech Engr 121, 650-656.

Sheehan, F. T., Derasari, A., Brindle, T. J. and Alter, K. E. 2009. Understanding patellofemoral pain with maltracking in the presence of joint laxity: complete 3D in vivo patellofemoral and tibiofemoral kinematics. J Orthop Research 27, 561-570.

Shelburne, K. B., Kim, H. J., Sterett, W. I. and Pandy, M. G. 2011. Effect of posterior tibial slope on knee biomechanics during functional activity. J Orthop Research 29, 223-231.

Shelburne, K. B. and Pandy, M. G. 1997. A musculoskeletal model of the knee for evaluating ligament forces during isometric contractions. J Biomech 30, 163-176.

Shelburne, K. B. and Pandy, M. G. 2002. A Dynamic Model of the Knee and Lower Limb for Simulating Rising Movements. Comp Meth in Biomech and BME 5, 149-160.

Shelburne, K. B., Pandy, M. G., Anderson, F. C. and Torry, M. R. 2004. Pattern of anterior cruciate ligament force in normal walking. J Biomech 37, 797-805.

Shelburne, K. B., Torry, M. R. and Pandy, M. G. 2005a. Effect of Muscle Compensation on Knee Instability during ACL-Deficient Gait. Med Sci Sports Exerc 37, 642-648.

Shelburne, K. B., Torry, M. R. and Pandy, M. G. 2005b. Muscle, Ligament, and Joint-Contact Forces at the Knee during Walking. Med Sci Sports Exerc 37, 1948-1956

Shelburne, K. B., Torry, M. R. and Pandy, M. G. 2006. Contributions of muscles, ligaments, and the ground reaction force to tibiofemoral joint loading during normal gait. J Orthop Research 24, 1983-1990.

Shin, C. S., Chaudhari, A. M. and Andriacchi, T. P. 2007. The influence of deceleration forces on ACL strain during single-leg landing: a simulation study. J Biomech 40, 1145-1152.

Shoemaker, S. C. and Markolf, K. L. 1985. Effects of joint load on the stiffness and laxity of ligament-deficient knees. An in vitro study of the anterior cruciate and medial collateral ligaments. J Bone Joint Surg Am 67, 136-146.

Shoemaker, S. C. and Markolf, K. L. 1986. The role of the meniscus in the anterior-posterior stability of the loaded anterior cruciate-deficient knee. Effects of partial versus total excision. J Bone Joint Surg Am 68, 71-79.

Simon, W. H., Friedenberg, S. and Richardson, S. 1973. Joint congruence: A correlation of joint congruence and thickness of articular cartilage in dogs. J Bone Joint Surg 55, 1614.

Spoor, C. and Veldpaus, F. 1980. Rigid body motion calculated from spatial co-ordinates of markers. J Biomech 13, 391-393.

Stäubli, H. U., Schatzmann, L., Brunner, P., Rincón, L. and Nolte, L. P. 1999. Mechanical tensile properties of the quadriceps tendon and patellar ligament in young adults. Am J Sports Med 27, 27.

Steinke, H., Lingslebe, U., Böhme, J., Slowik, V., Shim, V., Hädrich, C. and Hammer, N. 2012. Deformation behavior of the iliotibial tract under different states of fixation. Med Engr and Physics in press, .

Stergiou, N., Stavros, R., Constantina, M. and Georgoulis, A. D. 2007. Tibial Rotation in Anterior Cruciate Ligament (ACL)-Deficient and ACL-Reconstructed Knees: A Theoretical Proposition for the Development of Osteoarthritis. Sports Medicine 37, 601-613.

Sugita, T. and Amis, A. A. 2001. Anatomic and biomechanical study of the lateral collateral and popliteofibular ligaments. Am J Sports Med 29, 466.

Sullivan, D., Levy, I. M., Sheskier, S., Torzilli, P. A. and Warren, R. F. 1984. Medical restrains to anterior-posterior motion of the knee. J Bone Joint Surg Am 66, 930-936.

Taylor, W. R., Heller, M. O., Bergmann, G. and Duda, G. N. 2004. Tibio-femoral loading during human gait and stair climbing. J Orthop Research 22, 625-632.

Thelen, D. G. 2003. Adjustment of muscle mechanics model parameters to simulate dynamic contractions in older adults. J Biomech Engr 125, 70-77.

Thelen, D. G. and Anderson, F. C. 2006a. Using computed muscle control to generate forward dynamic simulations of human walking from experimental data. J Biomech 39, 1107-15.

Thelen, D. G. and Anderson, F. C. 2006b. Using computed muscle control to generate forward dynamic simulations of human walking from experimental data. J Biomech 39, 1107-1115.

Thelen, D. G., Anderson, F. C. and Delp, S. L. 2003. Generating dynamic simulations of movement using computed muscle control. J Biomech 36, 321-328.

Thompson, W. O. and Fu, F. H. 1993. The meniscus in the cruciate-deficient knee. Clin Sports Med 12, 771-796.

Trent, P. S., Walker, P. S. and Wolf, B. 1976. Ligament length patterns, strength, and rotational axes of the knee joint. Clin Orthop Relat Res 117, 263.

Tsai, A. G., Wijdicks, C. A., Walsh, M. P. and LaPrade, R. F. 2010. Comparative Kinematic Evaluation of All-Inside Single-Bundle and Double-Bundle Anterior Cruciate Ligament Reconstruction. Am J Sports Med 38, 263-272.

Tsaopoulos, D. E., Baltzopoulos, V. and Maganaris, C. N. 2006. Human patellar tendon moment arm length: Measurement considerations and clinical implications for joint loading assessment. Clin Biomech 21, 657-667.

Tsaopoulos, D. E., Baltzopoulos, V., Richards, P. J. and Maganaris, C. N. 2007. In vivo changes in the human patellar tendon moment arm length with different modes and intensities of muscle contraction. J Biomech 40, 3325-3332.

van der Krogt, M. M., Delp, S. L. and Schwartz, M. H. 2012. How robust is human gait to muscle weakness? Gait & Posture 36, 113-119.

Van Eijden, T. M. G. J., Kouwenhoven, E. and Weijs, W. A. 1987. Mechanics of the patellar articulation Effects of patellar ligament length studied with a mathematical model. Acta Orthop 58, 560-566.

Vincent, K. R., Conrad, B. P., Fregly, B. J. and Vincent, H. K. 2012. The pathophysiology of osteoarthritis: A mechanical perspective on the knee joint. PM&R 4, S3-S9.

Walker, P. S., Rovick, J. S. and Robertson, D. D. 1988. The effects of knee brace hinge design and placement on joint mechanics. J Biomech 21, 965-74.

Wang, C. J. and Walker, P. S. 1974. Rotatory Laxity of the Human Knee Joint. J Bone Joint Surg Am 56, 161-170.

Westphal, C. 2009. Load Dependent Variations in Knee Kinematics Measured by Dynamic Magnetic Resonance Imaging. University of Wisconsin Madison.

Westphal, C., Reeder, S. B. and Thelen, D. 2012. Load-Dependent Variations in Knee Kinematics Measured with Dynamic MRI. J Biomech submitted, .

Westphal, C. and Thelen, D. 2009. Load Dependent Variations in Knee Kinematics Measured by Dynamics MR. ASB.

Wilson, D. R., Feikes, J. D., Zavatsky, A. B. and O'Connor, J. J. 2000. The components of passive knee movement are coupled to flexion angle. J Biomech 33, 465-473.

Winter, D. 1987. The biomechanics and motor control of human gait. University of Waterloo Press,
Wismans, J. 1980. A Three-Dimensional Mathematical Model of the Human Knee Joint. Eindhoven University of Technology.

Wismans, J., Veldpaus, F., Janssen, J., Huson, A. and Struben, P. 1980. A three-dimensional mathematical model of the knee-joint. J Biomech 13, 677-679, 681-685.

Woo, S. L. Y., Hollis, J. M., Adams, D. J., Lyon, R. M. and Takai, S. 1991. Tensile properties of the human femur-anterior cruciate ligament-tibia complex. Am J Sports Med 19, 217.

Yoshioka, Y., Siu, D. and Cooke, T. 1987. The anatomy and functional axes of the femur. J Bone Joint Surg Am 69, 873.

Zajac, F. E. 1989. Muscle and Tendon: Properties, Models, Scaling, and Application to Biomechanics and Motor Control. Crit Rev in BME 17, 359-411.